AEDC-TR-66-258

RESEARCH STUDY OF RADIATION HEAT FLUX FROM HIGH PRESSURE AIR ARCS

C. H. Marston, G. Frind, and V. Mishkovsky
General Electric Company

December 1966

Distribution of this document is unlimited.

ARNOLD ENGINEERING DEVELOPMENT CENTER
AIR FORCE SYSTEMS COMMAND
ARNOLD AIR FORCE STATION, TENNESSEE

NOTICES

When U. S. Government drawings specifications, or other data are used for any purpose other than a definitely related Government procurement operation, the Government thereby incurs no responsibility nor any obligation whatsoever, and the fact that the Government may have formulated, furnished, or in any way supplied the said drawings, specifications, or other data, is not to be regarded by implication or otherwise, or in any manner licensing the holder or any other person or corporation, or conveying any rights or permission to manufacture, use, or sell any patented invention that may in any way be related thereto.

Qualified users may obtain copies of this report from the Defense Documentation Center.

References to named commercial products in this report are not to be considered in any sense as an endorsement of the product by the United States Air Force or the Government.

RESEARCH STUDY OF RADIATION HEAT FLUX FROM HIGH PRESSURE AIR ARCS

C. H. Marston, G. Frind, and V. Mishkovsky
General Electric Company

Distribution of this document is unlimited.

AF - AEDC
Arnold AFS Tenn

FOREWORD

The work reported herein was sponsored by Headquarters, Arnold Engineering Development Center (AEDC), Air Force Systems Command (AFSC), Arnold Air Force Station, Tennessee, under Program Element 62405334, Project 8952, Task 895202.

The results of research presented were obtained by the General Electric Company, Space Sciences Laboratory and High Power Laboratory, under Contract AF40(600)-1126, and the manuscript was submitted for publication December 1, 1966.

The reproducibles used in the reproduction of this report were supplied by the authors.

The authors acknowledge the assistance of Captain T. L. Hershey, technical monitor. The assistance of Mr. J. J. Carroll, who designed part of the apparatus and ably assisted with all the measurements, and Mr. R. L. Bendorovich, who contributed to the skillful construction of the total radiation calorimeters, is also acknowledged. Dr. H. E. Weber's frequent advice and comment are gratefully acknowledged.

A. M. Schorn was also an author of this report.

This technical report has been reviewed and is approved.

Terry L. Hershey
Captain, USAF
Research Division
Directorate of Plans and Technology

Donald R. Eastman
Acting Director
Directorate of Plans
and Technology

ABSTRACT

A method has been developed for computation of radiant interchange within an electric arc where self absorption is important. Most or all radiation in the vacuum u.v. range is reabsorbed before it gets out of the arc. Present values of absorption coefficients are within an order of magnitude of predicting radiation losses as determined by direct experimental measurement.

An arc has been operated in air at 100 atmospheres sufficiently quiescent to measure a temperature profile at 100 amperes but great care must be taken to start symmetrically and avoid disturbances. At 400 amperes even extreme precautions are not sufficient to forestall instabilities. The air arc constrictor is uncooled and is designed for quasi-steady operation for 1 to 5 milliseconds depending on current level.

NOMENCLATURE

dA	Area element
b	dimension, Figure 44
C	constant, Equation 2.39
C_2	radiation constant h/k_B = 1.438 cm-$^{\circ}$K
c_c	specific heat of calorimeter ring
c_p	specific heat at constant pressure
D	Relative Cumulative Spectral Radiance Equation 2.4
d_o, d_1, d_2, d_3	Interpolation Differences Equations A.3-A.6
E	Voltage gradient
$f(x)$	Transmission integral Equation 2.16
$f_c(x)$	Calorimeter Integral Equation D.2
g	Transmission function Equation 2.17
g	dimension, Figure 44
H	dimensionless enthalpy
h	enthalpy
h	calorimeter half width, Figure 44
h	Plancks constant
I	Electric Current
I_B	Black Body Intensity
J_{thin}	Radiance, Optically thin, Equation 3.1
J_{thick}	Radiance, Optically thick, Equation 3.2
k	number of data points, Equations 2.36 and 2.37 only
k	linear absorption coefficient
k_A	Thermal conductivity of Air
k_B	Boltzmann Constant
k_C	Thermal Conductivity of Copper
$(\overline{k\,R})$	optical depth
L	length of transmission path, Figure 1

Lo	Loschmidt Number
m	mass of calorimeter ring
m	parameter in Equation 2.6
$\bar{N}$	Average particle density, Equation C.6
N	number of Annuli for radiant interchange model
n	wavenumber (reciprocal wavelength)
P	net power into unit volume ($\sigma E^2 - P_r$)
P_r	net radiated power per unit volume
p	pressure
(q/A)	heat flux per unit area
(q/z)	heat flux per unit length of arc
R_g	gas constant
R_{jqm}	sector radii Equation 2.24
r	radius of arc or arc annulus
s	dimension, Figure 44
s	number of sectors per quadrant, radiant interchange model, Equation 2.19
s	parameter in Interpolation, Equation A.3
T	temperature
t	time
t_I	Time of arc extinction
V	volume
v	$h\nu/k_B T$
$W_{B,n}$	Monochromatic emissive power of a black body
X_i	Mol fraction
x	dummy variable in transmission integrals
x	Temperature or enthalpy profile exponent, Equations 2.35 and 5.1
y	Temperature exponent, Equation C.1
z	axial distance

Greek Letters

α_c	Thermal diffusivity of calorimeter
α	Angle defined in Equation 2.22
α	absorptivity
α, β	Integration limits, calorimeter integral, Figure 44
γ	Angle from normal to radiating surface, Figure 1
Δ	increment, not necessarily uniform
ϵ	emissivity
ζ	ratio of radiant flux per unit length reaching calorimeter to total radiant flux at arc boundary
θ	Angle defined on Figure 1
λ	Wavelength
ν	Frequency
ξ	Function defined by Equation 2.40
π	3.14....
ρ	density
σ	Stefan Boltzmann radiation constant
σ_e	Electrical conductivity
σ_{SD}	Standard deviation
τ	transmissivity
Φ	Angle defined on Figure 2
ω	Solid angle

Subscripts and Superscripts

a	Zone 1 arc boundary
C	calorimeter
CL	centerline value
cond	conduction
e	emitted
i	inner boundary of an annulus
L	Inner boundary of outermost annulus
N	Arc core
o	reference state (1 atmosphere, 273°K)
o	outer boundary of an annulus
P	Plexiglas
rad	radiation
t	transmitted
W	wall

Indices

i	general summation index
i	annulus (counting inward from the outermost)
j	boundary of emitting surface
j'	complement of j, see section 2.3
m	angle increment
n	frequency
q	boundary of absorbing surface

TABLE OF CONTENTS

		Page
1.	INTRODUCTION	1
2.	ANALYSIS	3
	2.1 Model and Basic Assumptions	3
	2.2 Radiant Interchange Integral	4
	2.3 Sector Radii	8
	2.4 Radiant Interchange Summation Equations	9
	2.5 Two Zone Arc Model	12
	2.5.1 Temperature Profile	12
	2.5.2 Thermal Conduction	13
	2.5.3 Electrical Properties	15
3.	AIR ABSORPTION COEFFICIENTS AND RADIANCE	17
	3.1 Data Sources and Ranges	17
	3.2 Integral Results	18
4.	EXPERIMENTAL APPARATUS	22
	4.1 Arc Constrictor Configurations	22
	4.1.1 Design Principles	22
	4.1.2 The Heat Sink Type Cascade Constrictor	23
	4.1.3 The Ablation Type Constrictor	24
	4.2 High Pressure Test Apparatus	25
	4.3 Power Supply	25

Page

4.4 Instrumentation 26

4.4.1 Electrical 26

4.4.2 High Speed Photography 26

4.4.3 Time Resolved Spectrograph 27

4.4.4 Total Radiation Calorimeter 29

5. METHODS OF MEASURING TEMPERATURE 33

5.1 Continuum Radiation Intensity 33

5.2 Arc Temperature From Voltage Gradient 34

6. ARC STABILITY 35

7. RESULTS AND CONCLUSIONS 37

7.1 Electrical Gradients and Preliminary Arc Temperature Determination 37

7.2 Temperature Measurements From Continuum Intensities . . . 37

7.2.1 The 115 Ampere Arc 37

7.2.2 The 400 Ampere Arc 38

7.3 Application of ARCRAD III to Measured Profile 38

7.4 Total Radiant Heat Flux Measurements 39

7.5 Conclusions 41

BIBLIOGRAPHY 43

APPENDICES

A. TABULATION AND INTERPOLATION OF TRANSMISSION INTEGRAL 48

B. PROGRAM ARCRAD III 54

B.1 Purpose 54

Page

B.2 Glossary of Terms 54

B.3 Input 64

B.4 FORTRAN Listing, ARCRAD III and Subroutines 67

C. ANNULUS BOUNDARIES 73

C.1 Weighted Average Temperature 73

C.2 Outermost Annulus 74

D. TOTAL RADIATION CALORIMETER MODIFICATION TO RADIANT INTERCHANGE EQUATIONS 76

FIGURES 79

1. INTRODUCTION

Planned development of very high pressure electric arc heaters for re-entry simulation facilities has resulted in a need for reliable calculation and measurement of the radiant heat transfer from arcs operating at pressures of the order of 100 atmospheres. At this pressure level radiation is a critical loss mechanism from the standpoints both of arc heater efficiency and container wall cooling load. Depending on frequency, the plasma ranges from mildly self-absorbed to nearly black body, but over most of the spectrum self-absorption is important and the upper bounds on radiant intensity furnished by the optically thin and black body approximations are completely inadequate. Experimental data on the properties of plasmas in the pressure range around 100 ATM is scarce, though some information is available from the recent paper of Bohn, Beth and Nedder (Bo. 1)*, the well known papers of Anderson (A. 1) and Peters (Pe. 1) and a few more (e.g., Refs. Og. 1, Mi. 1, Bo. 1).

The objective of the combined analytical and experimental program described in this report was the determination of radiant heat flux from an axially symmetric air arc column operating at high pressure. In an operational arc heater the arc column is likely to be unconfined or only partially confined and its characteristics are likely to be further complicated by the presence of a transverse flow and perhaps also by an alternating current power supply, but restriction to a steady, axially symmetric arc with large length to diameter ratio and no flow was necessary to make both experiment and analysis manageable.

An analytical model for calculation of radiant flux density at the arc boundary had been developed under a previous contract and this served as the basis for a more advanced model with which local net radiant interchange and current voltage gradient can be calculated. The model considers steady state dependence of the radiant heat flux on frequency, temperature and density, including the effects of self-absorption, by breaking up the arc into a series of concentric constant property annuli and converting volume radiant emission from each annulus to an equivalent emission from the exterior and interior annulus surfaces.

The experimental arc was designed to provide a well defined arcing apparatus suitable for detailed studies of high pressure arc plasmas, based

---

*-References are listed alphabetically by first and second (occasionally third or fourth) letter of the senior author's last name and a number to distinguish more than one publication by the same author.

in part on previous experience with Argon filled lamps which had been operated at 70 atmospheres and 4000 amperes for one millisecond. It was designed for short duration (~ 700-800 μs) so that no cooling is needed despite the very large heat flux, thus keeping hardware design simple and flexible. Arc power supply is a capacitor bank supplying a constant current pulse for the requisite duration by means of an RLC network switched with spark gaps.

Analysis and experiment represented a coordinated effort to measure and calculate radiant heat flux from the arc. Radiant heat flux both leaving the arc and reaching a calorimeter were computed and compared to calorimeter measurements. The computations were based on a directly measured temperature profile and on analytic profiles constructed with some guidance from observations of electrical properties.

Though computation and experiment both depart from the reality of an operational arc heater both have given useful insights into problems and possibilities in the high pressure regime. Keynote of the experimental effort has been the struggle for operation sufficiently stable to obtain useful spectrographic data. From the analysis has come a quantitative indication of the remarkable distinction between "low frequency" and "high frequency" energy in the radiation process.

2. ANALYSIS

Even with the restrictions of steady state, axial symmetry and large length to diameter ratio, radiant emission from a high pressure electric arc is an extremely complex set of phenomena. These phenomena are characterized by optical depth, the dimensionless product of an absorption coefficient (dependent on frequency, temperature and density) with an orientation dependent characteristic length.

The objective of the analytical work has been to set up an analysis of the radiant interchange within the arc which:

1) exploits the data storage and handling capability of a large digital computer to take all these variables into account.

2) has a degree of refinement adjustable to suit requirements and is sufficiently economical of computer time that many cases can be run.

At least two different approaches may be taken to the problem. These are the astrophysical; in which the dimensionless optical depth is taken as the primary variable in a set of non-linear integral or integro-differential equations; (Ko. 1), and the engineering; in which the emission from a volume is converted to equivalent radiation at a surface (Ja. 1). Most of the work in the former category has been done for the plane parallel, or spherical case although there has also been some work recently on cylindrical geometry. Kesten (Ke. 1) has applied the method to arcs but its extreme complexity has limited it to calculation at only a few specific wave numbers (Ke. 1). DeSoto (De. 1) has calculated radiant transfer in a pipe flow for a limited spectral band.

2.1 MODEL AND BASIC ASSUMPTIONS

The engineering approach has been taken on this project and the computational model is a substantially revised and improved version of one previously reported (Ma. 1, Ma. 2). The radiating arc column is assumed to be cylindrically symmetric, with a length to diameter ratio sufficiently large (10 or more) to be "infinite". The arc cylinder is divided into annuli, each at a uniform temperature temperature and density. Then, taking into account the effect of self-absorption within an annulus, volumetric emission from each annulus is converted to an equivalent radiant flux from the annulus boundary surfaces. The assumption of local thermodynamic equilibrium (LTE) permits the application of Kirchoff's law relating absorption, transmission and emission. Except for the core, each annulus has an interior,

concave, surface as well as an exterior, convex, surface from which radiant emission must be taken into account. Radiant interchange among all annuli is computed by considering emission, absorption and transmission along a representative array of paths from all the emitting surfaces to the outside of the column.

Because self absorption is significant, the controlling parameter is optical depth, the dimensionless product of absorption coefficient and a characteristic length. Two optical depths are distinguished here, 1) absorption lengths along the transmission path and 2) emission lengths within each annulus. Since absorption coefficient varies with temperature and density (each a function of radius), absorption and emission lengths are computed as integrals or summations. For example, a typical absorption length (Fig. 1) is given by

$$(\overline{k\,R}) = \int_o^R k\,dr = \sin\theta \int_o^L k\,dl \qquad (2.1)$$

The basic geometrical element of volume used for calculation of emission and absorption is the infinitely long half-cylinder, with a typical element of emitting area, dA located on its axis, Fig. 1. In previous work (Ma. 1) an average value of emissivity (frequency dependent) was calculated for each annulus, but now the calculations of angle dependent emission are on the same basis as transmission.

Neither emission nor transmission from any surface element actually takes place through a half cylinder, but the true volume shape is effectively approximated by several cylindrical sectors of different radii, Fig. 2. Two typical paths are shown in Fig. 2, with emission lengths shown as solid lines and absorption lengths shown as dashed lines. Calculations of total emission and absorption in each wave number interval requires integration over 2π steradians, accomplished by integrating separately over angles Φ and θ(Fig. 1). The sector approximation decouples the angular dependence of absorption length or emission length on Φ within any sector.

2.2 RADIANT INTERCHANGE INTEGRAL

Solution of the problem of radiant interchange among the annuli proceeded as follows. Consider a surface element dA of an annulus, radiating with an average intensity I within a solid angle $d\omega$ over a wavenumber interval Δn in a direction making an angle γ with the normal to dA. This equivalent surface emission arises from the volume within the annulus contained within the projection of $d\omega$ back through dA. Some of the radiated energy will be absorbed by other annuli along the path and some will escape the arc column

entirely. Then the radiant heat flux emitted at one annulus surface and reaching some other surface inside or outside the arc is given by

$$d^2q = I_B \epsilon \tau \cos\gamma \, d\omega \, dA \tag{2.2}$$

where I_B is black body intensity, ϵ is equivalent surface emissivity and τ is transmissivity along the path.

Black body radiant intensity within a particular wave number interval can be written as

$$I_B = \frac{\sigma T^4}{\pi} \left[D(n) - D(n + \Delta n) \right] \tag{2.3}$$

where

$$D = \frac{\int_n^\infty W_{B,n} \, dn}{\int_o^\infty W_{B,n} \, dn} = \frac{\int_n^\infty W_{B,n} \, dn}{\sigma T^4} \tag{2.4}$$

and D is conveniently expressed for computer calculation as (Pi. 1),

$$D \cong 1 - \frac{15}{\pi^4} v^3 \left(\frac{1}{3} - \frac{v}{8} + \frac{v^2}{60} - \frac{v^4}{5040} + \frac{v^6}{272160} \right) \tag{2.5}$$

$$v \leq 1$$

$$D \cong \frac{15}{\pi^4} \sum_{m=1}^{4} \frac{e^{-mv}}{m^4} \left(\left(\left(mv+3 \right) mv+6 \right) mv+6 \right)$$

$$v > 1 \tag{2.6}$$

$$v = \frac{h\nu}{k_B T} \tag{2.7}$$

Referring to Fig. 1, the solid angle subtended along a typical path is

$$d\omega = (R/L)\ d\theta\ d\Phi = \sin\theta\, d\theta\, d\Phi \tag{2.8}$$

also

$$\cos\gamma = \sin\theta \cos\Phi \tag{2.9}$$

The radius of the cylindrical emitting surface, Fig. 2, is r_j so, by symmetry

$$dA = 2\pi\, r_j\, dz \tag{2.10}$$

Transmissivity along the path length L is

$$\tau_n = e^{-\int_o^L k dl} \tag{2.11}$$

where subscript n denotes wavenumber dependence, so, using Eq. (2.1)

$$\tau_n = e^{-(\overline{kR})_t / \sin\theta} \tag{2.12}$$

The subscript t on $(\overline{kR})_t$ refers to the transmission path. Frequency dependence is understood but not explicitly indicated.

Emissivity at the radiating surface, dA, is computed in an analagous way except that the absorption length is replaced by an emission length, the dashed and solid lines respectively in Figure. 2.

$$\epsilon_n = 1 - e^{-(\overline{kR})_e / \sin\theta} \tag{2.13}$$

Eq. (2.2) can now be rewritten in terms of radiant flux per unit arc column length as

$$d\left[\frac{d\,q}{d\,z}\right]_{\Delta n} = \frac{\sigma\,T^4}{\pi}\left[D(n) - D(n+\Delta n)\right]\left[1 - e^{-(\overline{kR})_e / \sin\theta}\right]\left[e^{-(\overline{kR})_t / \sin\theta}\right]\left[\sin^2\theta\, d\theta \cos\Phi d\,\theta\right]\left[2\pi r_j\right] \tag{2.14}$$

Absorption and transmission lengths are assumed constant within each sector, $\Delta\Phi$, so that Eq. (2.14) can be integrated over Φ and θ separately, with a factor of 4 arising because the integration is, by symmetry, over 1/4 the solid angle.

$$\left(q/z\right)^t_{\Delta n,\Delta\Phi} = 2\pi r_j \sigma T^4 \left[D(n) - D(n+\Delta n)\right]\left[\sin\left(\Phi + \frac{\Delta\Phi}{2}\right) - \sin\left(\Phi - \frac{\Delta\Phi}{2}\right)\right]$$

$$\frac{4}{\pi}\left[\int_o^{\pi/2} e^{-(\overline{kR})_t / \sin\theta} \sin^2\theta\, d\theta - \int_o^{\pi/2} e^{-\left[(\overline{kR})_t + (\overline{kR})_e\right] / \sin\theta} \sin^2\theta\, d\theta\right] \tag{2.15}$$

The symbol (q/z) refers to radiant flux per unit length of arc. Superscripts t, e, a will specify transmitted, emitted and absorbed respectively.

The remaining integrals are functions of optical depth, not integrable analytically but identical in form

$$f(x) = \frac{4}{\pi}\int_o^{\pi/2} e^{-x/\sin\theta} \sin^2\theta\, d\,\theta \tag{2.16}$$

A numerical integration has been performed and a table of differences prepared so that the function can be evaluated simply for any x, see Appendix A.

Defining a transmission function in terms of Eq. (2.16)

$$g = f\left[(\overline{kR})_t\right] - f\left[(\overline{kR})_t + (\overline{kR})_e\right] \tag{2.17}$$

Equation (2.15) becomes

$$(q/z)^{t}_{\Delta n, \Delta \Phi} = 2\pi\, r_j \sigma\, T^4 \left[D(n) - D(n + \Delta n)\right] \left[\sin\left(\Phi + \frac{\Delta\Phi}{2}\right) - \sin\left(\Phi - \frac{\Delta\Phi}{2}\right)\right] g \tag{2.18}$$

2.3 SECTOR RADII

Approximation of absorbing or emitting volumes as sectors of cylinders (Fig. 2) requires calculation of the radial distance from each annulus boundary surface to every annulus boundary surface between it and the outer surface of the arc. The distances, measured at angles $0 < \Phi < \pi/2$ from the normal to the surface, are referred to as sector radii. Surfaces are numbered through the arc from 1 to 2 N, where N is the total number of annuli including the core. Sector radii are then assigned a triple subscript denoting: 1) the number, j, of the originating surface; 2) the number, q, of the terminating surface; 3) an index m on angle Φ. Examples are shown in Fig. 3 for the case N = 3.

It should be noted that:

1) The number j is never less than q, and when q = j, R = 0.

2) The annulus radii r_i and r_{2N+1-i} are equal. They will be referred to as complements and denoted by primes. (e.g. if N = 3, $r_2 \equiv r_5'$ and $r_5 \equiv r_2'$).

3) Physical properties and radiant emission of an annulus are referred to by the subscript of the equivalent emitting surface, so that $(q/z)_i$ and $(q/z)_{2N-i}$ refer to the same annulus and are eventually combined. (e.g. if N = 3, $T_2 \equiv T_4$ and $k_{n,1} \equiv k_{n,5}$)

4) With s the number of sectors into which the quadrant $0 \leq \Phi \leq \pi/2$ is divided, and therefore also the number of angles at which sector radii are computed,

$$\Delta\Phi = \pi/2s \tag{2.19}$$

and, with $1 \leq m \leq s$

$$\Phi_m = \left(m - \frac{1}{2}\right) \Delta\Phi \tag{2.20}$$

$$\int_{\Phi_m - \frac{\Delta\Phi}{2}}^{\Phi_m + \frac{\Delta\Phi}{2}} \cos\Phi\, d\Phi = \sin(m\,\Delta\Phi) - \sin[(m-1)\,\Delta\Phi] \tag{2.21}$$

Trigonometry for typical sector radii is shown in Fig. 4 for the three possible relationships between j, q and N. For convenience in calculating the sector radii, an angle α measured from the outward normal of the boundary surface is defined such that

$$\begin{aligned} \Phi &= \alpha & \alpha &\leq \pi/2 \\ \Phi &= \pi - \alpha & \alpha &\geq \pi/2 \end{aligned} \tag{2.22}$$

For either Fig. 4a or 4b the sector radius is related to the radii of the originating and terminating boundaries by

$$\left(R_{jqm} \cos\alpha + r_j\right)^2 + \left(R_{jqm} \sin\alpha\right)^2 = r_q^2 \tag{2.23}$$

The sector radius is then given by

$$R_{jqm} = -r_j \cos\alpha + \sqrt{r_j^2 \cos^2\alpha + (r_q^2 - r_j^2)} \qquad q \leq N$$

$$R_{jqm} = -r_j \cos\alpha - \sqrt{r_j^2 \cos^2\alpha + (r_q^2 - r_j^2)} \qquad q > N \tag{2.24}$$

with the condition that

$$r_q \geq r_j \sin\alpha \tag{2.25}$$

If condition (2.25) is not met, the sector radius does not exist for that combination of j, q and m. (e.g., Fig. 3, R_{542} does not exist. This means that the radius of surface q is too small for the path originating at surface j at angle Φ_m to intersect. When this situation occurs, appropriate deletions must be made from the summation equations to follow.

2.4 RADIANT INTERCHANGE SUMMATION EQUATIONS

In terms of sector radii and the appropriate (frequency dependent) absorption coefficients, the transmission functions, Eq. (2.17), become

$$g_{jqm} = f\left[(\overline{k}\,\overline{R})_{jqm}\right] - f\left[(\overline{k}\,\overline{R})_{jqm} - (\overline{k}\,\overline{R})_{j'qm}\right] \tag{2.26}$$

where

$$(\overline{k\,R})_{jqm} = \sum_{i=q}^{j-1} k_i \left(R_{jim} - R_{j,\,i+1,\,m}\right) \tag{2.27}$$

Emission lengths, $(\overline{k\,R})_{j'qm}$ are computed using the shortest existing complementary sector radius, either $R_{j',j'-1,m}$ or $R_{j'jm}$. For example, referring to Fig. 3 emission length for radiation along sector radius R_{522} is computed using R_{212} $(j=5\,,\ j'=2,\ j'-1=1,\ m=2)$.

Energy emitted by an annulus is just the special case of zero transmission length, for which Eq. (2.26) reduces to

$$g_{j\,j\,m} = 1 - f\left[(\overline{k\,R})_{j'qm}\right] \tag{2.28}$$

and, within a particular frequency interval, radiant emission per unit length from each surface, j, is

$$(q/z)^e_j = 2\pi\sigma T_j^4 r_j \left[D(n) - D(n+\Delta n)\right] \sum_{m=1}^{s} \left\{\sin(m\Delta\Phi) - \sin\left[(m-1)\Delta\Phi\right]\right\}\left[g_{j\,j\,m}\right] \tag{2.29}$$

Total emission from any annulus is found by adding together results for the j and 2N-j surfaces (the "exterior" and "interior" surfaces of the annulus)

$$(q/z)^e_i = \sum_n \left[(q/z)^e_{j=i} + (q/z)^e_{j=2N-i}\right]\left[D(n) - D(n+\Delta n)\right] \qquad 1 \leq i \leq N-1 \tag{2.30a}$$

$$(q/z)^e_n = \sum_n (q/z)^e_{j=N}\left[D(n) - D(n+\Delta n)\right] \tag{2.30b}$$

Frequency summation is over those wavenumbers, indexed by n, which are included within the limits $.2 \leq h\nu/k_B T_j \leq 15$.

These expressions for radiant emission per unit length include self-absorption within the emitting annulus. In the limiting case where an individual annulus reaches the back body limit within a particular frequency interval, the function $g_{j\,j\,m}$ becomes unity in that interval for all m and Eq. (2.29) reduces to the back body emission of a cylindrical surface of circumference $2\pi r_j$.

Radiant energy emitted at one annulus and absorbed by another annulus is computed as the difference between energy transmitted to and through the annulus. Absorption between surface q and surface q + 1 of emission from all surfaces j is thus

$$\left(q/z\right)_q^a = \sigma \left[D(n) - D(n + \Delta n)\right] \sum_{j=q+1}^{2N-1} T_j^4 r_j \sum_{m=1}^{s} \left\{ \left(g_{j,\, q+1,\, m} - g_{jqm}\right) \left[\sin m\Delta\Phi - \sin (m-1)\Delta\Phi \right] \right\} \tag{2.31}$$

Total absorption, by any annulus, of emission from all other annuli, analagous to Eqs. (2.30), is

$$(q/z)_i^a = \sum_n \left[(q/z)_{q=i}^a + (q/z)_{q=2N-i}^a \right] \left[D(n) - D(n + \Delta n)\right] \qquad 1 \leq i \leq N-1 \tag{2.32a}$$

$$(q/z)_N^a = \sum_n (q/z)_{q=N}^a \left[D(n) - D(n + \Delta n) \right] \tag{2.32b}$$

The net radiation from each annulus can be positive or negative and is given by

$$(q/z)_i^{rad} = (q/z)_i^e - (q/z)_i^a \tag{2.33}$$

and finally, the radiant flux per unit length which reaches the outside surface of the arc is given by

$$(q/z)^{rad} = \sum_{i=1}^{N} (q/z)_i^{net} \tag{2.34}$$

The above procedure is a massive sorting and summing job ideally suited for a digital computer. The fact that not all transmission paths intersect all annuli results in the absence of some terms in the above equations. These omissions have not been indicated explicitly but are taken care of in the scheme for indexing the summation loops of the computer program called ARCRAD III. Details of this program, including a Fortran listing, will be found in Appendix B.

2.5 TWO ZONE ARC MODEL

Application of the foregoing radiant interchange equations to a specific arc requires additional information and boundary conditions. If the temperature profile is known by direct measurement, then ARCRAD III can be used to compute radiant interchange, and existing information on transport properties employed to calculate voltage gradients, current and power dissipation in the arc, for comparison with measurements of these parameters. If the temperature profile is unknown, then one might hope to establish it from known boundary conditions supplemented by measurements of electrical characteristics.

Both radiant intensity and electrical conductivity in air change very rapidly with temperature, so that the lower temperature, outer part of, the arc contributes relatively little, either to power dissipation or to radiant emission. Also, the accurate determination of temperature profiles in the outer region is very difficult. For these reasons the arc is divided into two zones - interior (Zone I) and exterior (Zone II).

In Zone I, once the temperature profile has been established, as discussed below, the annulus boundaries are so determined that the weighted average temperature of each annulus is a multiple of $1000^{\circ}K$. This procedure results in a representative but tractable number of annuli and eliminates the need for temperature interpolation of absorption coefficent data. It is further discussed in Appendix C.

In Zone II, the profile is assumed linear and the boundaries of annulus i set at radii corresponding to $T_i \pm 500^{\circ}K$, where T_i is a multiple of $1000^{\circ}K$ greater than or equal to $3000^{\circ}K$. The outermost annulus includes the temperature range from $2500^{\circ}K$ down to wall temperature. Molecular absorption of vacuum uv radiation is the only significant radiation effect below $2500^{\circ}K$ and calculation of absorption coefficients for this annulus is a special case, also treated in Appendix C. Inclusion of Zone II in the radiant emission-absorption calculation changes the Zone I results by less than 1%. However, the vacuum u.v. absorption in Zone II is strong enough in most cases to prevent any of this radiation from reaching the wall (see Section 7.3).

2.5.1 Temperature Profile

An analytic expression for temperature profile in which the fullness of the profile is governed by a single parameter is

$$\frac{T - T_a}{T_{CL} - T_a} = 1 - \left(\frac{r}{r_a}\right)^x \qquad (2.35)$$

For any x greater than 1.0 this equation satisfies the basic condition of zero slope at the centerline and generates a family of curves ranging from essentially linear variation with radius ($x \tilde{=} 1$), to uniform temperature ($x \rightarrow \infty$).

The value of x which most closely maintains voltage gradient constant in the radial direction was the criterion which we used to compute profile shape. However, both radiant emission and thermal conduction change very rapidly with temperature, and computed voltage gradient is very sensitive to these, so no clear cut values of x could be established without some guidance from experimental measurements. Experimental temperature data were fitted to Eq. (2.35) using a standard least squares technique (Sb. 1). Application of the least squares criterion to Eq. (2.35) yields

$$x = \frac{\sum_{i=1}^{k} \left(\ln \frac{r_i}{r_a}\right) \left[\ln \left(1 - \frac{T_i - T_A}{T_{CL} - T_A}\right)\right]}{\sum_{i=1}^{k} \left(\ln \frac{r_i}{r_a}\right)^2} \qquad (r_i > 0) \qquad (2.36)$$

$$\sigma_{SD} = \sqrt{\frac{1}{k} \sum_{i=1}^{k} \left[x \ln \frac{r_i}{r_a} - \ln \left(1 - \frac{T_i - T_A}{T_{CL} - T_A}\right)\right]^2} \qquad (2.37)$$

where k is the number of data points (r_i, T_i), σ_{SD} is the standard deviation and T_a was chosen to minimize σ_{SD}.

2.5.2 Thermal Conduction

In the inner zone of a high pressure arc, where practically all the electrical dissipation takes place, energy loss is predominantly by radiation, so a relatively simple approximation was used to estimate thermal conduction. In the outer zone, radial conduction and absorption of vacuum u.v. radiation from Zone I are assumed to be the dominant modes of energy transfer.

The arc is assumed to be steady and cylindrically symmetric with no flow so that the Heller-Elenbaas equation (Sk. 1) is satisfied. This equation can be written in terms of enthalpy gradient as

$$\frac{1}{r} \frac{d}{dr} \left(r \frac{k}{c_p} \frac{dh}{dr}\right) + P = 0 \qquad (2.38)$$

where P is net power into a unit volume due to the combined effects of

electrical dissipation and radiation. Note P is positive when radiant absorption exceeds emission even if electrical dissipation is negligible.

Weber (We. 1, We. 2) has correlated the ratio k_A / c_p as a function of enthalpy (Fig. 5) in the form

$$k_A / c_p = C\, h^{0.5} \tag{2.39}$$

He has also pointed out that by defining a function

$$\xi = C\, h^{1.5} \tag{2.40}$$

one can simplify the first term of Eq. (2.38). Applying this transformation

$$\frac{1}{r}\,\frac{d}{dr}\left(r\,\frac{d\xi}{dr}\right) + 1.5\,P = 0 \tag{2.41}$$

In Zone II the boundary conditions are

$$r = r_w \qquad h \cong 0$$

$$r = r_a \qquad h = h_a$$

When P is constant, Eq. (2.41) yields an enthalpy profile for Zone II

$$\frac{h}{h_a} = \left\{ \frac{\ln\left(\frac{r_w}{r}\right)}{\ln\left(\frac{r_w}{r_a}\right)} - \frac{3\,P\,r_a^2}{8\,C\,h^{1.5}} \left[\left(\frac{r^2}{r_a^2} - 1\right) - \left(\frac{r_w^2}{r_a^2} - 1\right) \frac{\ln\left(\frac{r}{r_a}\right)}{\ln\left(\frac{r_w}{r_a}\right)} \right] \right\}^{2/3} \tag{2.42}$$

and an enthalpy gradient at the zone boundary, $r = r_a$

$$\left[\frac{dh}{dr}\right]_{r=r_a} = -\frac{2}{3}\,\frac{h_a}{r_a \ln\left(\frac{r_w}{r_a}\right)} \left\{ 1 - \frac{3}{8}\,\frac{P\,r_a^2}{C\,h_a^{1.5}} \left[\frac{r_w^2}{r_a^2} - 1 - 2\ln\left(\frac{r_w}{r_a}\right) \right] \right\} \tag{2.43}$$

A positive value of P in Zone II tends to reduce the enthalpy gradient at the zone boundary, so, as a first approximation, P was set equal to zero. Conduction heat flux at $r = r_a$ is then given by

$$(q/z)^{cond}_{r=r_a} = \frac{4\pi C h_a^{1.5}}{3 \ln (r_w / r_a)} \tag{2.44}$$

Because the conduction term is relatively small in Zone I, and by symmetry must vanish at r = 0, and also because transport properties in the high temperature zone are ill-defined, heat loss from the arc by conduction in Zone I was assumed to be proportional to $(r/r_a)^2$ rather than make use of the derivative of an empirical temperature profile. For any annulus, i

$$(q/z)^{cond}_i = (q/z)^{cond}_{r=r_a} \left[\left(\frac{r_i}{r_a}\right)^2 - \left(\frac{r_{i+1}}{r_a}\right)^2 \right] \tag{2.45}$$

2.5.3 Electrical Properties

For any annulus, i, the local energy balance is

$$E^2 G_i = \left(\frac{q}{z}\right)^{rad}_i - \left(\frac{q}{z}\right)^{cond}_i \tag{2.46}$$

where $(q/z)^{rad}_i$ is given by Eq. (2.31) and $(q/z)^{cond}_i$ is given by Eq. (2.45). Conductance G_i of an annulus of unit length is defined as

$$G_i = 2\pi \int_{r_{i-1}}^{r_i} \sigma_e \, r dr \tag{2.47}$$

where r_i is the outside radius of the i^{th} annulus counting inward from the arc boundary. Local electrical conductivity σ_e is computed from Weber's correlation (We. 1), Fig. 6.

$$\sigma_1 \text{ [mho/cm]} = 7.35 \times 10^{-9} H^{3.44}$$

$$\sigma_2 \text{ [mho/cm]} = .338 P^{0.22} H^{0.74}$$

$$\text{if } \sigma_1 < \sigma_2 \text{ then } \sigma_e = \sigma_1$$

$$\text{if } \sigma_1 > \sigma_2 \text{ then } \sigma_e = \sigma_2 \tag{2.48}$$

where $H = h/R_g T_o$, $R_g T_o = 7.874 \times 10^8$ cm^2/sec^2, p is measured in atmospheres and local values of enthalpy are obtained from the temperature profile (not the annulus average temperature used for computing radiant interchange).

Equation (2.46) was used to calculate local voltage gradient. Average gradient for Zone I is

$$E_{avg} = \sqrt{\frac{\sum_i E_i^2 G_i}{\sum_i G_i}} = \sqrt{\frac{(q/z)_{r=r_a}^{rad} + (q/z)_{r=r_a}^{cond}}{G}} \tag{2.49}$$

where

$$G = 2\pi \int_o^{r_a} \sigma_e \, r \, dr \tag{2.50}$$

and the weighted rms deviation of local values from E_{avg} is

$$\sigma_{SD,E} = \sqrt{\frac{\sum_i \left(E - E_{avg}\right)^2 G_i}{G}} \tag{2.51}$$

Total current carried by the arc is simply

$$I = G \, E_{avg} \tag{2.52}$$

3. AIR ABSORPTION COEFFICIENTS AND RADIANCE

3.1 DATA SOURCES AND RANGES

Equilibrium radiant emission and absorption in an air plasma is a complex set of phenomena including:

1. Free-free continuum radiation (Bremsstrahlung)
2. Free-bound deionization continua
3. Molecular bands
4. Molecular absorption of vacuum ultraviolet radiation
5. Lines

Items 1, 2, and 3 were included in the calculations of Nardone, Breene, Zeldin and Riethof (Na. 1) which were the source of absorption coefficients used in computations with ARCRAD I (Ma. 1).

As part of this project a revised tabulation of absorption coefficients was undertaken. The tabulation is a composite of information from several sources as shown on Fig. 7. The Nardone, et. al. results were retained at wavenumbers to 59,000 cm^{-1} and below, since they are most complete; but were multiplied by the factor $(1-e^{-h\nu/k_B T})$ to correct for stimulated emission (Sh. 1).

From 59,000 cm^{-1} shown in Fig. 7, the recent results of Sherman and Kulander (Sh. 1) for Free-Bound radiation were used together with Kramer's formula (U. 1) for free-free radiation.

Sherman and Kulander used the more sophisticated "quantum defect" method of Burgess and Seaton (Bg. 1) rather than Breene's hydrogenic model to calculate radiation due to radiative recombination of singly ionized nitrogen and oxygen atoms with electrons, and these are the dominant contributors at high frequencies.

A quantum mechanical correction to Kramer's formula, the Gaunt factor, was assumed to be unity because: 1) Nardone, et. al., used unity in their calculation of Free-Free radiation at low frequency. 2) The number is of order one and some disagreement exists as to whether it is greater or less than one. (No. 1) (Ka. 1).

Molecular absorption in the vacuum ultraviolet was accounted for by averaging the experimental data for molecular absorption collected by Schultze, et. al. (Sc. 1). Molecular absorption takes place at temperatures too low ($T \leq 10,000^{\circ}K$) for equilibrium emission to be significant at high

frequencies, but the absorption process is an important one in that vacuum ultraviolet radiation is blocked from reaching any solid boundary.

The effect of line radiation has not been accounted for in the tabulation of absorption coefficients.

Absorption coefficients on the input data tape are tabulated at 75 wavenumbers, equally spaced to 13,000 cm^{-1} and, from there to 200,000 cm^{-1}, at spacings chosen by Sherman and Kulander to be close together where absorption edges cause sharp changes in k and widely separated where changes in k are gradual. Values are averages over the interval between the tabulated wavenumber and the next higher tabulated wavenumber.

The data of Nardone were available at decade intervals of log density ratio, and that of Sherman and Kulander on a per particle basis. Tabulation for this project was by both density and pressure using equilibrium thermodynamic data of Browne (B.1). Density range was from 10^{-3} to 10^{2} ρ/ρ_o and pressures tabulated were 1, 5, 10, 30, 50, 100, 150, 200 and 300 atmospheres. Temperature range was from 3000°K to 20,000°K at 1000° intervals with an additional tabulation, at 273°K, of molecular absorption data in the vacuum ultraviolet.

Fig. 8 is a sample plot of k for several temperatures with p = 100 atmospheres.

3.2 INTEGRAL RESULTS

Condensation of the enormous amount of data represented by frequency, temperature and pressure or density dependent absorption coefficients is highly desirable. This can be done by summing over all frequency intervals, but such summations must be treated with care because any effort to include self-absorption must inevitably be associated with a specific geometry.

Several such summations have been performed with the data assembled for this project, as follows:

1) Radiance from an infinitesimal volume element (watts/cm^3-ster);

$$J_{thin} = \frac{\sigma T^4}{\pi} \sum_n k_n \left[D(n) - D(n + \Delta n) \right] \tag{3.1}$$

This form is independent of geometry but is not black body limited and is thus applicable only when the gas is optically thin at <u>all</u> frequencies. Figure 9 is a plot of summation Eq. (3.1), for p = 200 atm, T = 15,000°K, and gives an indication of the relative importance of any wavenumber interval.

TABLE 3.1
COMPARISON OF RADIANCE VALUES

Pressure (atm)	Temperature (°K)	This report, composite J_{thin} (kw/cm^3-ster)	This report, composite J_{thick} L = 1 cm (kw/cm^2-ster)	Breene and Nardone* (Na. 1) J_{thin} (kw/cm^3-ster)	Breene and Nardone* (Na. 1) J_{thick} L = 1 cm (kw/cm^2-ster)	Yos ** (Yo. 1) J_{thin} (kw/cm^3-ster)	Biberman*** (Bi. 1) J_{thick} L = 1 cm (kw/cm^2-ster)
1	12000	.100	.080	.202	.140	.06	.49
	14000	.495	.379	1.26	.743	.35	2.22
	17000	.924	.858	-	-	.66	4.85
10	12000	1.22	.625	2.47	.771	.86	1.76
	14000	8.81	3.25	21.3	4.12	7.3	6.45
	17000	35.13	13.96	-	-	35.	28.8
100	12000	18.2	6.37	27.1	6.19	-	-
	14000	109.2	22.9	249.	26.4	-	45.0
	17000	656.	78.9	-	-	-	90.7

* not corrected for stimulated emission factor $(1-e^{-(h\nu/k_B T)})$

** from curves of radiated power

*** from tabulation of equivalent surface emissivities

Yos (Yo. 1) presents the results of his calculations as total radiated power per unit volume, i.e., $4 \pi J_{thin}$, Table 3.1.

2) Radiance from a slab of unit thickness (watts/cm^2-ster, L = 1cm);

$$J_{thick} = \frac{\sigma T^4}{\pi} \sum_n \left(1 - e^{-k_n L}\right) [\, D(n) - D(n + \Delta n) \,] \tag{3.2}$$

Radiance is tied to the doubly infinite slab geometry and reduces to black body intensity, $\sigma T^4/\pi$, in the limit when $kL >> 1$ at all frequencies. As long as $kL >> 1$ the magnitude of L is irrelevant and the units of J_{thick} are watts/cm^2-ster). When $kL << 1$ at all frequencies, radiated power is proportional to slab thickness, L, and J_{thick} is identical to J_{thin} in magnitude and units. Nardone, et.al. (Na. 1) present their integrated results as radiance from a slab and this form can also be related to results of Biberman, et.al. (Bi. 1), who tabulate equivalent surface emissivities for a slab, Table 3.1.

3) Radiant Flux density at the surface of an optically thin, uniform temperature, infinite cylinder (watts/cm^2);

$$(q/A)_{thin} = 4 \pi J_{thin} \left(\frac{\text{Volume}}{\text{Surface}}\right) = 2 \pi r_a J_{thin} \tag{3.3}$$

This is simply the application of J_{thin} to the infinite cylinder geometry.

4) Radiant flux density at the surface of an optically thick uniform temperature infinite cylinder (watts/cm^2);

$$(q/A)_{thick} = \sigma T^4 \sum_n \left(1 - e^{-1.9 k_n r_a}\right) [\, D(n) - D(n + \Delta n) \,] \tag{3.4}$$

Here the mean beam length concept (Ec. 1) has been applied to calculate the equivalent surface emissivities of the cylindrical volume and thus account for self-absorption. Figure 10 shows curves of $(q/A)_{thick}$ at 1, 10, 100, and 300 atmospheres for $.05 \leq r \leq 1.0$ (cm) and $7000 \leq 20{,}000^\circ K$.

In Fig. 11 the ratios $(q/A)_{thin} / (q/A)_{thick}$ and $(q/A)_{thick} / \sigma T^4$ are plotted as a function of pressure, for a temperature-radius combination typical of experimental observations at 100 atmospheres, to illustrate the significance of self-absorption in arcs. The small arc radius encountered at 100 atmospheres tends to reduce optical depth. Thus self-absorption, while significant is not overwhelming, as shown by the ratio $(q/A)_{thin} / (q/A)_{thick}$ when radiation at wavenumbers up to 59,000 cm^{-1} is considered.

However, when vacuum ultra-violet radiation is included, self absorption is very important.

Now let us compare $(q/A)_{thick}$ to the black body limit. As pressure increases, the vacuum u.v. appears less important because, having reached black body maximum at low pressure, its relative contribution decreases as low frequency radiation becomes stronger.

4. EXPERIMENTAL APPARATUS

Our experimental efforts to operate and make useful measurements on high pressure electric arcs operating in air were directed toward achieving steady state arcs while depending on the transient characteristics of a capacitor power supply and an uncooled constrictor. This permitted simplicity and flexibility in apparatus design but required fast response instrumentation, both to ascertain if, when and for how long a steady arc was established, and to make useful measurements within the steady period. Figures 12 and 13 are photographs of the setup.

Figure 14 is a schematic which shows the principles of operation. Time resolving element for the temperature measurements is a rotating mirror M_1, on which light from the arc is focused by lens L_1. From the mirror the light falls on lens L_2 and is then focused on the slit S_1 of a spectrograph. Another light beam from the arc is focused by lens L_3 on slit S_2 of the drum camera, which provides a simultaneous record of arc stability. The electrical and electronic setup for the generation of the high current pulse and for the proper synchronization of the measurements is also indicated in Fig. 14. Details of all the experimental equipment and its operation are discussed below.

4.1 ARC CONSTRICTOR CONFIGURATIONS

4.1.1 Design Principles

Quantitative information as to plasma properties can best be gained with simple arcing devices, specifically, cylindrically symmetric ones without flow. A particularly successful arc constrictor, in which cylindrical arcs have been operated for long periods of time, is the so called cascade type or Maecker arc. (M.1, M.2). This constrictor consists essentially of a stack of mutually insulated, water-cooled, copper discs with a central circular hole for the arc. The principal limit of this device appears to be a maximum acceptable steady state wall heat flux of the order of 10 KW/cm^2 of wall surface, (Co.1, Cu.1, Ga.1). Unfortunately this number is too small to operate high current arcs in the 100 atm range, where radiative losses can reach values which are 10 or even 100 times as high. There was hope, however, that the excellent properties of the Maecker arc could be retained by operating on a transient rather than on a steady state basis. Then the copper walls could be used as a heat sink and the arc switched off before melting occurred. Figure 15 shows the result of a rough calculation of the maximum permissible operational time of such a constrictor, using conventional heat transfer calculation technique (Ca.1). The copper walls can be expected to absorb heat flux densities of 100 KW/cm^2 for about 1 millisecond and this pair of parameters was attractive enough to warrant a further study of such a device.

A second, quite different, solution for a cylindrical arc constrictor which can be operated at very high radial heat flux densities, is the ablation type arc (A. 1, Bu. 1, Fr. 1, Og. 1). This is a constrictor in which the fluid or solid walls evaporate by the heat from the arc. If proper precautions are taken, the arc then burns in the ensuing radially symmetric flow field. From a theoretical point of view this device is not as simple as the cascade type constrictor when the latter is operated with no flow. However, the flow field of an ablation type arc is well defined and it appears that a number of arc properties, especially radiation, can be studied conveniently. Moreover, a recent theoretical treatment of this arc type opens the road further for experimental work (Sm. 1). We have built both types of constrictors for the purpose of investigating high current air arcs in the 100 atm range, but most of our work to date has been done on the cascade arc.

4.1.2 The Heat Sink Type Cascade Constrictor

To avoid shorting of the arc at the high electrical gradients encountered (about 200 v/cm) the copper disc elements of the cascade constrictor must be thin. The discs used are 20 mil (1/2 mm) thick solid copper with a central hole 2.0, 2.5 or 5.0 mm diameter. They are each separated by a 20 mil air gap and held by two thin ribs of Plexiglas to which they are glued, Figs. 16 and 17. During the assembly operation the discs and electrodes are aligned by a steel rod through the constrictor holes. The length of the cascade type arc constrictor is 7 cm, thus ℓ/d is about 28. As can be seen from Fig. 17, the copper constrictor is radially open, permitting a fast initial expansion of the arc plasma after ignition. This initial flow phenomenon was the slowest transient process in the arc and in a radially closed constrictor lasted several milliseconds, which was much too long for our purpose.

Elimination of water cooling has several important advantages. It constitutes a remarkable saving in design and operation, permitting economical experimentation with a large number of modifications to constrictor diameter and thickness and to spacing of the discs. Also, frequent mishaps such as melting of the copper discs by faulty arc operation can be borne philosophically. Another advantage of the omission of water cooling is the convenient accessibility of the arc for optical observations. This helped immeasurably when arc stability was being studied with high speed photographic techniques.

Arc electrodes are made of graphite. They are held centered by a thicker copper washer at a distance of 60 mils from the first copper disc of the cascade. For additional support, and to aid in obtaining a good electrical contact between the graphite electrodes and the power supply leads, the rather light constrictor cage was mounted in a strong Plexiglas holder with two copper end caps, in which the graphite electrodes were held smoothly but tightly, Figs. 16 and 17. The Plexiglas holder fits into the pressure vessel described in a later section.

To improve the optical quality of the spectroscopic measurements, the two central elements of the constrictor were modified considerably from those described above, Fig. 17. They were cut to a rather long, nearly rectangular shape with two additional tapers designed to minimize stray light entering the optical system from the highly reflecting copper walls. The special constrictor elements also permitted the use of a rather large aperture for the optics, which helped in obtaining a high time resolution with the photographic spectroscopic technique.

Special precautions had to be taken with the copper discs to prevent arc contamination. The punchings as delivered by the manufacturer had loose particles and small greenish crystals on the surface of the hole. Also, a burr of rather loose copper material was apparently unavoidable, Figure 18. The situation grew worse when the die used for punching lost it sharpness. Loose crystals and copper particles will naturally evaporate much more rapidly when exposed to the arc than indicated by Figure 15. Copper vapor will then enter the arc in uncontrolled amounts, possibly affecting electrical conductivity and radiation, and/or giving rise to local unsymmetric blowing which may cause arc instabilities. To avoid these effects, all copper discs were carefully degreased and then chemically etched. This process removed the loose particles along with about 2 mil of the copper surface, Fig. 18.

Placing of the fuse wire for arc ignition in the copper constrictor was an important and rather time consuming operation. To minimize contamination, tungsten wires as thin as 1/2 mil (0.0005") were used. For maximum arc stability these had to be strung straight, and accurately centered, in the little cascade. This was achieved by replacing the two graphite electrodes having a central hole the same diameter as the copper discs, which were used for alignment, by two others with a tiny central hole. Through this hole the 1/2 mil tungsten wire was strung and held taut by little blobs of putty, hung on its ends. Then the wire was fixed at the ends of the electrodes with two more little blobs of putty.

To further reduce tungsten contamination of the arc, 1/4 mil diameter wire was tried. This, however, proved to be such a tedious task that it was abandoned.

A good indication of successful (i.e. reasonably stable) operation of the arc was the state of the copper constrictor after arc firing. Symmetrically burning arcs did not melt copper; unsymmetric arcs burned the discs badly, Fig. 19.

4.1.3 The Ablation Type Constrictor

An ablation type constrictor was also built for some exploratory tests of arc stability. To check on stability, complete visibility of the arc is

advantageous and therefore Plexiglas was used. The internal diameter of the Plexiglas tube was 3 mm and its length 3 cm. In the form shown in Figs. 16 and 17, without the use of special windows to exclude the lens action of the Plexiglas tube, the assembly of the constrictor was very simple. Operation was also simplified by the radial gas flow from the walls which automatically centered and stabilized the arc so that location of the ignition wire was not critical.

4.2 HIGH PRESSURE TEST APPARATUS

The arc constrictors were placed in a strong Plexiglas holder, and this was mounted in an aluminum pressure vessel, Figs. 20 and 21, capable of withstanding at least 5000 psi. The pressure vessel consists essentially of an aluminum block, into which several openings are drilled. First, there is a large central hole for the mounting of the Plexiglas holder with the arc constrictor. The block also has two rectangular holes which are used for arc observation, and optical measurements. Finally, there are two more small round holes for auxiliary purposes such as locating the over-pressure relief membrane. Caps for all holes were sealed with O-rings.

Flow of electric current inside the pressure chamber is schematically indicated by Fig. 22a. The vessel is grounded and provides a return path for the current. This helps to symmetrize the magnetic field lines and thus avoid unsymmetric magnetic forces on the arc. To further reduce stray light, two apertures were mounted in each of the light paths before the large windows, Fig. 22b.

4.3 POWER SUPPLY

Power is supplied to the arc by a 20 KV, 360 μf capacitor bank. A nearly rectangular current pulse is produced by a network of capacitors, inductors and resistors. Essentially three parallel circuits are used, Fig. 14; a weakly damped LC circuit, an RC circuit and a strongly damped LC circuit with about three times the frequency of the first one. The currents of the individual circuits and their composite are shown in Fig. 23, which also illustrates the flatness of the current pulse. Arc resistance has some effect, but resulting deformation of the current pulse is corrected by small adjustments in the circuit components.

The pulse is triggered by the rotating mirror which also provides the time resolution for the spectroscopic measurements so a rapid and precisely timed start of the current must be ensured. This is done with a

tri-electrode spark gap, G1 (Fig. 14) fired at a pre-determined position of the rotating mirror. The trigger pulse is initiated by a light beam reflected from the mirror to a light sensitive transistor. The transistor in turn discharges a capacitor through the primary winding of a pulse transformer, delivering a steep pulse of about 10 KV peak voltage.

To limit the dissipation of arc energy in the constrictor, a second spark gap, G2 is used to terminate the current pulse. This gap works under rather unusual conditions (Fig. 14). It must withstand high transient voltages which occur both at the time of ignition of gap G1, and during the subsequent explosion of the tungsten fuse wire. Later the gap must break down with only a limited voltage supplied to its electrodes. Therefore, a special trigger gap was built, Fig. 24, with a separate energy supply to a fourth electrode which generates additional plasma for the breakdown of the gap. The design of the 4 electrode gap is shown schematically in Figure 24. Between the usual insulated central trigger electrode E3, and the graphite electrode E2, a fourth concentric electrode E4 is mounted, slightly recessed into the Delrin insulator. The four electrode gap operates as follows:

When the initial trigger spark flashes from E3 to E2, the path between electrode E4 and E2 also breaks down, discharging the capacitor C. This discharge creates a plasma jet by evaporating material from the narrow slot of Delrin. The plasma jet is directed towards E1 and assists greatly in breaking down the path between E1 and E2, even when only a small voltage difference exists between these electrodes.

4.4 INSTRUMENTATION

4.4.1 Electrical

The arc current was measured with a coaxial shunt having a time constant of 2.4 nanoseconds, a resistance of 0.01 ohm and an I^2 Rt value of 500 joules. Arc voltages were measured with Tektronix high voltage probes which have a band width from DC to 10 M Hz.

All electrical measurements were monitored with Tektronix oscilloscopes model #551 or #502A. The 502A instrument was used for the heat flux measurements with thermocouples, which required only low time resolution, but high sensitivity.

4.4.2 High Speed Photography

Arc stability problems were investigated with the Beckman & Whitley high speed cameras models 326 (Dynafax) and 307. The Dynafax is a framing camera with a maximum framing rate of 26,000 pps and exposure

times down to about 1 microsecond. The 307 is a drum camera producing "smear" pictures with a time resolution as short as 100 nanoseconds. For this project both cameras were used only at intermediate speeds, often simultaneously with good success.

4.4.3 Time Resolved Spectrograph

Our basic spectrograph was the Hilger medium glass instrument. The dispersion of this instrument in the near infrared spectrum is only about 100 Å/mm but this is sufficient to resolve the strongly broadened infrared lines of oxygen and nitrogen and to observe the effect of self-absorption on the oxygen 7772-7775 Å triplet. Time resolution for our spectral measurements was achieved by the use of a mirror, Fig. 14, rotating at 135 revolutions/sec. Timing of the spectroscopic picture within the duration of the power current pulse was controlled by an electronic delay and was usually chosen to be near the end of the pulse. In the optical system between arc and spectrograph two Kodak lenses designed for aerial cameras were used. Because of the limited aperture of the spectrograph (f:12), they were stopped down to a fraction of their maximum aperture. The optical system clearly resolved a 1/2 mil tungsten ignition wire on the slit of the spectrograph.

Spectra were recorded on Kodak IN plates, which are sensitive up to 9000 Å, and developed for 5 minutes in 1:1 Kodak Dektol developer. The unusually long developing time resulted in high contrast plates, but it enabled us to photograph the spectrum of the carbon standard with the same exposure time as the air arc by using a larger spectrograph slit width. The high-pressure air arcs were photographed with a slit width of .025 mm or .050 mm and the carbon-standard needed a .600 mm wide slit.

Intensity steps for the absolute measurements of arc brilliancy were generated by geometrical apertures placed in the spectrograph between the first lens and the prism in the parallel light beam. They were made rectangular with a variable height, h, and a constant width, b, Fig. 25. Because it leaves the base of the prism unchanged, this procedure does not impair spectral resolution.

The carbon crater of McPherson (Mc. 1) was used as an intensity standard. There is some conflict between Euler's (Eu. 1) data from this standard and that of Null and Lozier (Nu. 1), which are the two best known sources. We have plotted both sets of data in Fig. 26. Euler's curve was calculated using his crater temperature of 3995°K, his absorption coefficients as listed in Table 4.1, and the black body brilliancies of Pivovonski and Nagel (Pi. 1). Null and Lozier's curve was obtained using their value of 3800°K for crater temperature and a constant absorption coefficient of 0.98. Null and Lozier's

TABLE 4.1
WAVELENGTH DEPENDENCY OF CARBON CRATER INTENSITY

λ (Microns)	2500	3000	4000	5000	6000	7000	8000	9000	10,000
α (Eucler)	0.706	0.718	0.736	0.748	0.756	0.763	0.767	0.772	0.776
I(erg/cm^2 -Å-ster)									
(Euler)	4.81^3	2.16^4	1.06^5	2.13^5	2.88^5	3.18^5	3.13^5	2.91^5	2.60^5
(Null & Lozier)	3.19^3	1.60^4	8.88^4	1.93^5	2.74^5	3.14^5	3.17^5	3.00^5	2.72^5

values are also included in Table 4.1. The brilliancy values disagree considerably in the ultra-violet and in the blue region of the spectrum but agree very closely in the vicinity of 8330 Å where we have measured continuum intensities.

Carbon crater intensity was recorded by removing the high pressure arc assembly and locating the carbon crater in exactly the same position. Except for the slit width of the spectrograph and the aperture before the prism, the optical system was unchanged. However, the crater is viewed directly, while the air arc is seen through a Plexiglas window in the high pressure vessel so the transmission of this window (calculated to be 90%) was taken into account in our evaluations. The crater was operated closely to its hissing current and in a 90° mounting.

4.4.4 Total Radiation Calorimeter

The calorimeter developed for total radiant heat flux measurement is shown in Figs. 27 and 28. The unit is a temperature sensing element surrounded by insulation, except for the surface exposed to the arc, and sandwiched between two copper discs of the type used to make up the remainder of the arc cage so that the calorimeter could be installed as an integral part of the arc cage. The sensing element is a copper ring, to which is welded a copper-constantan thermocouple.

As indicated in Fig. 28, three designs were built. The first two were to determine the relative effect of dishing the copper disc covers. The third represented an attempt to increase surface absorption and reduce conduction but was not tested.

The very large voltages across the arc cage (up to 15 kv at ignition) precluded measurements during the shot. Two vacuum switches, triggered by the rotating mirror which controls arc firing and spectrograph timing, isolated both leads from the recording oscilloscope until approximately 15 ms after the arc was extinguished, so measured temperature rise was the result of an integrated heat flux during and after the arc pulse (700-800 μs).

The radiant flux per unit length may be determined from measurements of temperature rise, ΔT and time of arc pulse Δt.

$$(q/z)^{rad} = \frac{m_c c_c}{2h} \frac{\Delta T}{\Delta t} \times \frac{1}{\alpha_c} \times \frac{1}{\zeta} \qquad (4.1)$$

The mass, m_c, specific heat c_c and half-width, h, of the calorimeter ring are fixed for a particular calorimeter and ζ is the ratio of radiation per unit arc length actually reaching the calorimeter to that leaving the arc. The method used to calculate this ratio is discussed in Appendix D.

Absorptivity, α_c, of the calorimeter sensing surface was made close to unity by blackening and, on model 3, threading to get the effect of a wedge shaped cavity.

Several other corrections to the thermocouple reading have been considered. Applying the conduction equation, Eq. (2.41), from r_a to the calorimeter radius yields a thermal conduction heat flux per unit length from the arc of the order of 1 kw/cm, but this must be considerably reduced by the relatively cool copper disc covers, especially with the dished configuration Models 1 and 3. Energy in the arc heated air after power is cut off was estimated from enthalpy and density and is only a few percent of the total energy dissipated.

An estimate of response time was made using a simplified model of the calorimeter with the following assumptions:

1). During the arc pulse the radiant flux is uniform and constant and the calorimeter sensing element is a semi-infinite solid.

2). After the arc is extinguished the sensor is completely insulated and the heat flux within is 1-dimensional.

The temperature distribution at time of arc extinction, t_1, was computed using the following equation based on a solution given by Carslaw and Jaeger (Ca. 1).

$$T(x, t_1) = 2 \frac{(q/A)}{k_c} \left[\sqrt{\frac{\alpha_c t_1}{\pi}}\, e^{(-x^2/4\alpha_c t_1)} - \frac{x}{2} \operatorname{erfc}\left(\frac{x}{2\sqrt{\alpha_c t_1}} \right) \right] \quad (4.2)$$

Temperature-time history was then computed with a standard finite difference method, again making use of the small digital computer. Results are shown in Fig. 29. The semi-infinite solid approximation is clearly valid during arcing since temperature rise at the outside radius is negligible at time t_1. For a radiant flux density of 5 kw/cm^2 at the calorimeter surface (a representative value) thermal equilibrium is approached to within 0.1 ^{o}K in slightly over 5 milliseconds. The thermocouple was located near the mean radius of the calorimeter and in that position apparent equilibration is even faster. This response time is substantially shorter than the time needed to switch in the thermocouple circuit.

The following estimates were made of heat loss through the surfaces in contact with the calorimeter ring. Consider first the Plexiglas disc which surrounds the outer surface. Assume that the temperature of the copper ring is constant and that the Plexiglas is a semi-infinite solid in perfect contact. Then, at any time t, the total amount of heat transferred through

unit area from time zero can be found by a spatial integration of the temperature rise in the semi-infinite solid. The latter is well known (e. g. Ref. Ro. 1). This heat must be supplied from the copper, and the approximate fractional change in calorimeter temperature is

$$\frac{(\Delta T)_C}{T_C - T_{P,\infty}} \cong \frac{4 r_o}{r_o^2 - r_i^2} \sqrt{\frac{\alpha_P}{\pi}} \left(\frac{\rho_P}{\rho_P}\right) \left(\frac{C_P}{C_C}\right) \sqrt{t} \tag{4.3}$$

Where subscripts C and P refer to calorimeter ring and Plexiglas. With property values from Table 4.2 the fractional change in calorimeter temperature is

$$\frac{(\Delta T)_C}{T_C - T_{P,\infty}} = 0.22 \sqrt{t(\text{sec})} \tag{4.4}$$

which amounts to a maximum possible error of 2.7% at the end of 15 ms.

The effect of heat transfer through the flat surfaces is somewhat less certain since it is dependent on the heating of the copper discs which form the covers of the calorimeter assembly. Ignoring heat transfer to the walls of the pressure vessel, the total energy dissipated in the arc (approximately 300 joules) would cause an average temperature rise of about 9° K in the cage and surrounding air. This is the same order rise as expected in the calorimeter ring so the driving temperature difference should be small. Comparing the heat transfer through the .02 inch thickness of alumina to that needed to cause a temperature change $(\Delta T)_C$ in (by symmetry) half the calorimeter ring yields

$$\frac{(\Delta T)_C}{T_C - T} = \frac{k_A}{z_A \, h \, \rho_C \, C_C} \tag{4.5}$$

where z is the thickness of the aluminum layer and h is again the half thickness of the calorimeter ring

$$\frac{(\Delta T)_C}{T_C - T} = 4.0 t(\text{sec}) \tag{4.6}$$

Assuming that $T_C - T$ remains of the same order as the net temperature rise in the calorimeter, this amounts to an error of approximately 6% at the end of 15 ms. Thus heat exchange with insulation has a relatively minor effect on the calorimeter during the time it takes to switch on the thermocouple, after which direct observation can be made of temperature change with time.

Conduction at the exposed surface both during and after arcing must be accounted for as discussed previously. However, re-radiation from the exposed surface is completely negligible because of the relatively small temperature rise involved.

TABLE 4.2
SELECTED PROPERTY VALUES USED IN CALORIMETER CALCULATIONS

Material	Density (g/cm^3)	Thermal Conductivity (watt/cm°K)	Specific Heat Joule/g°K	Thermal Diffusivity cm^2/sec
Copper[1]	8.95	3.80	.386	1.12
Plexiglas	1.2[2]	.0021[2]	1.47[3]	.0012
Alumina	--	.0017[4]	--	--
Air (300°K, 1 atm)[1]	.0011	.0028	1.0	.24

Sources:
(1) Ro. 1
(2) Ms. 1
(3) Mn. 1
(4) Estimated from values given in Wh. 1

5. METHODS OF MEASURING TEMPERATURE

Because of the high pressure and large electric current the arc was expected to be optically thick, though not "black" so that those methods depending on an optically thin plasma would not be applicable. For this reason we contemplated use of Bartel's method (Ba. 1) which depends on the phenomenon of self reversal of a spectral line in an optically thick plasma with a temperature gradient. However, the arcs at high pressure were smaller in diameter than expected, thereby reducing their optical depth and, while self-reversal of the oxygen 7772-7775Å triplet was observed at 400 amperes, use of Bartel's method appeared to be marginal.

On the other hand the optical depth of the continuum was also reduced to the point where it could be used for temperature measurement. A succession of difficulties with arc stability delayed the spectrographic results and an interim means of estimating temperature was also employed using electrical measurements and theoretical values of electrical conductivity as discussed below.

5.1 CONTINUUM RADIATION INTENSITY

The wavelength selected for determination of temperature from the absolute intensity of continuum radiation is in the near infrared at 8330 Å. Continuum radiation has frequently been used for temperature measurements in both low pressure (M. 3) and high pressure arcs (Bg. 1, Bo. 1, Mi. 1).

We have chosen as a theoretical basis the calculations of Nardone, Breene, et al (Na. 1). These calculations include free-free and free-bound radiation of the electron in the field of an ion, the free-free radiation of electron and atom and the O minus radiation. However, the amounts of free-free and of free-bound radiation obtained by Nardone, Breene, et al were multiplied with the slightly temperature dependent Gaunt factors determined by Karzas and Latter (Ka. 1). This was a correction of about 20%. To compare these results with those of other authors, we also calculated the intensity of the continuum radiation using Unsold's formula (Ma. 2), again with the Karzas and Latter gaunt factors. The result is plotted in Figure 30, along with the Nardone curve. The two curves agree fairly well, within 250°K at 15,000°K for example.

Besides the uncertainty in the theoretical results, our measurement of the arc temperature from the continuum intensity is also affected by self-absorption in the arc column. However, the optical depth of the arc

at the wavelength selected for measurements is considerably smaller than unity so self-absorption can be corrected for by a rather simple method. First, all evaluations are done with the assumption of an optically thin plasma. This leads to a first approximation for a radial intensity distribution, using a standard Abel inversion technique (Cr. 1). From the resulting temperature distribution and the known values of the local brilliancy, the absorption profile of the arc is obtained. This profile can then be numerically integrated for several values of axial distance to obtain total absoprtion along each path. Radiation originating in the arc will, on the average, see approximately half the total absorption. We have therefore corrected the originally measured I (x) distribution for 1/2 of the integrated absorption.

Such a simple correction of the absorption effect in the continuum can be made because: 1) the total absorption was small at the frequency measured, 2) the continuum radiation depends very sensitively on temperature. Therefore, the correction of the absorption effect leads to only a minor temperature correction.

5.2 ARC TEMPERATURE FROM VOLTAGE GRADIENT

A preliminary estimate of arc temperature at 500 amperes was obtained from voltage gradient measurements and observations or arc diameter. An enthalpy profile was assumed of the form

$$\frac{h - h_a}{h_{CL} - h_a} = 1 - \left(\frac{r}{r_a}\right)^x \tag{5.1}$$

where subscript a here refers to the visible edge of the arc. Weber's correlation (We. 1) Eq. (2.50), for electrical conductivity as a function of enthalpy and pressure was then used with Eq. (5.1) to obtain electrical conductivity as a function of radius. Then, writing ohms law in the form of an overall conductance

$$\frac{I}{\pi r_a^2 E_{avg}} = \int_o^1 \sigma_e \frac{r}{r_a} d\left(\frac{r}{r_a}\right) \tag{5.2}$$

the left hand side was determined from experimental measurements of current, voltage gradient and optical diameter and the equation solved graphically for centerline temperature by plotting the overall conductance as a function of centerline temperature.

6. ARC STABILITY

The achievement of arc stability at a pressure of 100 atmospheres turned out to be the crucial difficulty of the experimental part of this study. This was particularly so with the copper constrictor, which, for most of this work, was chosen over the ablation type constrictor because it permitted the investigation of air arcs.

Our first experiments at high pressures, with copper constrictors having a hole diameter of 5 mm, showed strong instabilities and a much contracted arc column, Fig. 31. An impression of the decrease of arc diameter with pressure may be conveyed by Fig. 32 in which arc diameters, as measured from the bright arc cores in high speed photographs, are plotted against pressure. Considerably improved arc stability was observed when constrictor diameter was reduced to 2.5mm and 2mm but a kink type of instability could never completely be eliminated.

We went to some length to prove that no simple experimental side effect caused the remaining arc motions:

1) Current flow in the arc apparatus was completely symmetrized by using the high pressure vessel as a back conductor. This measure minimized undesired magnetic forces on the arc.

2) The arc column was made rather long, 7 cm, to minimize electrode effects on the remote parts in the middle between the electrodes.

3) The copper discs were judiciously cleaned and etched, as described earlier, so that only a solid copper wall remained without loose particles of copper or crystals on the surface. Such particles would, under the heat load of the arc, evaporate at considerable shorter times than the solid copper wall and blow at the arc in an uncontrollable manner.

4) The 1/2 mil tungsten ignition wire was strung straight and in the very center of the constricting channel because it was observed that the arc tends to remain very close to the shape in which it was when the wire exploded for a rather long time (several hundred microseconds) after ignition. When started straight and in the very middle of the constrictor, the arc remains in that position for some time.

All these measures, however, did not prevent the arcs in the copper constrictor from eventually going unstable in a kink-like form.

As for the degree of instability, there was a difference between the 400 amp and the 100 amp arcs burned at 100 atmospheres in 2.5 mm constrictors. The 400 amp arcs were never really stable and showed motions at least in their outside parts. This is demonstrated with simultaneous high

speed photographs from a framing camera and a smear type camera in Fig. 33. At lower currents, the arcs can be operated for longer periods of time without melting the copper discs. Then three stages of arc development can be distinguished, as seen in detail in Figures 34, 35 and 36. During stage A the wire explodes and the arc plasma expands until it fills the constrictor. Then the arc remains rather stable in stage B as a diffuse plasma column filling the channel. Finally in stage C, a distinct thin arc core appears, which moves slowly in the constrictor. As seen from the discrete pictures of Fig. 36 complete stability is never achieved with the deviations from a cylindrical distribution growing in time.

We cannot say at this time what the reason is for the very characteristic formation of an arc core. However, it appears that the diffuse period of the arc is caused by the contamination of the plasma with the vapor of the 1/2 mill tungsten ignition wire. This problem requires further work.

In addition to the experiments using copper constrictors, a few tests were made with ablation type arc channels. The channels were made of Plexiglas (Fig. 16) with an inside diameter of 3 mm. The current was 400 amperes and the pressure 150 atmospheres. Fig. 37 shows these arcs to be remarkably stable after only a brief period of instability immediately following arc ignition.

The difference between arcs in the copper constrictor and those in the Plexiglas constrictor is quite remarkable. All arcs in the copper constrictors eventually go unstable, even if they were stable initially. Arcs in Plexiglas constrictors show just the opposite behavior and become stable after a short initial unstable time. It appears, therefore, that in the copper constrictor the destabilizing forces prevail and in the Plexiglas constrictor the stabilizing forces are stronger.

7. RESULTS AND CONCLUSIONS

As described in the last chapter, only the ablation type arcs were completely stable. However, most of our measurements were made on arcs in copper constrictors which were not completely stable.

7.1 ELECTRICAL GRADIENTS AND PRELIMINARY ARC TEMPERATURE DETERMINATION

Electrical gradients were determined from measurements of the total arc voltage and the length of the constrictor. The sum of cathode and anode fall, was, in all cases, estimated to be 50 volts. At 1500 psi the assumption of a linear potential distribution along the arc column was checked by using 4 of the copper discs of the cascade as probes. This measurement confirmed the linear potential distribution.

Voltage gradients of 500 ampere air arcs, burning in copper constrictors of 2.5 mm diameter and 7 cm length, are plotted as a function of pressure in Fig. 32. Using these gradients and the estimates of arc diameter also shown in Fig. 32, Eqs. (2.48, 5.1 and 5.2) were applied as discussed in Section 5.2 with results shown in Fig. 38. Three values of profile parameter are shown in Fig. 38; $x \rightarrow \infty$ corresponds to uniform temperature and $x = 2$ corresponds to a parabolic profile. The bars at 100 atmospheres indicate the effect of varying T_a from 8000°K to 10,000°K.

Since neither T_a nor the profile shape were known, precise values of centerline temperature could not be determined, but the following tentative conclusions were reached:

1) Since a uniform temperature profile is certainly a limiting case, centerline temperature is at least 16,000°K for a 500 ampere air arc at 100 atmospheres and is more likely between 18,000°K and 20,000°K,

2) Temperature changes only slowly with pressure, and appears to have a minimum value somewhere between 20 and 100 atmospheres.

7.2 TEMPERATURE MEASUREMENTS FROM CONTINUUM INTENSITIES

Measurement of the radial temperature distribution were made on arcs with a pressure of 103 atmospheres and currents of 115 and 400 amperes.

7.2.1 The 115 Ampere Arc

The result of the measurements at the 115 ampere arc is shown in Fig. 39. An axis temperature of 17,650°K was obtained and a radial distribution with "core formation."

This measurement was made close to the end of a 2300 microsecond current pulse where a rather stable arc core had formed, as demonstrated by Fig. 40. This figure shows a "smear" picture of the arc core during the spectroscopic exposure time. The photograph shows that the core did not burn in the very center of the arc constrictor and this fact was confirmed by a slight asymmetry in the photometer curve of the radial distribution of the brilliancy. The curve was folded and smoothed for the further evaluation. Fig. 40 also shows the infrared spectrum of the arc with strong and very broad oxygen and nitrogen lines and, in addition to these, a continuum of considerable strength. The temperature measurement was made at the continuum wavelength of 8330 Å.

7.2.2 The 400 Ampere Arc

For the 400 ampere arc, no reasonable radial temperature distributions were obtained. This arc, as shown in Fig. 33, fluctuates strongly in the constrictor, which tends to lower the spectroscopically measured axis temperature. Consistent with this argument, an axis temperature of only 16,600°K was measured.

It was also observed that the radial distribution of the continuous radiation extended well beyond the wall of the copper cage. There are several possible explanations, including a penetration of arc plasma into the area between the copper discs. Further experimental work is needed to clarify this point.

7.3 APPLICATION OF ARCRAD III TO MEASURED PROFILE

Using the least squares procedure, Eqs. (2.38 and 2.39), a temperature profile of the form of Eq. 2.35 was fitted to the measured profile as shown on Fig. 41. The fitted profile has T_a = 12,700°K, x = 1.1343 and σ_{SD} = 44°K, an average voltage gradient of 140 volts/cm, $\sigma_{SD,E}$ = 26 volts, and a current of 111 amperes. These compare with measured values of 160 v/cm and 115 amperes, respectively. The results are the correct order of magnitude and can therefore be considered reasonably successful but they do illustrate the difficulty of computing without experimental guidance.

As an illustration of the radiant energy redistribution predicted by the ARCRAD III analysis, Fig. 42 shows cumulative net radiation* computed using the arc profile of Fig. 41. The curves are normalized by the total radiant flux density at the arc boundary (8.36 kw/cm) and are plotted for three frequency ranges as well as for the sum over all frequencies. At a radius of .05 cm, vacuum u.v. radiation is over 25% of that which eventually leaves the arc, but practically all of the vacuum u.v. is reabsorbed in the outer layers so that effective emission is all below 59,000 cm^{-1}.

*By "cumulative net" at any radius, r, is meant the net radiant flux crossing a cylindrical surface of radius r.

7.4 TOTAL RADIANT HEAT FLUX MEASUREMENTS

All total heat flux measurements were made at the 400 ampere current level where no useful temperature profile data were obtained. Thus the correlation of ARCRAD III computations and total heat flux measurements cannot be direct. Evidence of instability obtained after the calorimeter measurements were made also casts some doubt on the assumption of steady state upon which the analysis is based.

Table 7.1 summarizes the results of the heat flux measurements. In view of the uncertainties regarding the arc itself no corrections have been made other than the geometrical one discussed in Appendix D.

The ratio ζ of radiation reaching the calorimeter to radiation at the arc boundary was computed using a profile estimated to be representative. This ratio appears to be quite insensitive to profile parameter as can be seen from Table 7.2 which shows results of a set of calculations for $x = 50$. The The latter value was chosen to reduce the number of annuli in the calculation since it could only be a rough approximation in any case and also to render the choice of T_a unimportant. The radiant fluxes per unit arc column calculated are of the same order as those measured although the voltage gradients are somewhat lower than measured.

Voltage, current and calorimeter thermocouple traces are shown in Fig. 43 for the case marked * in Table 7.1. The temperature continues to rise gradually as the entire high pressure container tends to thermal equilibrium. Traces taken with a slower sweep indicate that a peak is reached at about 200 milliseconds and after that temperature drops slowly. Temperature was measured as the difference between a reference sweep prior to the shot and the temperature trace projected back to the time of arc cutoff.

TABLE 7.1
TOTAL RADIATION HEAT FLUX MEASUREMENTS $(q/z)^{rad}$

Calorimeter Model	ζ	Pressure (atm)	Current (amp)	Voltage Gradient (volts/cm)	$(q/z)^{rad}$ (kw/cm)	EI (kw/cm)	$\left[\frac{(q/z)^{rad}}{EI}\right]$
1	.24	20	430	115	9.5	49.5	.19
		34	410	115	17.1	47.0	.36
		*100	410	196	33.6	80.3	.42
2	.44	20	440	122	15.4	53.6	.29
		100	390	203	32.2	79.0	.41
		100	400	183	33.3	73.0	.46

Note: based on T_{CL} = 18000°K T_a = 12500°K r_a = .086 cm
p = 100 atm x = 1.2 and 2.0

*Fig. 43

TABLE 7.2
ARCRAD III RADIANT FLUX CALCULATIONS FOR CONDITIONS REPRESENTATIVE OF THE 100 ATM 400 AMP ARC

Temperature °K	r_a (cm)	E (volts/cm)	I (amp)	$(q/z)^{rad}$ (kw/cm)	ζ (model 1)
16600	.08	127	282	25.2	.27
	.10	122	421	37.8	.27
	.12	117	584	52.2	.27
17000	.08	128	318	28.3	.29
	.10	122	473	42.2	.29
	.12	118	656	58.1	.30
18000	.08	138	423	39.0	.29
	.10	132	628	57.8	.29
	.12	126	867	79.0	.29

7.5 CONCLUSIONS

A tractable model of the frequency dependent radiant interchange within a steady, cylindrically symmetric arc has been developed. Results of computations with the model show that radiation in the vacuum ultraviolet strongly influences the distribution of energy within the arc and the gas immediately surrounding it. However, this radiation does not contribute to the wall cooling load in an arc chamber because of very strong molecular absorption.

The capability for prediction of temperature profiles without some guidance from experimental observations is limited because of uncertainties in input radiation data (such as the effect of lines), and in thermal and electrical conductivities at high pressures. These uncertainties led to retention of a single parameter temperature profile which matched the measured profile quite well and gave local voltage gradients of the correct order of magnitude but did not justify a more detailed solution.

The relative significance of line radiation from a high pressure arc might be evaluated by examining a few typical lines in some detail (i.e. estimating or measuring line broadening effects and taking perhaps 10 wave number intervals over several half-breadths). Direct experimental verification would also be possible by measuring average intensity on a plate on which the lines are deliberately smeared by using a large slit and comparing the results to measurements of continuum intensity only from a sharp plate.

Constricted air arcs have been studied under conditions where very little quantitative experimental work has been done. Arcs with currents from 100 to 500 amperes have been run at 100 atmospheres pressure. Wall stabilization was not effective for maintaining a stable arc at such high pressure. However, at the lower current level of 100 amperes, a meta-stable state was maintained in the air arc for sufficient time to expose a spectrographic plate from which a temperature profile was determined. Such a plate also contains a great deal of additional information on spectral distribution of continuum and line radiation intensities. Much additional data reduction, including use of an Abel inversion which accounts for self-absorption (Gr.1, Bo.1) will be needed to extract this information. Radiant heat flux measurements are in reasonable agreement with calculations in view of the uncertainty in arc state at the 100 atm, 400 amperes condition where heat flux measurements were made.

Arcs which are flow stabilized by ablation from the constrictor wall are stable even at 150 atmospheres and probably higher. Although the resultant plasma is a mixture corresponding to the wall composition (typically some combination of C, H and O) rather than air, the inherent stability of the ablating constrictor type arc offers the prospect of studying both local spectral radiant intensities and total radiant flux density over a broad range of pressure and arc current. It is recommended that future work on high pressure plasma

radiation place primary emphasis on the ablating constrictor type arc because of its much greater stability and flexibility of operation. Theoretical data on continuum radiation of the atomic species are available and the importance of line radiation could be assessed as described above.

BIBLIOGRAPHY

A.1 Anderson, J. A., "Spectral Energy Distribution of the High Current Vacuum Tube", Astrophys. Jour. 75, 394-406, (1932).

B.1 Browne, W. G., "Thermodynamic Properties of the Earths Atmosphere", GE MSD, Radiation and Space Physics, TM #2 (1962).

Ba.1 Bartels, H. Bull. Acad. Sci. USSR, Phys. Ser., 22, 737 (1958).

Bg.1 Bogen, P., Conrads, H., and Rusbuldt, D., "Bestimmung von Temperatur und Dichte Eines Gleitfunkens Aus Der Bremsstrahlung im Infrarot", Z. Physik, 186, 240-248 (1965).

Bi.1 Biberman, L. M., Vorobev, V. S., Norman, G. E. and Iakubov, I.T., "Radiation Heating in Hypersonic Flow", Kosmich, Issled, 2, 441-454 (1964)

Bo.1 Bohn, W. L., Beth, M. V. and Nedder, G., "Spectroscopic Investigation of an Argon Plasma with Self Absorption", 7th Int. Conf. of Ion. Phen. in Gases, Belgrade (1965).

Br.1 Burgess, A. and Seaton, M. F., "A General Formula for the Calculation of Atomic Photo-ionization Cross Sections", Monthly Notices Royal Astronautical Soc., 120, 121-151 (1960).

Bu.1 Burhorn, F., Maecker, H. and Peters, T., "Temperatur Messungen An Wasserstabilisierten Hoch Leistungs Bogen", Z. Physik, 131, 28-40 (1951).

Ca.1 Carslaw and Jaeger, Conduction of Heat in Solids, (Oxford Univ. Press, London, 1947).

Cn.1 Cann, G. L., Teem, J. M., Buhler, R. D. and Branson, L. K., "Magnetogas Dynamic Accelerator Techniques," Tech. Documentary Report, AEDC TDR-62-145, Arnold Engineering Development Center (July 1962).

Co.1 Cordero, J., Diederich, F. W. and Hurwicz, H., "Aerothermodynamic Test Techniques for Re-entry Structures and Materials," Aerospace Eng. 22, 166-191 (1963).

Cr.1 Cremers, C. J. and Birkebak, R. C., "Application of the Abel Integral Equation to Spectrographic Data," Applied Optics 5, 1057-1064 (1966).

BIBLIOGRAPHY (Cont'd)

De. 1 DeSoto, S., "Coupled Radiation Conduction and Convection in Entrance Region Flow," AIAA Paper Number 66-136 (Jan. 1966)

Ec. 1 Eckert, E.R.G. and Drake, R. M., Heat and Mass Transfer, (McGraw Hill Book Co., New York, 1959) 2nd ed.

Eu. 1 Euler, J., "Der Graphitbogen Als Spectralphotometrisches Strahldichtenormal im Gebiet Von 0.25 Bis. 1.8 μ," Annalen Phys. 11, 203-224 (1953).

Fr. 1 Frind, G., "An Ablation Type Plasma Generator," Journ. Spacecraft and Rockets, 2, 458-460 (1965).

Ga. 1 Gambill, W. R. and Greene, N. D., "A Preliminary Study of Vortex Boiling Burnout Heat Flux," Jet Propulsion, 28, 192-194 (1958).

Gr. 1 Griem, H. R., Plasma Spectroscopy, (McGraw Hill Book Co., New York, 1964) p. 178.

Hi. 1 Hildebrand, F. B., Introduction to Numerical Analysis, (McGraw Hill Book Co., New York, 1956).

Ja. 1 Jakob, M., Heat Transfer, (John Wiley and Sons, New York, 1957), Vol. II.

Ka. 1 Karzas, W. J. and Latter, R., "Electron Radiative Transitions in a Coulomb Field," Astrophysical Journal Supplement Series, 6, 167-212 (1961-62).

Ke. 1 Kesten, A. S., "Radiant Heat Flux Distribution in a Cylindrically Symmetric Non-Isothermal Gas with Temperature Dependent Absorption Coefficient", GE JILA, U. of Colo., NBS and ONR Sponsored Symposium on Interdisciplinary Aspects of Radiative Energy Transfer, Philadelphia, Pa. (February 1966) Symposium Volume to be published.

Ko. 1 Kourganoff, V., Basic Methods in Transfer Problems, (Dover Publications, Inc., New York, 1963).

M. 1 Maecker, H., "Ein Zylindrischer Bogen fur Hohe Leistungen", Z. F. Naturf. 11a, 457-459 (1956).

M. 2 Maecker, H., "Messung und Auswertung von Bogencharacteristiken (A, N_2)," Z. Physik, 158, 392-404 (1960).

BIBLIOGRAPHY (Cont'd)

M. 3 Maecker, H., "Das Elektronenkontinuum in der Saule des Hochstromkohlebogens und in Anderen Bogen", Z. Physik. 139, 448-463 (1954).

M. 4 Maecker, H., "Experimental and Theoretical Studies of Properties of N_2 and Air at High Temperatures," NATO AGARD Combustion Conference, Braunschweig, Germany (April 1962).

Ma. 1 Marston, C. H., "Air Arc Radiation with Self Absorption", General Electric Co., Philadelphia, Pa. TIS R65SD20 (May 1965).

Ma. 2 Marston, C. H., "Study of Radiation Heat Flux from High Pressure Air Arcs", Contract Report AF 40(600)-1080, Arnold Engineering Development Center, Arnold Air Force Station, Tennessee (1964).

Mc. 1 McPherson, "The Carbon Arc as a Radiation Standard," J. Opt. Soc. Am. 30, 189-193 (1940).

Mi. 1 Maisenhalder, F. and Schoeck, P. A., "The Energy Balance of Electric Arcs Without and With Superimposed Gas Flow", 7th Int. Conf. of Ion Phen. in Gases, Belgrade (1965).

Mn. 1 Mantel, C. L. (ed), Engineering Materials Handbook, (McGraw Hill Book Co., New York, 1958) 1st ed., p. 33-22.

Ms. 1 Mason and Manning, "The Technology of Plastics and Resins, (D. VanNostrand, Inc., N. Y., 1947).

Na. 1 Nardone, M. C., Breene, R. G., Zeldin, S. S. and Riethof, T. R., "Radiance of Species in High Temperature Air", General Electric Co., Philadelphia, Pa., TIS R63SD3 (June 1963).

No. 1 Norman, G. E., "Free-Free Transitions of the Electron in the Ion Field", Opt. Spectr. 14, 277-279 (1963).

Nu. 1 Null, M. R., and Lozier, W. W., "Carbon Arc as a Radiation Standard", J. Opt. Soc. Am. 52, 1156-1162 (1962).

Og. 1 Ogurtsova, N. N., Podmoshenskii, V. M. and Shelemina, V. M., "Characteristics of the Plasma Jet of a Powerful Capillary Discharge", Opt. Spectr. 15, 404-406, (1963).

P. 1 Peters, Th., "Temperatur-und Strahlungsmessungen am Wasserstabilisierten Hochdruckbogen," Z. Physik. 135, 573-592 (1953).

BIBLIOGRAPHY (Cont'd)

Pe. 1 Peng, T. and Pindroh, A. L., "An Improved Calculation of Gas Properties at High Temperatures-Air", Magnetohydrodynamics Proc. Fourth Biennial Gas Dynamics Symposium, (Northwestern University Press, Evanston, Illinois, 1962) pp. 67-88.

Pi. 1 Pivovonsky, M. and Nagel, M. R., "Tables of Black Body Radiation Functions, (The MacMillan Co., New York, 1961), p. xiv.

Ro. 1 Rohsenow, W. M. and Choi, H., Heat Mass and Momentum Transfer (Prentice-Hall, Inc., Englewood Cliffs, N. J. 1961), p. 288.

Sb. 1 Scarborough, J. B., Numerical Mathematical Analysis (The Johns Hopkins Press, Baltimore, 1962) 5th ed.

Sc. 1 Schultz, E. O., Holland, A. C., and Marmo, F. F., "Planetary Aeronomy, VIII:A Congeries of Absorption Cross Sections for Wavelengths Less than 3000 Å", NASA CR-15 (Sept. 1963).

Sh. 1 Sherman, M. P. and Kulander, J. L., "Free-Bound Radiation from Nitrogen, Oxygen and Air", General Electric Co., Philadelphia, Pa., TIS R65SD15 (May 1965).

Sk. 1 Skifstad, J. G., "Review of Theoretical Analyses of Arc Heating in a Tube", Aerospace Research Laboratories, Wright-Patterson AFB, Ohio, Report ARL 65-207 (Oct. 1965).

Sm. 1 Schmitz, G., Druxes, H., and Patt, H. J., "Zur Modelltheorie des zylindersymmerischen Lichtobogens mit radialer Masseneinströmung", Z. Physik, 187, 271-289 (1965).

Th. 1 Thomas, M., "Transport Properties of High Temperature Gases," Magnetohydrodynamics, Proc. Fourth Biennial Gas Dynamics Symposium, (Northwestern University Press, Evanston, Illinois 1962). pp. 89-107.

U. 1 Unsold, A., Physik der Sternatmosphären (Springer, Berlin 1955)

Vi. 1 Viegas, J. R. and Peng, T. C., "Electrical Conductivity of Ionized Air in Thermodynamic Equilibrium", ARS Journal, 31, 654-657 (1961).

We. 1 Weber, H. E., "Skin Friction and Heat Transfer for High Temperature Equilibrium Boundary Layer Flows with and without Blowing", General Electric Co., Philadelphia, Pa., Report TIS R66SD9 (March 1966).

BIBLIOGRAPHY (Cont'd)

We. 2 Weber, H. E., "Constricted Arc Column Growth", Proc. 1964 Heat Transfer and Fluid Mechanics Inst., (Stanford Univ. Press Stanford, Calif. 1964), pp. 245-259.

Wh. 1 Whittemore, "Properties and Uses of Pure Oxide Refractories", J. of the Am. Ceramic Soc., 32, 40 (1949).

Yo. 1 Yos, J. M., "Transport Properties of Nitrogen, Hydrogen, Oxygen, and Air to 30,000°K", AVCO Report No. RAD-TM-63-7 (1963).

APPENDIX A
TABULATION AND INTERPOLATION OF TRANSMISSION INTEGRAL

An integral arises in the radiant transfer model used in this work which cannot be solved in closed form, namely

$$f(x) = \frac{4}{\pi} \int_0^{\pi/2} e^{-x/\sin\theta} \sin^2\theta \, d\theta \tag{A.1}$$

The original computer program ARCRAD (Ma.1, Ma.2) took advantage of the close resemblance of the integral to an exponential decay by using an empirical representation which was the product of an exponential decay and a polynominal. Since Program ARCRAD III, which includes angular variation of emission, requires the difference between two values of the integral, a more precise evaluation was needed. The function was integrated numerically to an error less than 1.0×10^{-6} using the parabolic (Simpson's) rule. A table of differences was then calculated and stored in the computer to facilitate evaluation of the integral by means of Bessel's interpolation formula (Hi.1)

$$f(x) = d_o(x_i) + (s-1/2)\, d_1(x_i) + s(s-1)\, d_2(x_i) + s(s-1)(s-1/2)\, d_3(x_i) \tag{A.2}$$

where x_i is the next lower value for which x is tabulated and

$$s = \frac{x - x_i}{x_{i+1} - x_i} \tag{A.3}$$

$$d_o(x_i) = \frac{f(x_i) + f(x_{i+1})}{2} \tag{A.4}$$

$$d_1(x_i) = f(x_{i+1}) - f(x_i) \tag{A.5}$$

$$d_2(x_i) = \frac{f(x_{i+2}) - f(x_{i+1}) - f(x_i) + f(x_{i-1})}{2 \times 2!} \tag{A.6}$$

$$d_3(x_i) = \frac{f(x_{i+2}) - 3f(x_{i+1}) + 3f(x_i) - f(x_{i-1})}{2 \times 3!} \tag{A.7}$$

The interval was varied with optical depth to keep the table of differences as small as possible while retaining a precision of interpolation equaling the precision of the tabulated values of the function.

Table A.1 lists tabulated values of f(x) and associated differences for x = 0 to x = 14. At larger optical depths interpolation of ln(f(x)) proved more convenient, so, in the range $6 \leq x \leq 14$, the table lists ln (f(x)) and its associated differences. At an optical depth of 14, $f(x) < .5 \times 10^{-6}$ so this was chosen as the cutoff. Fortran compatible notation was used in the table with $f(x_i) \leftrightarrows$ F(NX), $d_o(x_i) \leftrightarrows$ F(NX, 1), etc.

TABLE A.1
TRANSMISSION INTEGRAL AND INTERPOLATION DIFFERENCES

NX	f(NX)	F(NX,1)	F(NX, 2)	F(NX, 3)	F(NX, 4)
.00	+9.99999[illegible]6E-01	+9.8746170E-01	-2.5075430E-02	+3.86450E-04	-3.79166E-06
.02	+9.7497403E-01	+9.6276135E-01	-2.4325330E-02	+3.65672E-04	-3.13833E-06
.04	+9.5059870E-01	+9.387923[illegible]E-01	-2.3612740E-02	+3.48232E-04	-2.68583E-06
.06	+9.2698596E-01	+9.1551975E-01	-2.2932400E-02	+3.33010E-04	-2.39166E-06
.08	+9.0405356E-01	+8.9291320E-01	-2.2280700E-02	+3.19375E-04	-2.16333E-06
.10	+8.8177286E-01	+8.7094540E-01	-2.1654900E-02	+3.06960E-04	-1.98000E-06
.12	+8.6011796E-01	+8.4959150E-01	-2.1052860E-02	+2.95482E-04	-1.8550[illegible]E-06
.14	+8.39[illegible]E-01	+8.2882860E-01	-2.0472970E-02	+2.84772E-04	-1.72166E-06
.16	+8.1859213E-01	+8.0863520E-01	-1.9913770E-02	+2.74742E-04	-1.62500E-06
.18	+7.9867836E-01	+7.8899135E-01	-1.9374000E-02	+2.65310E-04	-1.52750E-06
.20	+7.7930436E-01	+7.6987805E-01	-1.8852530E-02	+2.56367E-04	-1.45500E-06

NX	f(NX)	F(NX,1)	F(NX,2)	F(NX,3)	F(NX,4)
.20	+7.7930436E-01	+7.5620860E-01	-4.6191460E-02	+1.56528E-03	-2.18550E-05
.25	+7.3311290E-01	+7.1151690E-01	-4.3191970E-02	+1.44178E-03	-1.93133E-05
.30	+6.8992093E-01	+6.6970875E-01	-4.0424330E-02	+1.33197E-03	-1.72916E-05
.35	+6.4949660E-01	+6.3056455E-01	-3.7864070E-02	+1.23346E-03	-1.55525E-05
.40	+6.1163253E-01	+5.9388725E-01	-3.5490470E-02	+1.14445E-03	-1.41166E-05
.45	+5.7614206E-01	+5.5949890E-01	-3.3286260E-02	+1.06355E-03	-1.28600E-05
.50	+5.4285580E-01	+5.2723765E-01	-3.1236270E-02	+9.89782E-04	-1.17300E-05
.55	+5.1161963E-01	+4.9695594E-01	-2.9327130E-02	+9.22257E-04	-1.07833E-05
.60	+4.8229240E-01	+4.6851878E-01	-2.7547240E-02	+8.60217E-04	-9.90250E-06
.65	+4.5474516E-01	+4.4180203E-01	-2.5886260E-02	+8.03117E-04	-9.13333E-06
.70	+4.2885690E-01	+4.1669151E-01	-2.4334770E-02	+7.50472E-04	-8.42166E-06
.75	+4.0452413E-01	+3.9308194E-01	-2.2884370E-02	+7.01785E-04	-7.80833E-06
.80	+3.8163976E-01	+3.7087594E-01	-2.1527630E-02	+6.56692E-04	-7.22750E-06

TABLE A-1. (Continued)

NX	I(NX)	F(NX, 1)	F(NX, 2)	F(NX, 3)	F(NX, 4)
.85	+3.6011213E-01	+3.4998333E-01	-2.0257600E-02	+6.14925E-04	-6.69666E-06
.90	+3.3985453E-01	+3.3032056E-01	-1.9067930E-02	+5.76130E-04	-6.23583E-06
.95	+3.2078660E-01	+3.1181006E-01	-1.7953080E-02	+5.40052E-04	-5.79083E-06
1.00	+3.0283352E-01	+2.9437966E-01	-1.6907720E-02	+5.06507E-04	-5.39083E-06
1.0	+3.0283352E-01	+2.8641613E-01	-3.2834770E-02	+1.96793E-03	-4.17291E-05
1.1	+2.6999875E-01	+2.5542411E-01	-2.9149200E-02	+1.73385E-03	-3.62975E-05
1.2	+2.4084947E-01	+2.2789979E-01	-2.5899360E-02	+1.53000E-03	-3.16533E-05
1.3	+2.1495011E-01	+2.0343547E-01	-2.3029280E-02	+1.35197E-03	-2.76883E-05
1.4	+1.9192083E-01	+1.8167510E-01	-2.0491460E-02	+1.19679E-03	-2.42733E-05
1.5	+1.7142937E-01	+1.6231691E-01	-1.8244920E-02	+1.05933E-03	-2.13108E-05
1.6	+1.5318405E-01	+1.4505739E-01	-1.6254110E-02	+9.39152E-04	-1.87508E-05
1.7	+1.3693034E-01	+1.2968610E-01	-1.4488310E-02	+8.33325E-04	-1.65250E-05

NX	I(NX)	F(NX, 1)	F(NX, 2)	F(NX, 3)	F(NX, 4)
1.8	+1.2244203E-01	+1.1598162E-01	-1.2930810E-02	+7.40022E-04	-1.45758E-05
1.9	+1.0952122E-01	+1.0375711E-01	-1.1528220E-02	+6.57667E-04	-1.28766E-05
2.0	+9.7993006E-02	+9.2847930E-02	-1.0298146E-02	+5.84865E-04	-1.13908E-05
2.1	+8.7702860E-02	+8.3108480E-02	-9.1887570E-03	+5.20449E-04	-1.00813E-05
2.2	+7.8514103E-02	+7.4409925E-02	-8.2083500E-03	+4.63399E-04	-8.93500E-06
2.3	+7.0315753E-02	+6.6638135E-02	-7.3351600E-03	+4.12823E-04	-7.92441E-06
2.4	+6.2975938E-02	+5.9692260E-02	-6.5570570E-03	+3.67953E-04	-7.03275E-06
2.5	+5.6413536E-02	+5.3481860E-02	-5.8633460E-03	+3.28115E-04	-6.24775E-06
2.6	+5.0550190E-02	+4.7927893E-02	-5.2445940E-03	+2.92720E-04	-5.55133E-06
2.7	+4.5305596E-02	+4.2959364E-02	-4.6924630E-03	+2.61251E-04	-4.93833E-06
2.8	+4.0613133E-02	+3.8513339E-02	-4.1995870E-03	+2.33255E-04	-4.39466E-06
2.9	+3.6413546E-02	+3.4533825E-02	-3.7594410E-03	+2.08336E-04	-3.91275E-06
3.0	+3.2654085E-02	+3.0970984E-02	-3.3662420E-03	+1.86144E-04	-3.48516E-06

TABLE A-1. (Continued)

NX	f(NX)	F(NX, 1)	F(NX, 2)	F(NX, 3)	F(NX, 4)
3.1	+2.9287863E-02	+2.778043ØE-02	-3.Ø148650E-03	+1.66368E-04	-3.10666E-06
3.2	+2.6272998E-02	+2.4922614E-02	-2.7007680E-03	+1.48741E-04	-2.76908E-06
3.3	+2.3572230E-02	+2.236228ØE-02	-2.4199088E-03	+1.33022E-04	-2.47866E-06
3.4	+2.1152330E-02	+2.ØØ6799ØE-02	-2.1686808E-03	+1.18996E-04	-2.20441E-06
3.5	+1.898365ØE-02	+1.8011693E-02	-1.9439130E-03	+1.06478E-04	-1.96850E-06
3.6	+1.7039737E-02	+1.6168353E-02	-1.7427680E-03	+9.52992E-05	-1.75775E-06
3.7	+1.5296969E-02	+1.4515611E-02	-1.5627160E-03	+8.53175E-05	-1.56953E-06
3.8	+1.3734253E-02	+1.3033504E-02	-1.4014980E-03	+7.63977E-05	-1.40375E-06
3.9	+1.2332755E-02	+1.1704192E-02	-1.2571250E-03	+6.84247E-05	-1.25391E-06
4.Ø	+1.1075630E-02	+1.Ø511730E-02	-1.127799ØE-03	+6.12982E-05	-1.12166E-06
4.1	+9.9478313E-03	+9.4418645E-03	-1.Ø119327E-03	+5.49242E-05	-1.ØØ3ØØE-06
4.2	+8.9358986E-03	+8.481847ØE-03	-9.Ø81Ø23ØE-04	+4.92230E-05	-8.97441E-07
4.3	+8.Ø277963E-03	+7.6202755E-03	-8.158407ØE-04	+4.41215E-05	-8.Ø3133E-07
4.4	+7.2127556E-03	+6.8469475E-03	-7.3161600E-04	+3.95559E-05	-7.18858E-07
4.5	+6.4811396E-03	+6.1527310E-03	-6.5681700E-04	+3.54691E-05	-6.43466E-07
4.6	+5.8243226E-03	+5.5294525E-03	-5.8973960E-04	+3.18097E-05	-5.76383E-07
4.7	+5.2345830E-03	+4.9697940E-03	-5.2957800E-04	+2.85323E-05	-5.16216E-07
4.8	+4.7050050E-03	+4.4671998E-03	-4.7561040E-04	+2.55966E-05	-4.62333E-07
4.9	+4.2293946E-03	+4.Ø157988E-03	-4.2719160E-04	+2.29663E-05	-4.14416E-07
5.Ø	+3.8022030E-03	+3.6103305E-03	-3.8374500E-04	+2.06094E-05	-3.71300E-07
5.1	+3.4184580E-03	+3.2460811E-03	-3.4475370E-04	+1.84969E-05	-3.32833E-07
5.2	+3.Ø737043E-03	+2.9188257E-03	-3.Ø975710E-04	+1.66030E-05	-2.98425E-07
5.3	+2.7439472E-03	+2.6247764E-03	-2.7834160E-04	+1.49051E-05	-2.67525E-07
5.4	+2.4856156E-03	+2.3605374E-03	-2.5013640E-04	+1.33825E-05	-2.4ØØ8ØE-07
5.5	+2.2354692E-03	+2.1230635E-03	-2.2481130E-04	+1.20168E-05	-2.15225E-07
5.6	+2.Ø1Ø6579E-03	+1.9Ø96234E-03	-2.Ø2Ø689ØE-04	+1.07919E-05	-1.93091E-07

NX	f(NX)	F(NX, 1)	F(NX, 2)	F(NX, 3)	F(NX,4)
5.7	+1.8085890E-03	+1.7177672E-03	-1.8164360E-04	+9.69290E-06	-1.73250E-07
5.8	+1.6269454E-03	+1.5452967E-03	-1.6329730E-04	+8.70675E-06	-1.55466E-07
5.9	+1.4636481E-03	+1.3902398E-03	-1.4681660E-04	+7.82177E-06	-1.39525E-07
6.0	+1.3168315E-03	+1.2508264E-03	-1.3201020E-04	+7.02747E-06	-1.25241E-07

NX	f(NX)	Ln(F(NX, 1))	Ln(F(NX, 2))	Ln(F(NX, 3))	Ln(F(NX, 4))
6.0	+1.3168315E-03	-7.1593245E-00	-1.0535963E-00	+3.02840E-03	-1.16450E-04
7.0	+4.5915480E-04	-8.2102420E-00	-1.0482386E-00	+2.42970E-03	-8.30166E-05
8.0	+1.6095886E-04	-9.2563000E-00	-1.0438775E-00	+1.99615E-03	-6.14916E-05
9.0	+5.6671490E-05	-1.0298366E+01	-1.0402540E-00	+1.67087E-03	-4.69416E-05
10.0	+2.0025711E-05	-1.1337090E+01	-1.0371940E-00	+1.42020E-03	-3.65666E-05
11.0	+7.0980700E-06	-1.2372973E+01	-1.0345730E-00	+1.22300E-03	-2.91666E-05
12.0	+2.5224984E-06	-1.3406411E+01	-1.0323020E-00	+1.06475E-03	-2.35833E-05
13.0	+8.9847906E-07	-1.4437719E+01	-1.0303140E-00	+9.35500E-04	-1.95000E-05
14.0	+3.2066249E-07	-1.5467156E+01	-1.0285600E-00	+8.28750E-04	-1.60833E-05

APPENDIX B
PROGRAM ARCRAD III

B.1 PURPOSE

The purpose of ARCRAD III is the calculation of radiation heat flux from arc heated air based on spectral emission-absorption characteristics of air and a measured or assumed temperature profile. Included are computations of flux reaching a total radiation calorimeter and of voltage gradient based on a local energy balance, and total electric current.

B.2 GLOSSARY OF TERMS

Fortran Name	Definition
A0, A1, A2, A3	Constants for polynomial which multiplies transmission function for calorimeter calculation.
AINT	Intermediate value in calculation of R array.
ALPHA (6)	Angles used in calculation of sector radii.
ANGLE	Angle sectors of quadrant. ($\phi + \Delta\phi/2$)
BCDREC (25)	Array in which alphameric identification of tape is read.
BIG (20)	Array for storing largest absorption length for each annulus.
BINT	Intermediate value in calculation of R array.
C2T (20)	Array of C_2/T used in calculation of v.
CEM	Calorimeter emission-transmission integral for particular value of ETKDR.
CONST	Average particle density of outermost (low temperature) annulus.
CQRAD (10)	Calorimeter integral summed over wave number group.
COSNA (6)	Cosines of ALPHA array.

CTEMP (21)	Array of temperatures for which electrical conductivity is tabulated.
CTR	Calorimeter transmission integral for particular value of TKDR.
CTRANS	Calorimeter transmission function, emitting annulus to arc boundary.
CURRNT	Current.
DALPHA	Angle difference in degrees between elements of ALPHA array.
DEV	Weighted standard deviation of calculated voltage gradient.
DIV	Length of subrange for numerical integration.
DH	Relative cumulative spectral radiance at upper wave number limit of a particular wave number increment.
DL	Relative cumulative spectral radiance at lower wave number limit of a particular wave number increment.
DSINA (6)	Difference in the sines of consecutive sector angles.
DSUM	Intermediate value for computing relative cumulative spectral radiance when $v > 1$.
E (21)	Annulus voltage gradient.
EAVG	Weighted average voltage gradient.
EM	Transmission integral for particular value of ETKDR.
EKDR	Dimensionless emission length.
EKDRMX (20, 76)	Temporary storage array.
ESUM	Intermediate value used in calculation of weighted average voltage gradient.

ETA	Black body energy fraction within a specified wave number interval (DH-DL).
ETKDR	Dimensionless emission, transmission length.
EX (10)	Temperature profile parameter.
EX1 (10)	Temperature profile parameter, Zone I, when Zone II is omitted.
EX2 (10)	Temperature profile parameter, Zone I, when Zone II is included.
F (88, 4)	Array of interpolation differences for dimensionless absorption length.
I	Wave number index or annulus subinterval index.
I1	Lowest wave number at a given temperature for which $\nu \geq .2$.
IF (10)	Array of index limits for breaking total radiation into wave number groups.
II	Subinterval index for evaluating electrical conductivity.
IJK	Index in calculation of relative cumulative spectral radiance.
IN	Index of outermost annulus for ARCRAD III calculation.
IN 1	IN + 1
INF	Consider a ray emitted from an interior annulus surface passing through an absorbing annulus. INF is the index of the first boundary of the absorbing annulus encountered. NF is the index of second boundary encountered. NF may equal INF-1 or NT + 1 - INF.
INN	Index for bypassing Zone II data when Zone I only is being calculated.

IPOS	Index on pressure.
IPST	Index for locating absorption coefficient on an input record.
IR	Index on output radiation values stored by wave number group.
ITEST	When index on absorbing annulus greater than NT, ITEST = 0; when index less than or equal, ITEST = 1.
IW	Wave number index used for finding I1.
IX	Index on profile parameter.
IZONE	IZONE = 0 when Zone II is omitted. IZONE = 1 when Zone II is included.
J	Index for temperature interpolation of conductivity.
KA	Index on annulus absorbing from interior surface of emitting annulus.
L	Index for reading title card.
N	Index on emitting annulus.
N1	Number of annuli exterior to an exterior emitting surface.
NA	Angle index.
NALPHA	Number of angular subintervals.
NANGLE	NALPHA + 1.
NB	IN - 1.
NC	IN
NCASE	Number of cases; each different combination of temperature and pressure constitutes a case.
NDIV	Number of subdivisions for integrating conductivity.

NF	See INF.
NIF	Number of wave number groups.
NJ	Index on absorbing annuli for exterior emission.
NJ2	Index used in calculating annulus and sector radii.
NP	Index used for summation.
NQ	Index used for annuli absorbing from exterior surface of emitting annulus.
NS	1) Index used in calculating annulus and sector radii. 2) Index used to select proper annulus and sector radius for the emission length of the emitting annulus.
NS 1	NS + 1.
NT	Number of annuli of the profile.
NT 1	NT + 1.
NT 2	2* NT.
NT 21	2*NT - NC.
NT 22	2*NT - NB.
NW	Number of wave numbers.
NWBCD	Control parameter (= 0 to read entire BCD record).
NWBIN	Control parameter (= 0 to read entire binary record).
NWI	First wave number of wave number group.
NWF	Last wave number of wave number group.

NX	NX = NX1 when Zone II omitted. NX = NX2 when Zone II included.
NX 1	Number of profile parameters when Zone II omitted.
NX 2	Number of profile parameters when Zone II included.
NXX	Index used to read array F (88, 4)
P	Pressure.
PCNT	Interpolation fraction.
PROP (20, 76)	Linear absorption coefficient.
PRTINT (20)	Electrical conductivity weighting factor (SIGINT(N)/SIGSUM).
QABS (20, 10)	Radiant flux per unit arc length absorbed by annulus from all other annuli (summed over a wave number group).
QCON (20)	Net thermal conduction per unit arc length from an annulus.
QCONA	Thermal conduction per unit arc length at boundary of Zone I.
QCOR	Total power per unit arc length.
QEMIT (20, 10)	Radiant flux per unit arc length emitted by annulus (self-absorption included).
QNET (20, 10)	QEMIT - QABS for one annulus.
QRAD (10)	Summation of QNET over all annuli.
QV (10)	Net radiation per unit volume.
R (40, 40, 3)	Array of annulus and sector radii.
RA	Radius at boundary of Zone I.
RAD (20)	Array of radii ordered from outermost annulus to core.

RDALPH	Angular increment in radians.
REC (700)	Array in memory for reading in tape records.
RL	Inner radius of outermost annulus divided by RA.
RR	Radius subinterval for conductivity calculation.
RW	Ratio of radii of Zone I and Zone II.
SIGINT (20)	$\int_{r_i}^{r_o} \sigma \, r dr$
SIGMA (21)	Input array of electrical conductivity at 1000°K increments (pressure dependent).
SIGSUM	$\int_{o}^{r_a} \sigma \, r dr$
SIGTA	Electrical conductivity at boundary of Zone I.
SINA (7)	Sines of consecutive angle sectors of the quadrant.
SQABS (20)	QABS summed over all wave numbers.
SQEMIT (20)	QEMIT summed over all wave numbers.
SQNET (20)	SQEMIT - SQABS.
SUM	Intermediate value used in several summations.
T(21)	Intermediate temperature for electrical conductivity integral.
TA	Temperature at boundary of Zone I.
TAA	TA/1000 - used in FINANN subroutine.
TCL	Centerline temperature.

TCLL	TCL/1000 - used in FINANN subroutine.
TEMP (20)	Array of annulus temperatures ordered from outermost annulus in to core.
TEMPRW (20)	$\pi \sigma T^4$
TL	Temperature of inner boundary of outermost annulus ($2500^{\circ}K$).
TKDR	Dimensionless transmission length.
TR	Transmission integral for a particular value of TKDR.
TRANS	Transmission function from emitting annulus through absorbing annulus.
TRANS 1	Transmission function from emitting annulus to absorbing annulus.
TT	Outer boundary temperature of annuli in Zone II.
TWALL	Temperature at outside boundary of Zone II (wall temperature).
V	$C_2 n/T = h\nu/k_B T$
V2	V^2
V4	V^4
V6	V^6
VINC	Radius increment for conductivity calculation.
WBB (20, 76)	TEMPRW (N) * ETA
WBBR	WBB (N, I) * RAD (N)
WN (76)	Wave number array.
WNS (10)	Largest wave number of wave number group.

WVNO (20)	Wave number for maximum emission length - associated with given annulus.
XT (88)	Dimensionless absorption length.

Subroutine FINANN

Fortran Name	Definition
C0, C1	Constants for linear interpolation or extrapolation of annulus inner radius from latest two trails.
DRAD	Radius increment.
F(I)	rT^x
FINTG	Integral function.
I	Index on Simpson rule integration.
J	Index used for matching subroutine results to main program.
K	Index for reshuffling RI(K) and TAVG(K) in preparation for new trial. RI(3)→RI(2), RI(2)→RI(1), etc.
L	Iteration index L is incremented 1 during each iteration but also set back one after third and subsequent trials.
LL	Index used for special case of core and innermost annulus.
N	Index on temperature and radius.
NT NTCL	Index on centerline temperature.
R(N)	Radius where temperature is T(N).
RAD(J)	Outside radius of J^{th} annulus in centimeters.
RAD 1	Local radius for integration.

RCK	Annulus outside radius minus RMIN. If RCK does not exceed R(N) then T(N) is skipped and calculation proceeds to next higher temperature level.
RCOL	Arc radius or Zone I radius, r_a.
RI(N)	Annulus inside radius.
RMIN	Minimum permitted value of RO(N) - R(N), set at .025 r_a; also see RCK.
RO(N)	Current value of RAD(J). Both designations used in order of simplify matching of subroutine in ARCRAD III.
SUM 1 SUM 2 SUM 3	Intermediate values in integration.
T(N)	Temperatures at which data are tabulated (divided by 1000°K for the subroutine).
TAVG(L)	Calculated average annulus temperature divided by 1000°K. Must match T(N) $\pm$ TTOL before going to next inner annulus.
TCL	Arc centerline temperature.
TDIFA	Absolute value of TDIF.
TDIF	TAVG(L) - T(N), see TAVG(L)
TDIFF	TCL - T(1), used in calculation of R(N) from profile.
TEMP(J)	T(N)*1000, see ROCM.
TEX	Exponent on temperature in integration, set at 8, see Appendix C.
TRD	Temperature at annulus outside radius calculated from temperature profile.
TTOL	Allowed difference between T(N) and TAVG(L), set at .002.

TXC TXC 1	$T(NTCL)^8$, used for special case of core and innermost annulus.
TXX	T(1), value from main program.
X	Parameter on analytic temperature profile.
Y	Local temperature for temperature average integration.

Subroutine LOOK

Fortran Name	Definition
AINC	Intervals for which F array is tabulated.
FX	Transmission integral for value of X.
FY	Calorimeter transmission integral for value of X.
NY	Integer variable which indexes the nearest tabulated value of F(x) for XT less than or equal to X.
S	Interpolation fraction.
X	Dimensionless absorption length.

B.3 INPUT

1. Tape

   Binary tape contains linear absorption coefficients for temperature 273° and 3000°K - 20,000°K. This is a tape with 19 files, one file per temperature.

2. Cards

   a. number of cases (fixed point)

   b. cards per case

1) identification card

2) NAM 1

TA	zone I boundary temperature
HA	zone I boundary enthalpy
RA	zone I boundary radius
TWALL	temperature at wall
RW	ratio of radii of zone II to zone I
TCL	centerline temperature

3) NAM2

DALPHA	angle difference in degrees of elements of ALPHA array
IPOS	pressure of the case index dependent on pressure used in picking off the proper absorption coefficient
SIGTA	electrical conductivity at zone I boundary

4) NAM3

NIF	number of wave number groups
NALPHA	number of members of ALPHA array
NX1	number of profile parameters to be used in zone I
NX2	number of profile parameters to be used in zone I and zone II

5) NAM4

WNS array of largest wave number of wave number group

6) NAM5

IF index array of wave number group

7) NAM6

EX1 array of profile parameter used for zone I

8) NAM7

EX2 array of profile parameter used for zone I and zone II

9) NAM8

CTEMP array of temperature $0^{\circ}K$ to $20000^{\circ}K$ in $1000^{\circ}K$ increments

10) NAM9

SIGMA array of electrical conductivity data

B.4 FORTRAN LISTING , ARCRAD III AND SUBROUTINES

08/03/66

```
      COMMON ALPHA(6),BCOREC(25),BUFFT(80),CZT(20),COSMA(6),
     1DS(NA(6),FMT(12),PROPT(20,76),REC(700),R(40,40,3),SINA(7),
     2TEMPRM(20),WWB(20,76),WM(76),T(21),FBIGMA(21),CTEMP(21),EIGINT(20)
     3,GCON(21),E(21),PMTINT(20),SIGMA(21),X1(80),F(80,4),WVNO(20),
     4BIG(20),EXDMMX(20,76),QV(10),QNET(20,10),QEMIT(20,10),QABS(20,10),
     5ETASUM(20),SQNET(20),SQEMIT(20),SQABS(20),IF(10),EX1(10),EX2(10),
     6EX(10),WNS(10),QRAD(10),CORAC(10)
      COMMON A0,A1,A2,A3
      COMMON /LABEL/ NT,RAD(20),TEMP(20)
    1 FORMAT(1H1)
    2 FORMAT (12A6)
    3 FORMAT)(I)
    9 FORMAT (9X5HRAD,8X4HTEMP,7X5HQEMT,8X5HQABS,8X5HQNET,9X4HQCON,10
     1X1HE,10X8HPATH(NT)
   10 FORMAT (1H 3(1PE14.7,3X))
   14 FORMAT )1H 1PE12.5,2X,E8.1,2X,8(1PE11.4,2X))
   15 FORMAT (1H09X4HTEMP,13X4HWVNO,11X6HMXEXDB)
   16 FORMAT (1H010X10HCURRENT = 1PE14.7,10X/MEAVB = 1PE14,7)
   17 FORMAT (1H010X9HSIGSUM = 1PE14,7)
   18 FORMAT (1H010X12HDEVIATION = 1PE14,7)
   19 FORMAT (F5.0,E14,7,E14,7,814,7,E14,7)
   20 FORMAT (1H 4HRAD,4X8(E11,4,2X))
   21 FORMAT (1H05X4HTEMP,14X2HBV)
   22 FORMAT (1H 2(1PE14,7,3X))
   23 FORMAT (1H 8X5HWN = F8.0,3X3(1PE11,4,2X))
   24 FORMAT )1H05X4HTEMP,12X6HETASUM)
   25 FORMAT (1H 2(1PE14,7,3X))
   26 FORMAT (1H 2HWN,6X8(F8,0,5X))
   30 FORMAT (1H 5HCORAD,3X8(E11,4,2X))
   31 FORMAT (1H010A8HSGRAD = 1PE14,7,10X9HSCORAD = 1PE14,7)
      NAMELIST /NAM1/ TA,HA,RA,TWALL,RW,TCL/NAM2/TZ,DALPHA,P,IPOS,SIGTA,
     1I)2/NAM3/NIF,NALPHA,NX1,MX2/NAM4 /WN5/NAM5/IP/NAM6/EX1/NAM7/EX2
     2/NAM8/CTEMP/NAM9/SIGMA/NAM10/A0,A1,A2
      IF (SETX)1(2)) 70,726,70                                          2
   70 DO 71 NXX=1,80
   71 READ(5,19) X1(NXX),F(NXX,1),F(NXX,2),F(NXX,3),F(NXX,4)           8
      READ (5,3) NCASE                                                 15
   72 READ (5,2) (FMT(L),L=1,12)                                       17
      CALL SPRNDR (FMT)                                                24
      READ (5,NAM1)                                                    25
      READ (5,NAM2)                                                    26
      READ (5,NAM3)                                                    27
      READ (5,NAM4)                                                    28
      READ (5,NAM5)                                                    29
      READ (5,NAM6)                                                    30
      READ (5,NAM7)                                                    31
      READ (5,NAM8)                                                    32
      READ (5,NAM9)                                                    33
      READ (5,NAM10)                                                   34
      WRITE (6,NAM1)                                                   35
      WRITE (6,NAM2)                                                   36
      WRITE (6,NAM3)                                                   37
      WRITE (6,NAM4)                                                   38
      WRITE (6,NAM5)                                                   39
      WRITE (6,NAM6)                                                   40
```

08/03/66

MAIN - EFN SOURCE STATEMENT - IFN(S) -

```
      WRITE )6,NAM7)                                                   41
      WRITE (6,NAM8)                                                   42
      WRITE (6,NAM9)                                                   43
      WRITE (6,NAM10)                                                  44
      I(21=1)2=1
      A3=A0=A1=10.=A2=100.
      M01V=11
      MM=75
      NWBCD=0
      IF (RREAD (10,BCUREC,NWBCD))75,74,75                             50
   74 CALL ERROR (3,18HEOF WHILE READ REC)                             53
   75 NWBIN=0
      IF (RREADB (10,MM,N=BIN))76,76,76                                56
   76 NWBIN=0
      IF )RREADB(10,REC,NWBIN))77,76,77                                60
   77 NWBIN=0
      IF (RREADB(10,REC,NWBIN)) 78,74,76                               64
   78 CALL CLOSE (10)                                                  67
      CALL RETP )10)                                                   69
      IPST=4
      TEMP(1)=273.
      RAD(1)=RA=RW
      TT=1500.
      DO 80 N=2,1121
      TT=TT-1000.
      IF(TEMP(N)=TT=500.
   80 RAD(N)=RA=(1.-((TT-TA)/(TWALL-TA))=(RW-1.))
      RL=RAD(2)/RA
      TL=2500.
      CONST=P=((2.=273.16)/(TL-TWALL))=((RW-RL)/(RW=RL))
     1=((TL/(TL-TWALL))=(RL/(RW-RL))=ALOG(TL/TWALL)-1.))              80
      DO 79 I=1,25
      PROP(1,I)=CONST=REC(IPST)
   79 IPST=IPST+6
      RDALPH=DALPHA=1.7453292E-2
      NANGLE=NALPHA+1
      ANGLE=0.
      SINA(1)=0.
      DO 190 NA=2,NANGLE
      ANGLE=ANGLE=RDALPH
      SINA(NA)=SIN(ANGLE)                                              94
  190 DSINA(NA-1)=SINA(NA)-SINA(NA-1)
      ALPHA(1) = RDALPH/2.
      COSNA(1) = COS(ALPHA(1))                                         102
      DO 200 NA=2,NALPHA
      ALPHA(NA)=ALPHA(NA-1)+RDALPH
  200 COSNA(NA)=COS(ALPHA)NA))                                         110
      IZONE=0
      IN=)2
      IN1=)N+1
      NB=)121
      NC=)12
      MX=NX1
      DO 205 I=1,MX
  205 EX)IX)=EX1(IX)
  210 DO 719 I=1,MX
```

B.4 FORTRAN LISTING, ARCRAD III AND SUBROUTINES (Cont'd)

```
      MAIN      - EFN  SOURCE STATEMENT  - IFN(S) -  08/03/00

      TAA=T4/1000.
      T22=T2/1000.
      TCLL=TCL/1000.
      CALL FIN4NN (TAA,T22,I121,TCLL,EX(IX),RA)                          135
      NT2=2*NT
      NT22=NT2-NW
      NT1=NT-1
      NT21=NT2-NG
      DO 241 N=1,NT
      TEMPRM(N)=(TEMP(N)**4)*5.6856E-12+6.2631853
  241 C2T(N)=1.438/TEMP(N)
      DO 320 N=1,NT2
      DO 320 NJ=1,NT2
      DO 320 NA=1,NALPHA
  320 R(N,NJ,NA)=0.
      DO 350 N=1,NT1
      N1=N+1
      DO 350 NA=1,NALPHA
      AINT=RAD(N)*COSNA(NA  )
      DO 350 NJ=1,N1
  350 R(N,NJ,NA)=-AINT+(AINT**2+(RAD(NJ)**2-RAD(N)**2))**.5          90  173
      DO 400 N=NT1,NT22
      N3=NT2-N+1
      N32=N3-1
      DO 400 NA=1,NALPHA
      AINT=RAD(N3)*COSNA(NA)
      DO 375 NJ=1,N3
      BINT=AINT**2+(RAD(NJ)**2-RAD(N3)**2(
      BINT=BINT**.5                                                  71  192
      R(N,NJ,NA)=AINT-BINT
  375 CONTINUE
      IF (N32-NT1) 380,400,400
  380 DO 390 NJ=N31,NT
      BINT=AINT**2+(RAD(NJ)**2-RAD(N3)**2)
      IF (BINT) 400,388,385
  385 BINT=BINT**.5                                                  85  206
  388 R(N,NJ,NA)=AINT-BINT
      NJ2=NT2-NJ+1
      R(N,NJ2,NA)=AINT-BINT
  390 CONTINUE
  400 CONTINUE
      DO 410 N=1,NT
      DO 410 I=1,NW
  410 NBB(N,I)=0.
      NWRCD=0
      IF (BREAD(10,BCOREC,NWBLD1) 415,411,415                        225
  411 CALL ERROR (3,18HEOF WHILE READ REC)                           228
  415 DO 420 I=1,NB
      N=BIN=0
      IF (BREADB(16,REC,NWB(N))420,414,420                           233
  414 CALL ERROR (3,18HEOF WHILE READ REC)                           234
  420 CALL CLOSE(10)                                                 238
      IF (IZONE-1) 413,412,413
  412 INN=2
      GO TO 425
  413 INN=12
```

```
      MAIN      - EFN  SOURCE STATEMENT  - IFN(S) -  08/03/00

  425 DO 440 N=INN,NT
  426 NWB(N)=0
      IF (BREADB(16,REC,NWB(N)) 431,432,431                          290
  432 CALL ERROR (3,18HEOF WHILE READ REC)                           293
  431 IF (ABS(TEMP(N)-REC(1))-1.E-4) 433,433,4315
 4315 CALL CLOSE (16)                                                298
      GO TO 428
  433 NWB(N)=0
      IF (BREADB(16,REC,NWB(N)) 434,432,434                          302
  434 IPST=IPOB
      DO 437 I=1,75
      PROPIN,I)=REC(IPST)
  437 IPST=IPST+9
  440 CALL CLOSE (16)                                                274
      DO 445 N=1,NT
  445 ETASUM(N)=0.
      DO 461 N=INN,NT
      IW=1
  446 Y=C2T(N)*WN(IW)
      IF (Y-.2) 448,449,449
  448 IW=IW+1
      GO TO 446
  449 IF (IW-1) 450,4495,450
 4495 Y=C2T(N)*WN(1)
      I1=2
      GO TO 451
  450 Y=C2T(N)*WN(IW-1(
      I1=IW
  451 V2=V*V
      V4=V2*V2
      V8=V4*V4
      DL=1.-.1939897*(Y**3)*(.33333333-Y/8.+Y2/80.-Y4/5040.+
     1Y6/272160.)
      DO 460 I=I1,76
      Y=C2T(N)*WN(I)
      IF (Y-1.) 4505,4505,452
 4505 V2=V*V
      V4=V2*V2
      V6=V4*V2
      DM=1.-.1939897*(Y**3)*(.33333333-Y/8.+Y2/80.-Y4/5040.-Y6/272160.)
      ETA=DL-DM
      DL=DM
      GO TO 455
  452 DSUM=0.
      AM=0.
      DO 454 J=1,4
      AM=AM+1.
  454 DSUM=DSUM+((EXP(-AM*Y))/AM)**4)*(((AM*Y+3.)*AM*Y+8.)*AM*Y+6.)  310
      DM=DSUM*.1539897
      ETA=DL-DM
      DL=DM
  455 NWB(N,I-1)=ETA*TEMPRM(N)
      ETASUM(N)=ETASUM(N)+ETA
      IF (Y-19.) 460,461,461
  460 CONTINUE
  461 CONTINUE
```

```
08/03/66
      MAIN      - EFN   SOURCE STATEMENT  - IFN(S) -
      DO 463 I=1,NW
      DO 463 M=1,NT
  463 EKORM(M,I)=0.
      DO 465 M=1,NT
      BIG(M)=0.
  465 WYNO(M)=0.
      DO 467 M=1,NT
      DO 467 IN=1,NIF
      QEMIT(M,IR)=0.
      QABS(M,IR)=0.
  467 QNET(M,IR)=0.
      DO 468 IR=1,NIF
      CQRAD(IR)=0.
  468 QRAD(IR)=0.
      DO 9355 N=1,NT
      N1=N-1
      NS=NT2-N+1
      NF=NS+1
      DO 9355 NA=1,NALPHA
      IF (R(NS,NF,NA))  731,510,515
  510 NF=NT2-N
  515 DO 9355 IR=2,NIF
      NM=IF(IR-1)=1
      NMF=IF(IR)
      DO 9355 I=NM,NMF
      WBBR=WBB(N,I)=RAD(M)
      EKOR=R(NS,NF,NA)*PROP(N,I)
      IF (NA-1) 730,516,917
  516 EKORMX(N,I)=EKOR
  917 CALL LOOK (EKOR,EM,CEM)                                          379
      TRANS1=1.-EM
      CTRANS=1.-CEM
 9175 QEMIT(N,IR)=QEMIT(N,IR)+WBBR*OS(NA(NA)*TRANS1
      IF (N1-1) 518,520,920
  518 TRANS=TRANS1
      GO TO 939
  520 TKOR=0.
      DO 930 NQ=1,N1
      NQ=N-NQ
      TKOR=TKOR+(R(N,NQ,NA)-R(N,NQ+1,NA))*PROP(NQ,I)
      ETKOR=EKOR
      CALL LOOK (TKOR,TM,CTR)                                          395
      CALL LOOK (ETKOR,EM,CEM)                                         397
      TRANS=TR-EM
      CTRANS=CTR-CEM
  930 QABS(NQ,IR)=QABS(NQ,IR)+WBBR*OS(NA(NA)*(TRANS1-TRANS)
  939 TRANS1=TRANS
  935 QRAD(IR)=QRAD(IR)+WBBR*OS(NA(NA)*TRANS
 9355 CQRAD(IR)=CQRAD(IR)+WBBR*OS(NA(NA)*CTRANS
      DO 6001 M=NT1,NT21
      NS=N(2-N+1
      DO 6001 NA=1,NALPHA
      DO 6001 IR=2,NIF
      NN1=IF(IR-1)+1
      NMF=IF(1)
      DO 600 I=NM,NMF
```

```
08/03/66
      MAIN      - EFN   SOURCE STATEMENT  - IFN(S) -
      WBBR=WBB(NS-1,I)*NA0(NB)
      ITEST=0
      EKOR=R(NS,NS-1,NA)*PROP(NS-1,I)
      CALL LOOK (EKOR,EM,CEM)                                          436
      TRANS1=1.-EM
      QEMIT(NS-1,IR)=QEMIT(NS-1,IR)+WBBR*OS(NA(NA)*TRANS1
      TKOR=0.
      INF=N
      NF=N-1
  530 IF(R(N,NF,NA)) 731,540,537
  537 IF(NF-NT) 544,544,542
  542 NA=NT2-NF
      GO TO 546
  540 ITEST=1
      NF=NT2-N
  544 NA=NF
  546 TKOR=TKOR+(R(N,NF,NA)-R(N,INF,NA))*PROP(KA,I)
      ETKOR=(KOR+EKOR
      CALL LOOK (TKOR,TM,CTR)                                          456
      CALL LOOK (ETKOR,EM,CEM)                                         458
      TRANS=TM-EM
      CTRANS = CTR-CEM
  548 QABS(KA,IR)=QABS(NA,IR)+WBBR*OS(NA(NA)*(TRANS(-TRANS)
      TRANS1=TRANS
      IF (NF-(N) 731,600,550
  550 INF=NF
      NF=NF-1
      IF(ITEST-1( 536,544,762
  600 QRAD(IN)=QRAD(IR)+WBBR*OS(NA(NA)*TRANS
 6001 CQRAD(IN)=CQRAD(IN)+WBBR*OS(NA(NA(=CTRANS
      DO 6005 N=1,NT
      SQNET(N)=0.
      SQEMIT(N)=0.
 6005 SQABS(N)=0.
      DO 601 N=1,NT
      DO 601 IR=2,NIF
      QNET(N,IR(=QEMIT(N,IR)-QABS(N,IR)
      SQNET(N)=SQNET(N)+QNET(N,IR)
      SQEMIT(N)=SQEMIT(N(+QEMIT(N,IR)
  601 SQABS(N)=SQABS(N)+QABS(N,IR(
      SQRAD=0.
      SCQRAD=0.
      DO 6015 N=2,NIF
      SQRAD=SQRAD+QRAD(IR)
 6015 SCQRAD=SCQRAD+CQRAD(IR)
      DO 603 N=1,NT
      DO 603 I=1,N
      IF(BIG(N(-EKORMX(N,I)) 602,603,603
  602 BIG(N)=EKORMX(N,I(
      WYNO(N(=N(I)
  603 CONTINUE
      WRITE ( 8,1(                                                     527
      WRITE (6,15)                                                     529
      DO 604 N=1,NT
  604 WRITE( 6,10) TEMP(N),WYNO(N(,BIG(N)                              531
      WRITE (6,24)                                                     533
```

B.4 FORTRAN LISTING, ARCRAD III AND SUBROUTINES (Cont'd)

```
      MAIN      - EFN  SOURCE STATEMENT  - IFN(S) -                    08/03/68
      DO 6045 N=1,NT
 6045 WRITE (6,25) TEMP(N),ET*SUM(N)                                    939
      IF (IN-1) 733,605,610
  605 WRITE (6,1)                                                       943
      WRITE (6,21)                                                      944
      DO 606 N=1,IIZI
      QV(N)=(ESQNET(N))/(1)RAD(N)**2-RAD(N*1)**2)*3.1415926)
  606 WRITE (6,22) (EMP(N),QV(N)                                        953
  610 NP=NDIV/2-1
      DIV=NDIV-1
      T(NDIV)=14
      FSIGMA(NDIV)=SIBTA
      J=1
      DO 705 N=1,2,NT
      T(1)=T(NDIV)
      FSIGMA(1)=SIGMA(NDIV)
      VINC=(RAD(N)-RAD(N*1))/DIV
      RR=RAD(N)
      DO 600 I=2,NDIV
      RR=RR+VINC
      T(I)=TA*(TCL-TA)*(1.-(RR/RA)**EX(IX))                             971
  681 IF (CTEMP(J)- T(I))682,686,684
  682 J=J-1
      GO TO 681
  684 CNT=(ALOG(T(I))-ALOG(CTEMP(J-1)))/(ALOG(CTEMP(J))-ALOG(CTEMP(J-1)
     1))
      FSIGMA(I)=(EXP((ALOG(SIGMA(J)/SIGMA(J-1)))*PCNT+ALOG(SIGMA(J-1)(
     1))*RR                                                             982
      GO TO 686                                                         984
  686 FSIGMA(I)=SIGMA(J)=RR
  690 CONTINUE
      SUM=0.
      DO 695 I1=1,NP
  695 SUM=SUM+6.*FSIGMA(2*I1)*2.+FSIGMA(2*I1+1)
  700 SIDIN(N)=V(NC-(5)SIGMA(1)*SUM+4.*FSIGMA(NDIV-1)+FSIGMA(NDIV)/(/3.
      ESUM=0.
      SIGSUM=0.
      QCONA=3.1415926*1.3333333*82.68*1.556-4*(HA)**1.5/(ALOG(RW))      812
      DO 715 N=1,NT
      QCON(N)=WCONA*((R*D(N)/HA)**2-(RADIN=1)/RA)**2(
      QCOR=SQNET(N)-QCON(N)
      IF (QCOR) 711,713,714
  711 E(N)=0.
      GO TO 712
  714 E(N)=(WCOR/(0.2831853*SIG(NT(N)))**.5                             827
  715 SIGSUM=SIGSUM+SIG)NT(N)
      DEV=0.
      DO 716 N=1,2,NT
      PRT)NT(N)=SIG)NT(N)/SIGSUM
  716 ESUM=ESUM+E(N)**2*PRT)NT(N)
      EAVG=ESUM=0.5                                                     841
      DO 7165 N=1,2,NT
 7165 DEV=DEV+ (E(N)-EAVG)**2*PRT)NT(N)
      DEV=DEV**.5                                                       848
      CURRNT=6.2831853*EAVG*SIGSUM
      WRITE (6,1)                                                       849
```

```
      MAIN      - EFN  SOURCE STATEMENT  - IFN(S) -                    08/03/68
      WRITE (6,8)                                                       850
      DO 718 N=1,NT
      WRITE (6,14) RAD(N),TEMP(N),SQEMIT(N),SQABS(N),SQNET(N),QCON(N),
     1E(N),PRTINT(N)                                                    852
      DO 717 IN=2,NIF
  717 WRITE (6,23) WNS((R(,QEMIT(N,IR),QABS(N,IR),QNET(N,IR)            864
  718 CONTINUE
      WRITE (6,20)(WNS(IR),IR=2,NIF)                                    870
      WRITE (6,30) (QRAD)(N),IR=2,NIF)                                  875
      WRITE (6,30) (QCRAD(IR),IR=2,NIF)                                 880
      WRITE (6,31) SQRAD,SCQRAD                                         885
      WRITE(6,16) CURRNT,EAVG                                           886
      WRITE(6,17) SIGSUM                                                887
      WRITE (6,18) DEV                                                  888
  719 CALL REWIP(10)                                                    890
      IZONE=IZONE+1
      IF (IZONE-1) 733.,720.72N
  720 NX=NX2
      DO 721 IA=1,NX
  721 EX(IX)=EXZ(IX)
      IN=1
      IN1=IN+1
      NB=0
      NC=1
      GO TO 210
  726 NCASE=NCASE-1
      IF (NCASE) 730,740,727
  727 GO TO 72
  730 CALL ERROR (3,18HNCASE OUT OF LIMIT)                              715
  731 CALL ERROR (2,12HRAD NEGATIVE)                                    717
  732 CALL ERROR (2,12H ITEST WRONG)                                    719
  733 CALL ERROR (2,12H IZONE WRONG)                                    721
  734 CALL ERROR (2,12H IN NEGATIVE)                                    723
  735 CALL ERROR (2,12HIYTEST WRONG)                                    725
  740 CALL RUN)IP(10)                                                   727
      STOP
      END
```

```
ANNUL  - EFN  SOURCE STATEMENT - IFN(S) -                    08/03/66

      SUBROUTINE FINANN (TXX,T22,T(21),TCL,X,NCOL)
      COMMON /LABEL/NT,RAD(20),TEMP(20)
      DIMENSION T(24),ND(24),R(24),TAVG(3),F(17),R(24)
    3 FORMAT (1H0,5X4HTCL=F5.1,2X2HX=F6.2,2X6HDELTA=F9.2,2HCM)
    7 FORMAT (1H1)
    8 FORMAT (1H 2XF5.1,1XF9.3,1XF9.3)
    9 FORMAT (1H0,4X4HITEMP    RADIUS  RO/DELTA  RO(CM)    T(ND))
  201 FORMAT (1H 4XF5.1,2XF7.4,2XF7.4,2XF7.4,2XF7.3)
      T(2)=T22
      N=2
   15 N=N+1
      T(N)=T(N-1)+1.
      IF (TCL-T(N)) 20,20,15
   20 NTCL=N
      LL=0
      TDIFF=TCL-T(1)
      I=NTCL-1
      DO 30 N=1,NTCL
   30 RO(N)=0.
      DO 100 N=1,I
      R(N)=(1.-(T(N)-T(1))/TDIFF)**(1./X)                          32
  100 WRITE (6,281) T(N),R(N)                                      34
      R(NTCL)=0.
      RCK=R(1)-RMIN
      N=1
  200 N=N+1
      IF (RCK-R(N))200,201,201
  201 RO(N)=1.
      IF (NTCL-N-1) 267,267,202
  202 L=0
      RI(1)=R(N)
  205 L=L+1
  210 DRAD=(RO(N)-RI(L))/10.
      RAD1=RI(L)
      DO 220 I=1,11
      Y=T(1)-TDIFF*(1.-RAD1**X)                                    58
      F(I)=Y**(EX-RAD1                                             59
  220 RAD1=RAD1+DRAD
      SUM1=F(1)+F(11)
      SUM2=F(2)+F(4)+F(6)+F(8)+F(10)
      SUM3=F(3)+F(5)+F(7)+F(9)
      FINTG=.66666667*DRAD*(SUM1+4.*SUM2+2.*SUM3)
      IF(ILL) 1000, 227, 274
  227 TAVG(L)=(FINTG/(RO(N)-RI(L)))**(1./EX)                       70
  229 IF(L-2) 230, 240, 250
  230 RI(2)=R(N-1)
      GO TO 205
```

```
ANNUL  - EFN  SOURCE STATEMENT - IFN(S) -                    08/03/66

  240 C1=(TAVG(L-1)-TAVG(L))/(RI(L-1)-RI(L))
      C0=TAVG(L-1)-C1*RI(L-1)
      RI(3)=(T(N)-C0)/C1
      IF(RI(3))    249, 205, 242
  242 IF(RI(N)-RI(3)) 248,246,205
  246 RI(3)=(RI(N)+RI(2))/2.
      GO TO 205
  248 RI(3)=0.
      GO TO 205
  250 TDIF=TAVG(L)-T(N)
      IF(RI(3)) 254, 254, 258
  254 IF(TDIF) 269, 258, 258
  258 TEMP=SQRT (TDIF*TDIF)                                        101
      IF(TEMP-TTOL) 262, 262, 260
  260 DO 261 K=1, 2
      TAVG(K)=TAVG(K-1)
  261 RI(K)=RI(K+1)
      L=L-1
      GO TO 240
  262 RCK=RI(3)-RMIN
      IF(RCK-RI(NTCL-2)) 266, 265, 265
  265 N=N-1
      IF(RCK-RI(N)) 263, 265, 269
  269 RO(N)=RI(3)
      GO TO 202
  266 IF(RI(3)-RI(NTCL-1)) 267, 269, 269
  267 RI(3)=RO(N)
      RO(N)=0.
  268 N=NTCL-1
      RO(N)=RI(3)
      LL=1
      L=1
      RI(1)=0.
      GO TO 210
  274 TXC=T(NTCL)**TEX                                             139
      TXC1=T(N)**TEX                                               141
      RO(NTCL)=SQRT ((1.)(NTG-TXC)*RO(N)*RO(N))/(TXC-TXC1))        144
      IF(1.-RO(NTCL)-RMIN) 275, 280, 280
  275 RO(NTCL)=1.
      RO(NTCL-1)=0.
  280 WRITE (6,3) TCL,X,RCOL                                       151
      WRITE (6,9)                                                  152
      J=I-2
      N=2
  285 IF (RO(N)) 1000,296,295
  295 ROCM=RO(N)*RCOL
      TRO=T(1)-TDIFF*(1.-RO(N)**X)
      WRITE (6,281) T(N),R(N),RO(N),ROCM,TRO                       160
                                                                   161
      J=J+1
      TEMP(J)=T(N)*1000.
      RAD(J)=ROCM
  296 N=N+1
      IF (NTCL-N) 301,295,285
 1000 CALL EXIT                                                    173
  301 NT=J
      RETURN
      END
```

B.4 FORTRAN LISTING, ARCRAD III AND SUBROUTINES (Cont'd)

```
*INTP      - 6FN   SOURCE STATEMENT - IFN(S) -                    08/03/66

      SUBROUTINE LOOK (X,FX,FY)
      COMMON ALPHA(6),BCORREC(25),BUFFT(86),C2T(20),COSNA(6),
     1DSINA(6),FMT(12),PROP(20,76),REC(700),W(40,40,3),SINA(7),
     2TEMPRW(20),WBB(20,76),WN(76),T(21),FSIGMA(21),CTEMP(21),SIGINT(20)
     3,GCON(21),E(21),PRTINT(20),SIGMA(21),XT(88),F(88,4),WVNO(20),
     4BIG(20),BKURMX(20,76),QV(10),QNET(20,10),QEMIT(20,10),QABS(20,10),
     5ETASUM(20),SQNET(20),SQEMIT(20),SQABS(20),IF(10),EX1(10),EX2(10),
     6EX(10),WNS(10),QRAD(10),CQRAD(10)
      COMMON A0,A1,A2,A3
      IF (X-.2) 20,20,5
    5 IF (X-1.) 30,30,10
   10 IF (X-6.) 40,40,15
   15 IF (X-14.) 50,50,70
   20 AINC=.02
      NX=1.+X/AINC
   25 S=(X-X1(NX))/AINC
      FX=F(NX,1)+(S-.5)*F(NX,2)+.5*(S-1.)*F(NX,3)+S*(S-1.)*(S-.5)*F(NX,4)
      IF (X-10.) 26,26,27
   26 FY=(A0+A1*X+A2*X**2)*FX
      GO TO 28
   27 FY=A3*FX
   28 RETURN
   30 AINC=.05
      NX=X/AINC+8.
      GO TO 25
   40 AINC=.1
      NX=X/AINC+10.
      GO TO 25
   50 AINC=1.
      NX=X/AINC+74.
      S=(X-X1(NX))/AINC
      FX=EXP(F(NX,1)+(S-.5)*F(NX,2)+S*(S-1.)*F(NX,3)+S*(S-1.)*(S-.5)*
     1F(NX,4))                                                        32
      IF (X-10.) 55,55,57
   55 FY=(A0+A1*X+A2*X**2)*FX
      GO TO 58
   57 FY=A3*FX
   58 RETURN
   70 FX=0.
      RETURN
      END
```

APPENDIX C
ANNULUS BOUNDARIES

C.1 WEIGHTED AVERAGE TEMPERATURE

In order to avoid interpolation of absorption coefficients for temperature, the boundaries of each annulus were so calculated that the weighted average annulus temperature was an exact multiple of 1000°K. The FINITE ANNULUS computer program to accomplish this was an improved version of the ANALYTIC TEMPERATURE PROFILE program described in Appendix B of Ref. Ma. 1. FINITE ANNULUS was developed in its present form on the small computer but eventually incorporated into the main program. Even though the arc as a whole is not optically thin, the assumption that radiation from an individual annulus varies as the product of annulus volume and T^y is reasonable. Thus the weighted average temperature of annulus i can be defined as

$$T_i = \frac{2}{(r_i)^2 - (r_i+1)^2} \left[\int_{r_{i+1}}^{r_i} \left[T(r)\right]^y \, r\,dr \right]^{1/y} \qquad (C.1)$$

The exponent on T was determined by comparing curves of T^y for values of y from 4 to 10 with curves of pressure-dependent total radiance which had been cross-plotted from density-temperature results of Nardone, et. al. (Na. 1). No single exponent matches all the curves, of course, but the best fit is in the range from 7 to 9 and numerical calculations showed that results are insensitive to choice of y, Table C. 1. The exponent was therefore arbitrarily fixed at 8. The calculation is started at the outer boundary (i = 1) where temperature and radius are presumed known, and proceeds inward to the centerline.

TABLE C.1

COMPARISON OF CALCULATED ANNULUS RADII FOR SEVERAL VALUES OF TEMPERATURE EXPONENT ($x = 4$, $r_a = 1$ cm, $T_c = 14{,}000°K$)

T(°K)	5000	7000	9000	11000	13000	14000
z						
7	.9293	.8847	.8200	.7451	.6305	.3805
8	.9311	.8847	.8212	.7454	.6319	.3822
9	.9325	.8850	.8222	.7458	.6330	.3842
% Variation	.3%	.05%	.3%	.1%	.4%	1%

Since the desired values of T_i are predetermined, the unknown is the inner radius of the annulus, r_{i+1}. Annulus radius appears both explicitly and as a limit of integration, and must therefore be found by iteration as described in Ref. Ma. 1. The procedure involves selection of two trial values, interpolation (or extrapolation) to a third trial value and, if necessary, repetition of the interpolation step using results of the latest two trials until T_i matches its preselected value within $\pm 2^{\circ}K$.

In FINITE ANNULUS an exception was made for the core and innermost annulus. Equation C. 1 was modified to

$$(T_N)^y (r_N{}^2) + (T_{N-1})^y (r_{N-1}{}^2 - r_N{}^2) = 2 \int_o^{r_{N-1}} \left[T(r)\right]^y r \, dr \qquad (C.2)$$

where subscript N refers to the core. For this special case the core radius, r_N, only appears explicitly and can be solved for without iteration.

A minimum annulus thickness was also established. If a calculated annulus thickness was less than 5% or r_a, that average temperature was automatically omitted and the annulus volume included in the next higher temperature step. A listing of the FINITE ANNULUS program is included in Appendix B as subroutine FINANN of ARCRAD III.

C.2 OUTERMOST ANNULUS

Below $3000^{\circ}K$ radiant emission from the arc is totally negligible. However, absorption of vacuum ultra violet radiation is still very important. This absorption is proportional to particle density, so it is convenient to compute an average particle density for the outside annulus in Zone II, where the temperature ranges from $2500^{\circ}K$ at the inner boundary to the assumed wall temperature of $500^{\circ}K$.

By assumption, the temperature profile in this region is linear.

$$T = T_L + \frac{r - r_L}{r_W - r_L} \left[T_W - T_L\right] \qquad (C.3)$$

Subscripts L and W refer to values at the inner and outer radii, respectively.

The average particle density is given by

$$\overline{N} = \frac{N}{V} = \frac{Lo}{V} \int_V (\rho/\rho_o) \, dV \qquad (C.4)$$

where Lo is the Loschmidt Number ($2.69 \times 10^{+19}$ particles/cm^3 at STP). Assuming that air at these temperatures is a perfect gas, and making use of the cylindrical geometry

$$\overline{N} = \frac{Lo\left(\frac{p}{p_o}\right)To}{(r_W^2 - r_L^2)} \int_{r_L}^{r_W} \frac{r\,dr}{T} \tag{C.5}$$

With equation C.3 this integrates to

$$\overline{N} = 2\,Lo\left(\frac{p}{p_o}\right)\left(\frac{To}{T_L - T_W}\right)\left(\frac{r_W - r_L}{r_W + r_L}\right)\left\{\left[\left(\frac{T_L}{T_L - T_W}\right) + \left(\frac{r_L}{r_W - r_L}\right)\right]\left[\ln\left(\frac{T_L}{T_W}\right)\right] - 1\right\} \tag{C.6}$$

Absorption coefficients are then directly calculated from values tabulated for density corresponding to STP

$$k = (k)_{STP}\, X_i\, \frac{\overline{N}}{Lo} \tag{C.7}$$

where X_i is the mol fraction of species i (O_2, N_2 or NO).

APPENDIX D
TOTAL RADIATION CALORIMETER MODIFICATION TO RADIANT INTERCHANGE EQUATIONS

The sensing element of the calorimeter designed for measurements of total radiation was ring shaped to maintain rotational symmetry. However, in order to minimize the effect of thermal conduction, the ring was recessed and therefore exposed only to a relatively short length of the arc.

Applying the radiant interchange integral, Eq. (2.15), to this situation, integration in the ϕ direction is unchanged but now both the upper and lower limits of the θ integral are functions of axial position, z, and an axial integration is necessary. Fig. 44.

$$\left(\frac{q}{z}\right)^{t}_{n,m} = (2\pi r_j)(\sigma T^4)\left[D(n) - D(n+\Delta n)\right]\left[\sin\left(\phi + \frac{\Delta\phi}{2}\right) - \sin\left(\phi - \frac{\Delta\phi}{2}\right)\right]$$

$$\frac{2}{\pi}\int_{-\left(\frac{z}{h}\right)_{max}}^{0}\int_{\alpha\left(\frac{z}{h}\right)}^{\beta(z/h)}\left[e^{-(k\bar{R})_t/\sin\theta} + e^{-\left[(k\bar{R})_t + (k\bar{R})_e\right]/\sin\theta}\right]$$

$$\sin^2\theta\, d\theta\, d\left(\frac{z}{h}\right) \qquad (D.1)$$

Here h is the half width of the calorimeter ring and $(z/h)_{max}$ is the greatest relative axial displacement at which any part of the calorimeter sensing surface is visible. Definition of half-width and choice of negative (z/h) were made for convenience in working with the angle variables. The former changes the symmetry factor on the integral from 4 in Eq. (2.15) to 2 in Eq. (D.1).

The dependence of limits α and β on (z/h) is illustrated in Fig. 44. Two cases are distinguished, one where the shield overlaps the sensing ring and one where it does not. In both cases the axial integration is divided into 3 zones and, for each zone, the angle limits are given in Table D.1 in terms of their tangents.

As before, the integral can be written as the sum of two integrals identical in form

$$f_c(x) = \frac{2}{\pi}\int_{(z/h)_{max}}^{0}\int_{\alpha(z/h)}^{\beta(z/h)} e^{-x/\sin\theta}\sin^2\theta\, d\theta\, d(z/h) \qquad (D.2)$$

The required double numerical integration was carried out on a digital computer. For the geometries of interest, the value of the integral turns out to be nearly independent of the location of the radiating surface relative to constrictor wall (dimension b, Fig. 44). Therefore the ratio of the calorimeter integral to the complete integral, Eq. (2.16), is plotted in Fig. 45 as a function of absorption length only. A polynomial was fitted to this curve so that radiation reaching the calorimeter could be computed as an extra step in the ARCRAD III program. The ratio of the summation over all annuli and all frequencies of radiation reaching the calorimeter to the equivalent summation of radiation leaving the arc is the term ζ in Eq. (4.1).

TABLE D.1

TANGENTS OF INTEGRATION LIMIT ANGLES α and β (See Fig. 44)				
	All Zones	Zone 1	Zone 2	Zone 3
$s \geq 0$	$\tan \alpha = \frac{b + g}{-z + h}$	$\tan (\pi - \beta) = \frac{b + g}{z + h}$	$\tan \beta = \frac{b + g}{-h - z}$	$\tan \beta = \frac{b}{-z - h - s}$
$s < 0$	$\tan \alpha = \frac{b + g}{-z + h}$ or $\tan \alpha = \frac{b}{-z + h + s}$ whichever is larger	$\tan (\pi - \beta) = \frac{b + g}{z + h}$	$\tan (\pi - \beta) = \frac{b}{h + s + z}$	$\tan \beta = \frac{b}{-z - h - s}$

Note: $-z$ is a positive number since integration is from $-(z/h)_{max}$ to zero.

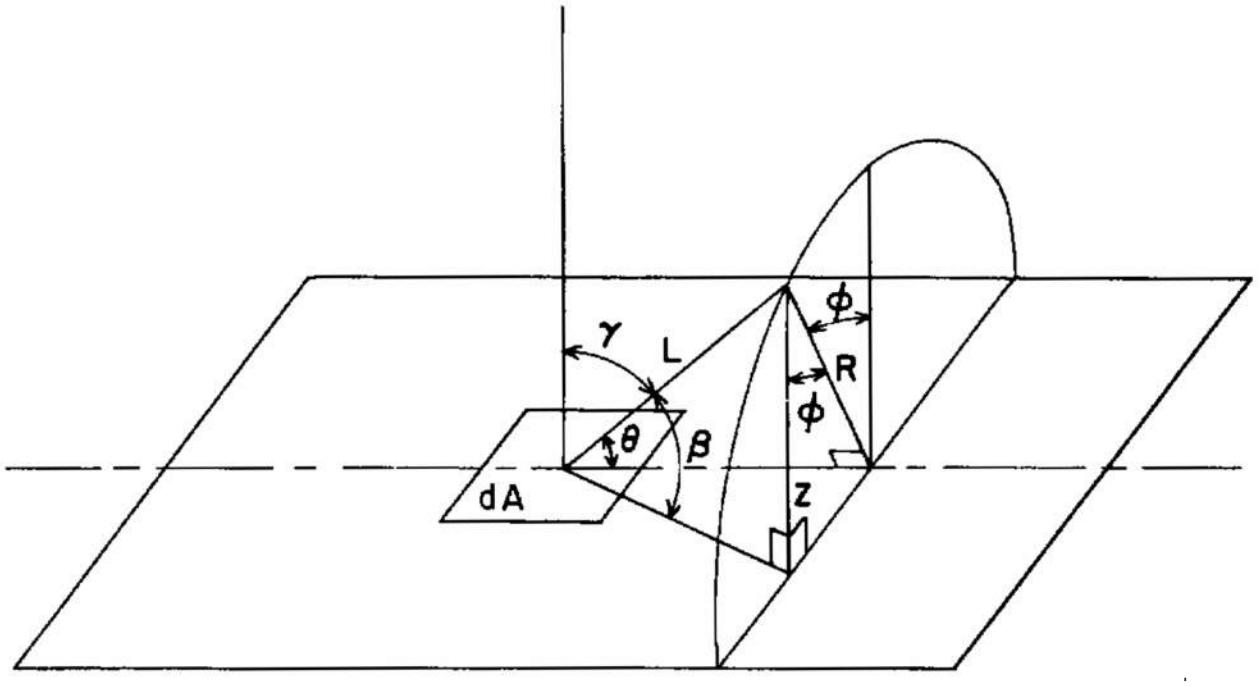

AI01A875

a. Geometry

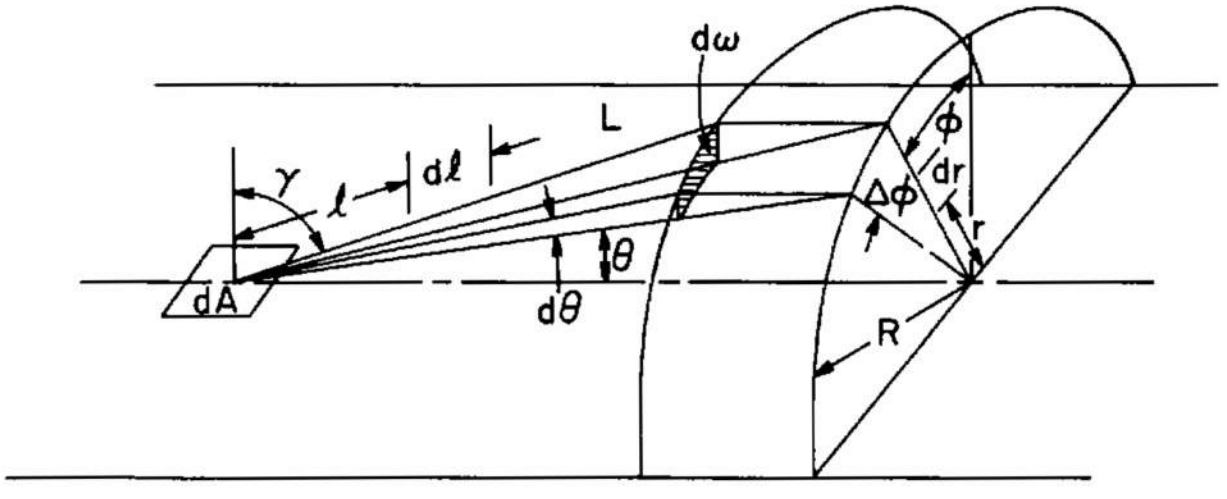

b. Typical Absorption Path

Fig. 1 Absorption by an Infinitely Long Half-Cylinder

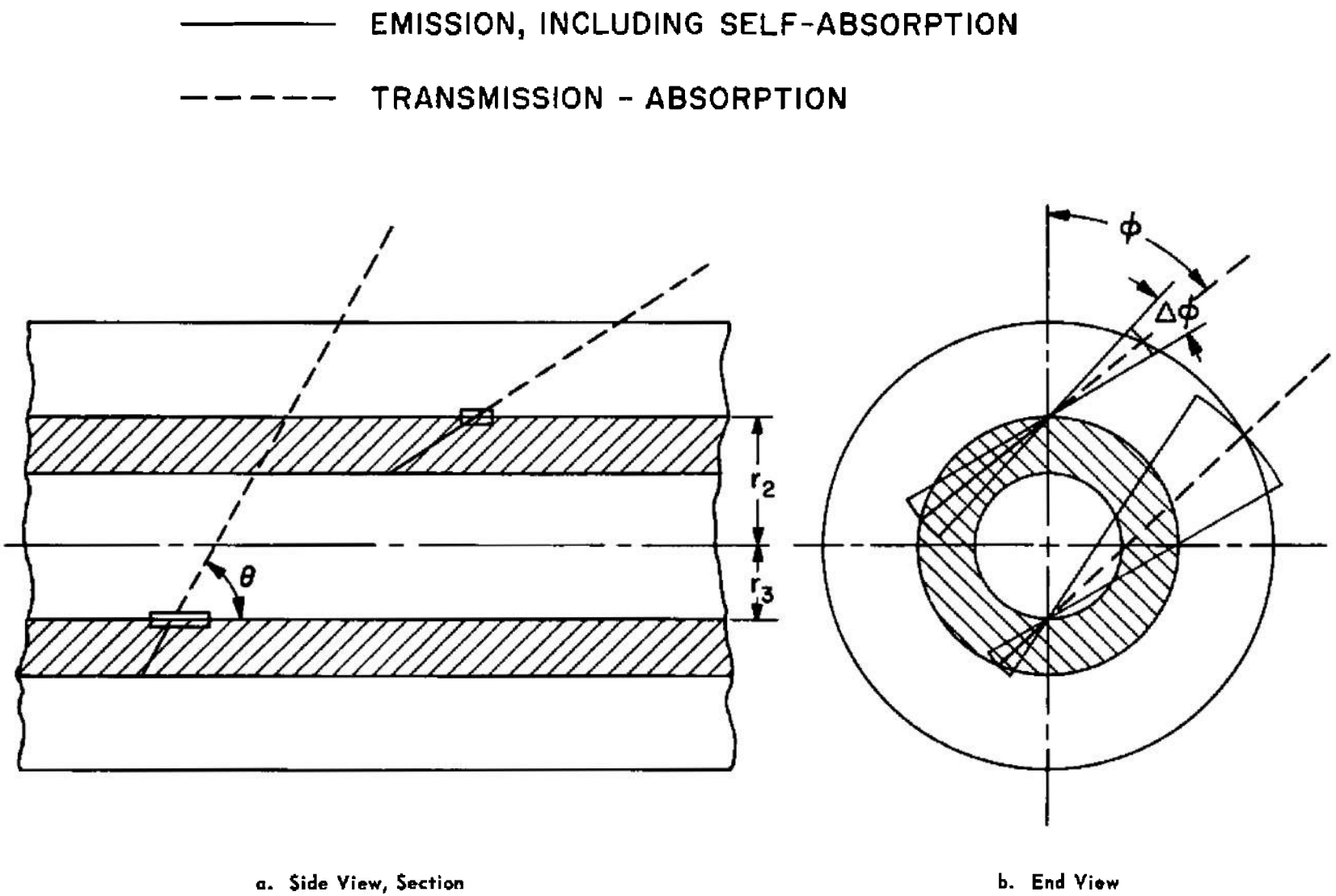

a. Side View, Section

b. End View

Fig. 2 Typical Emission and Absorption Paths to be Accounted for by Radiant Interchange Model

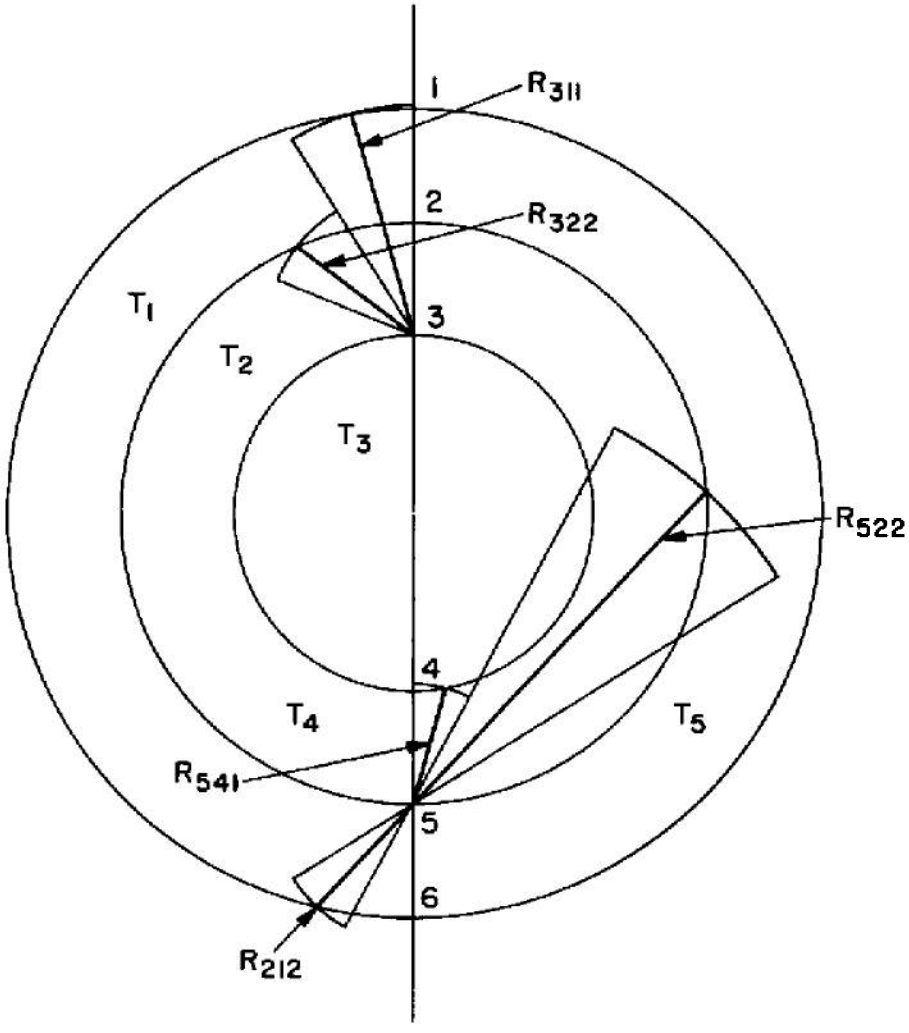

Fig. 3 Examples of Subscripting Notation for Annulus Boundaries, Annulus Properties and Typical Sector Radii (N= 3, m = 3)

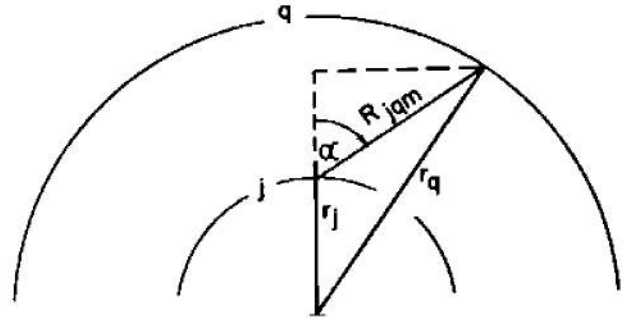

a. $\phi = \alpha$, N>j>q

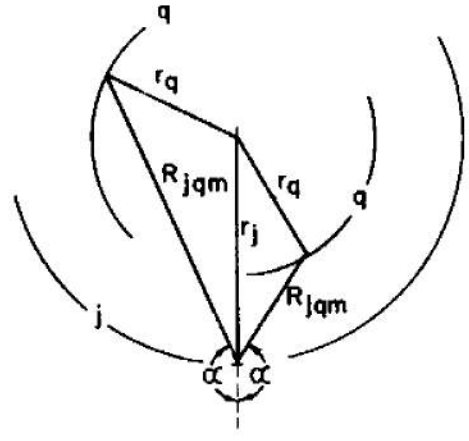

b. $\phi = \pi - \alpha$: Left Side, j>N>q; Right Side j>q>N

Fig. 4 Trigonometric Relationships for the Calculation of Sector Radii

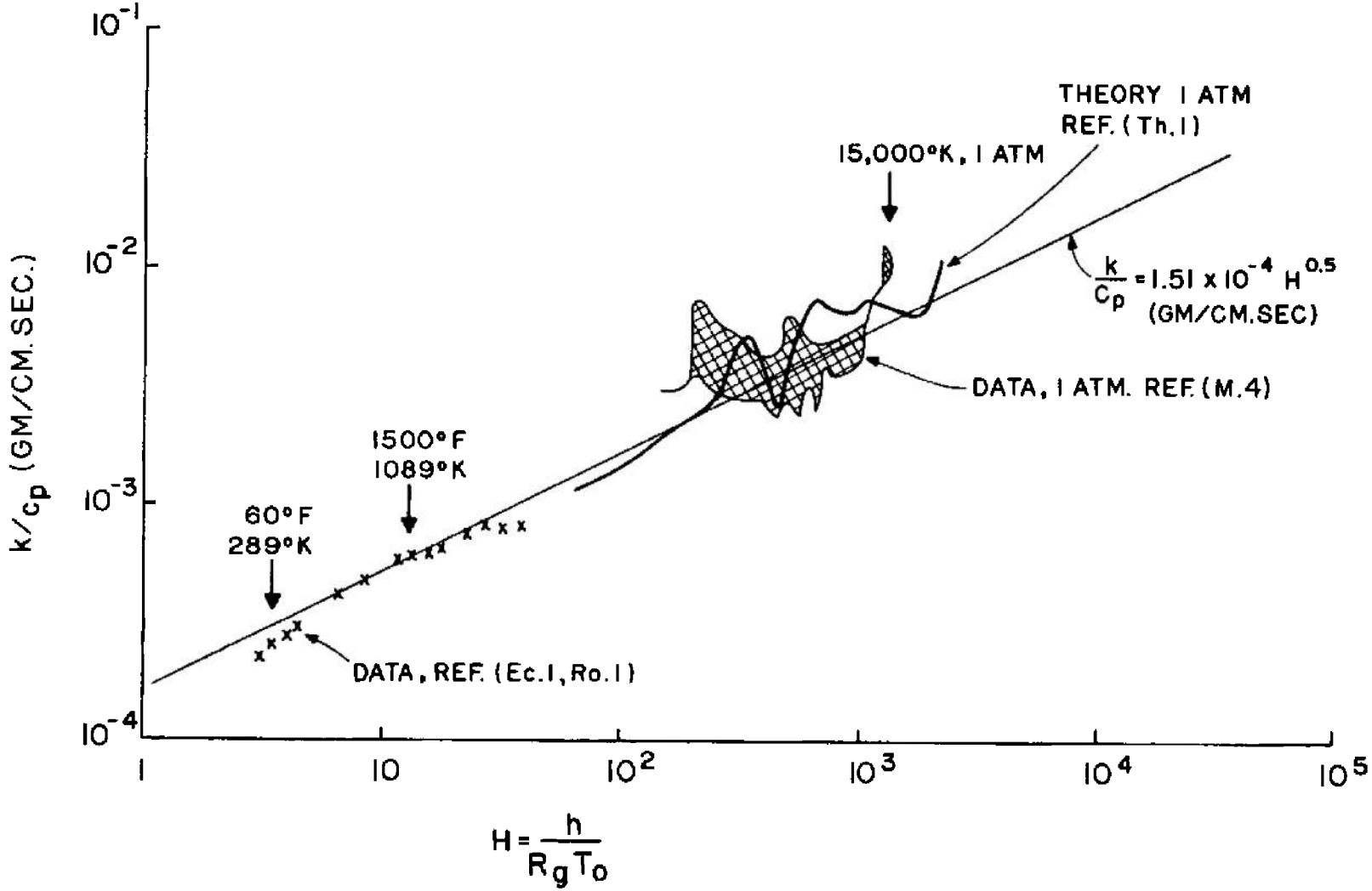

Fig. 5 Weber's Correlation of k/c_p with Enthalpy

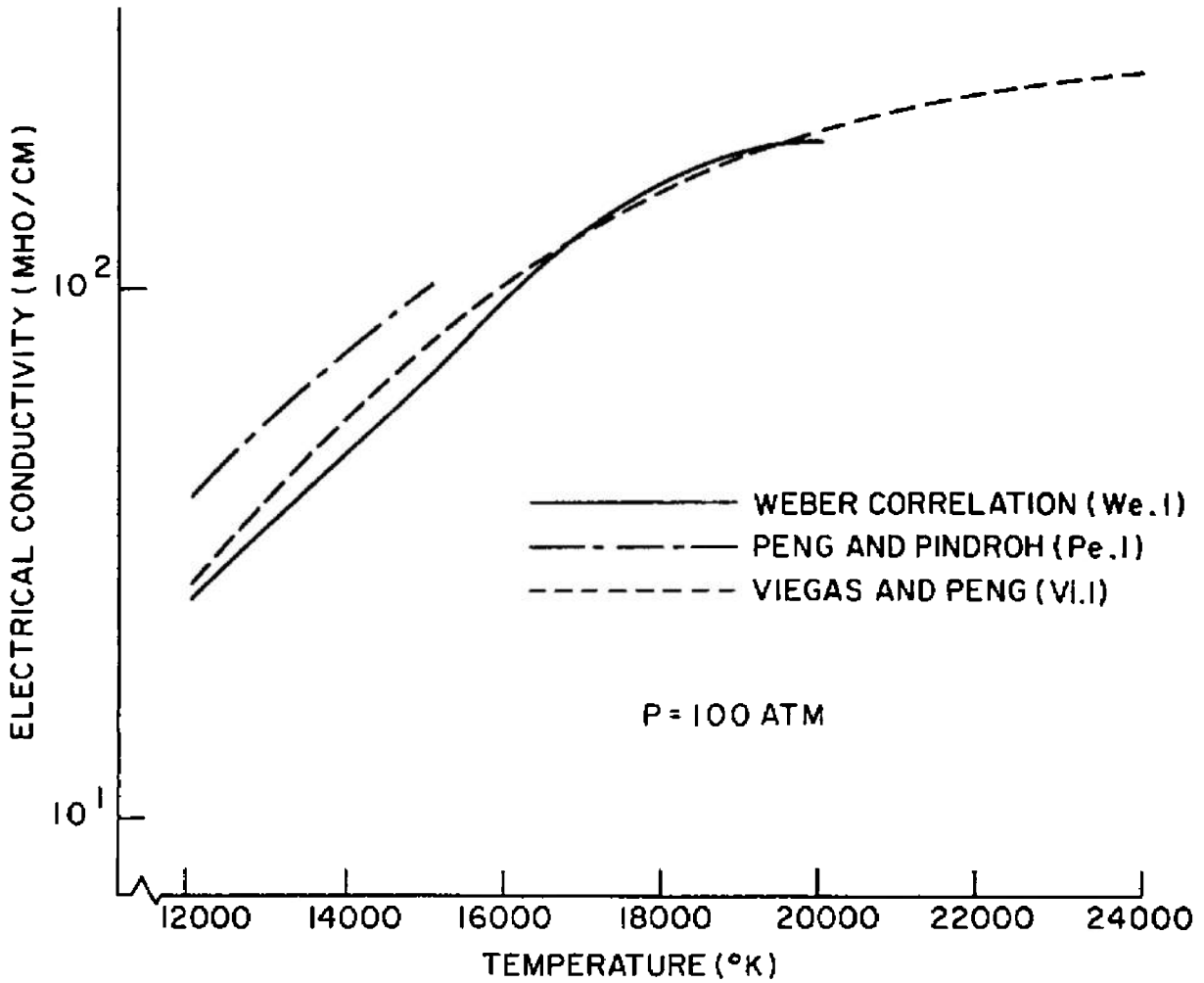

Fig. 6 Electrical Conductivity at P = 100 Atmospheres

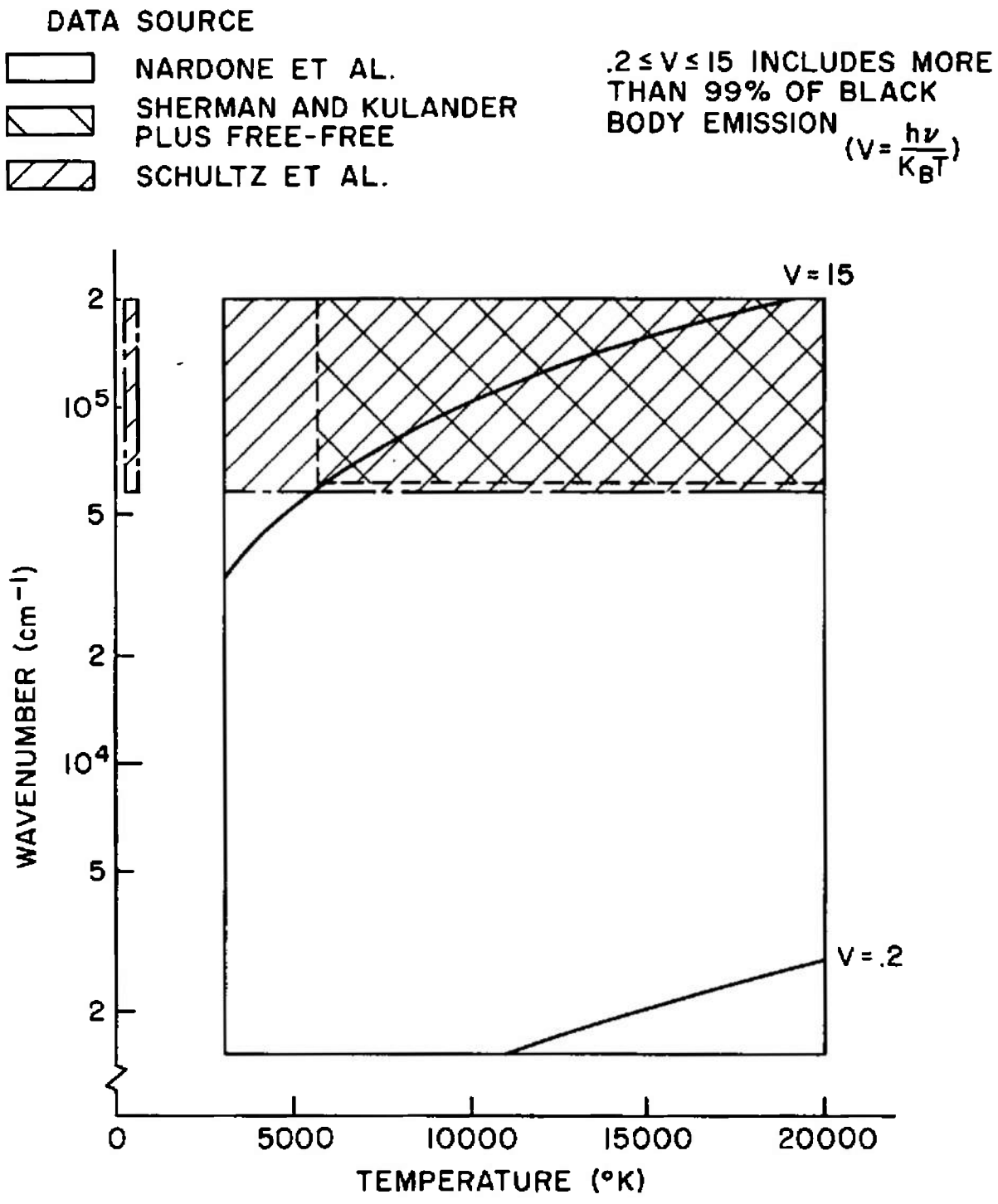

Fig. 7 Range and Sources for Absorption Coefficients

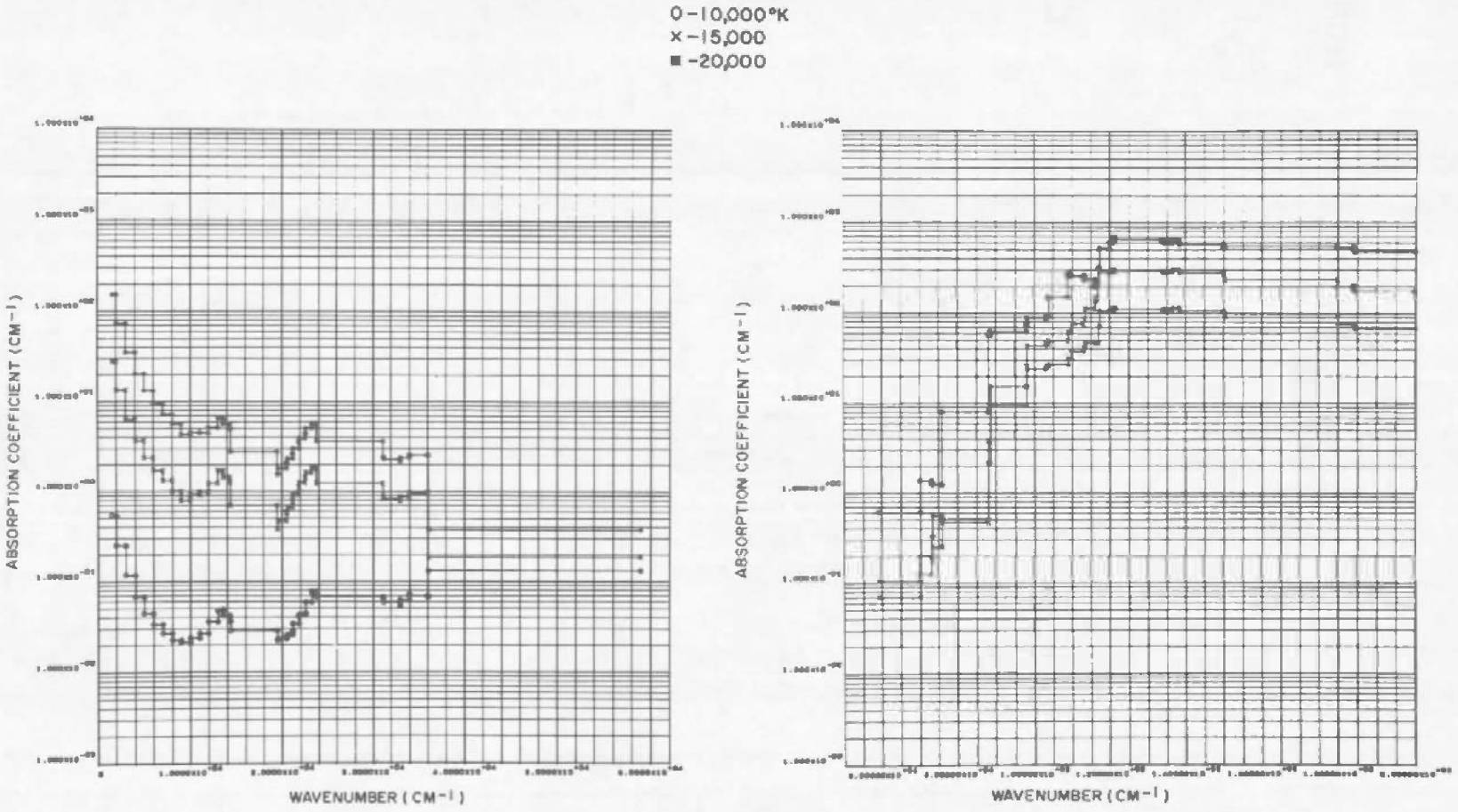

a. 1500-59,000 cm^{-1}

b. 59,000-200,000 cm^{-1}

Fig. 8 Continuum Absorption Coefficient for Air at 100 Atmospheres and Temperatures of 10,000°K, 15,000°K and 20,000°K

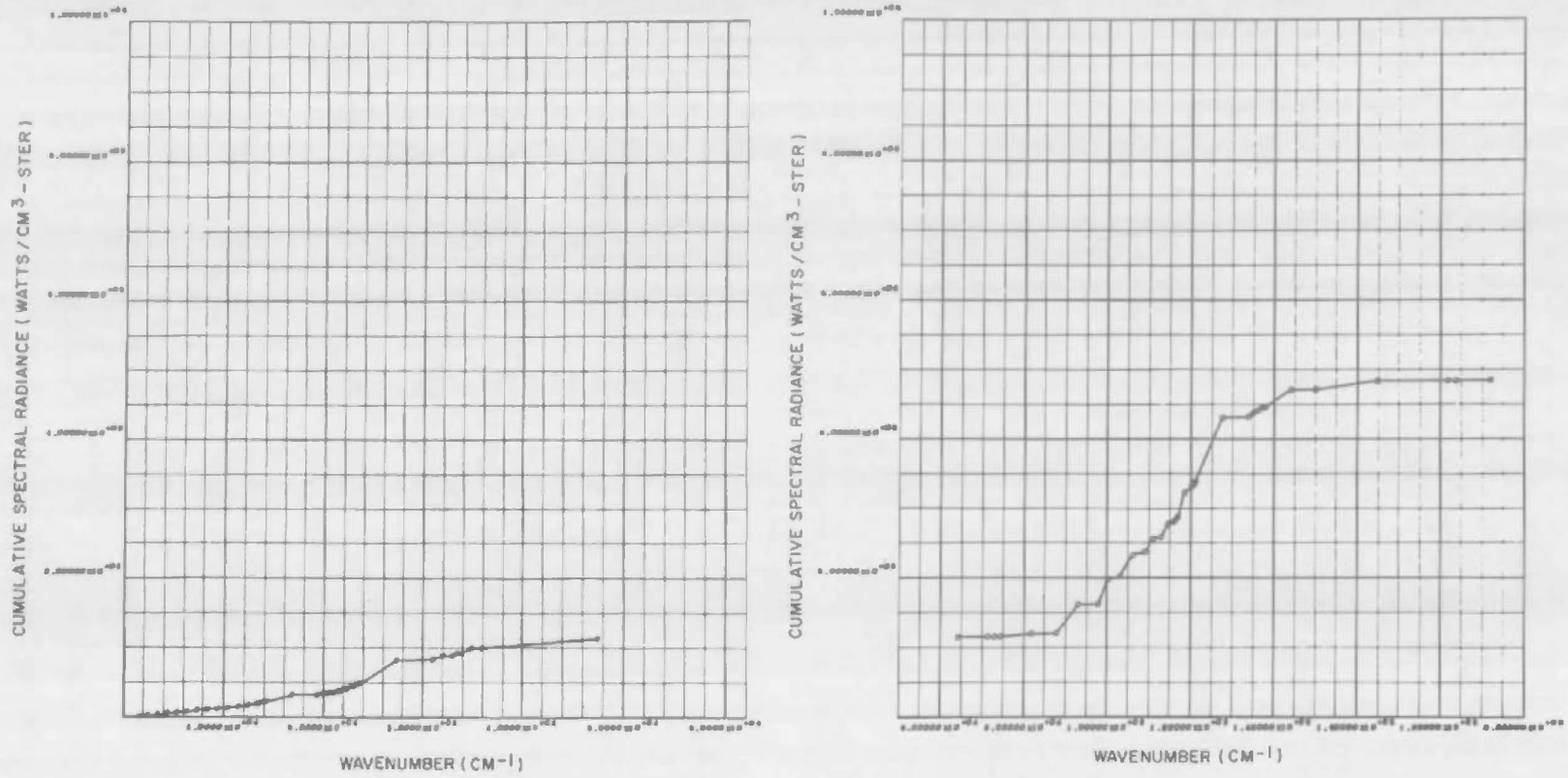

a. 1500 – 59,000 CM^{-1}

b. 59,000 – 200,000 CM^{-1}

Fig. 9 Optically Thin Spectral Radiance, Cumulative Summation, 200 Atmospheres, 15,000°K

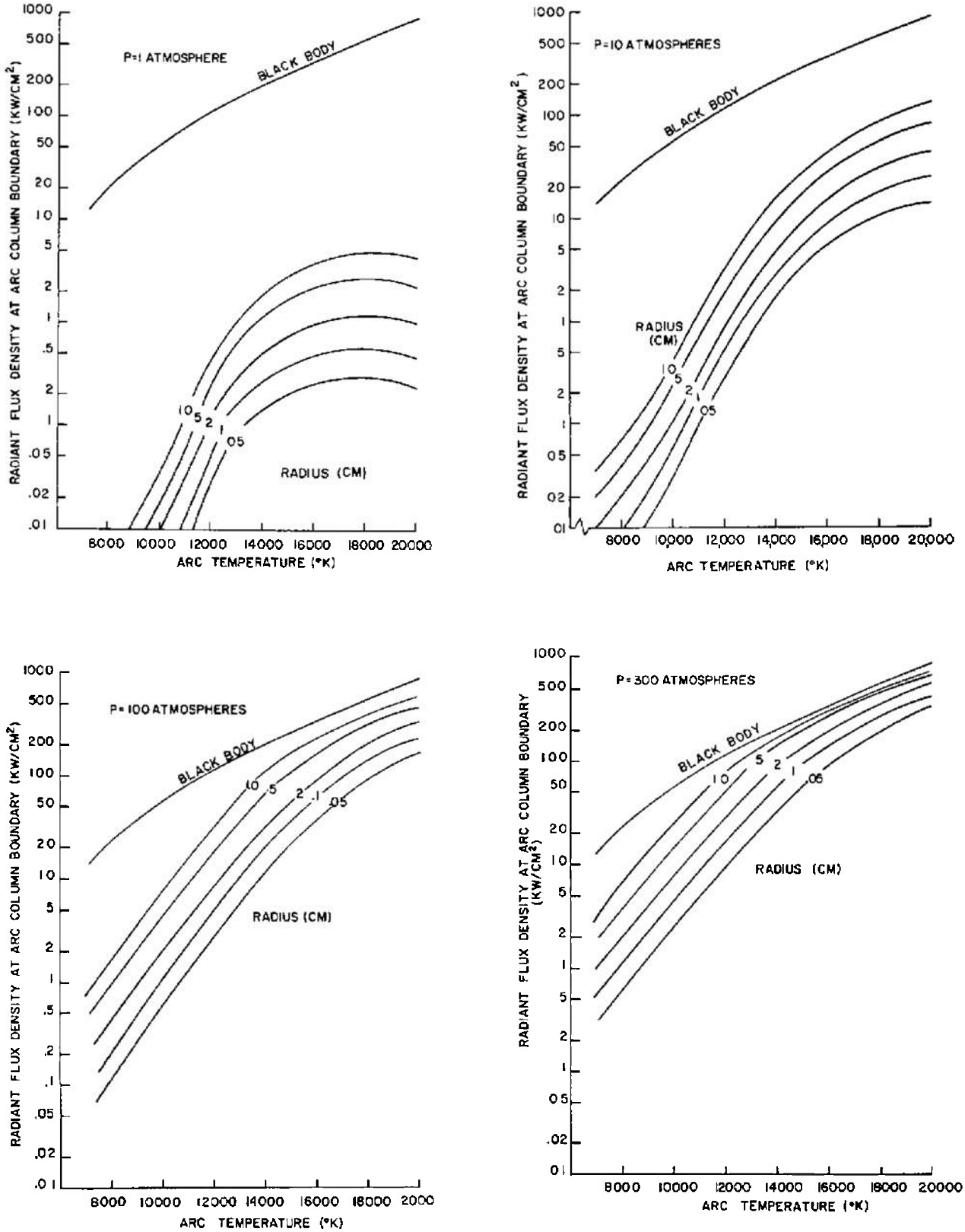

Fig. 10 Radiant Flux Density at Arc Column Boundary

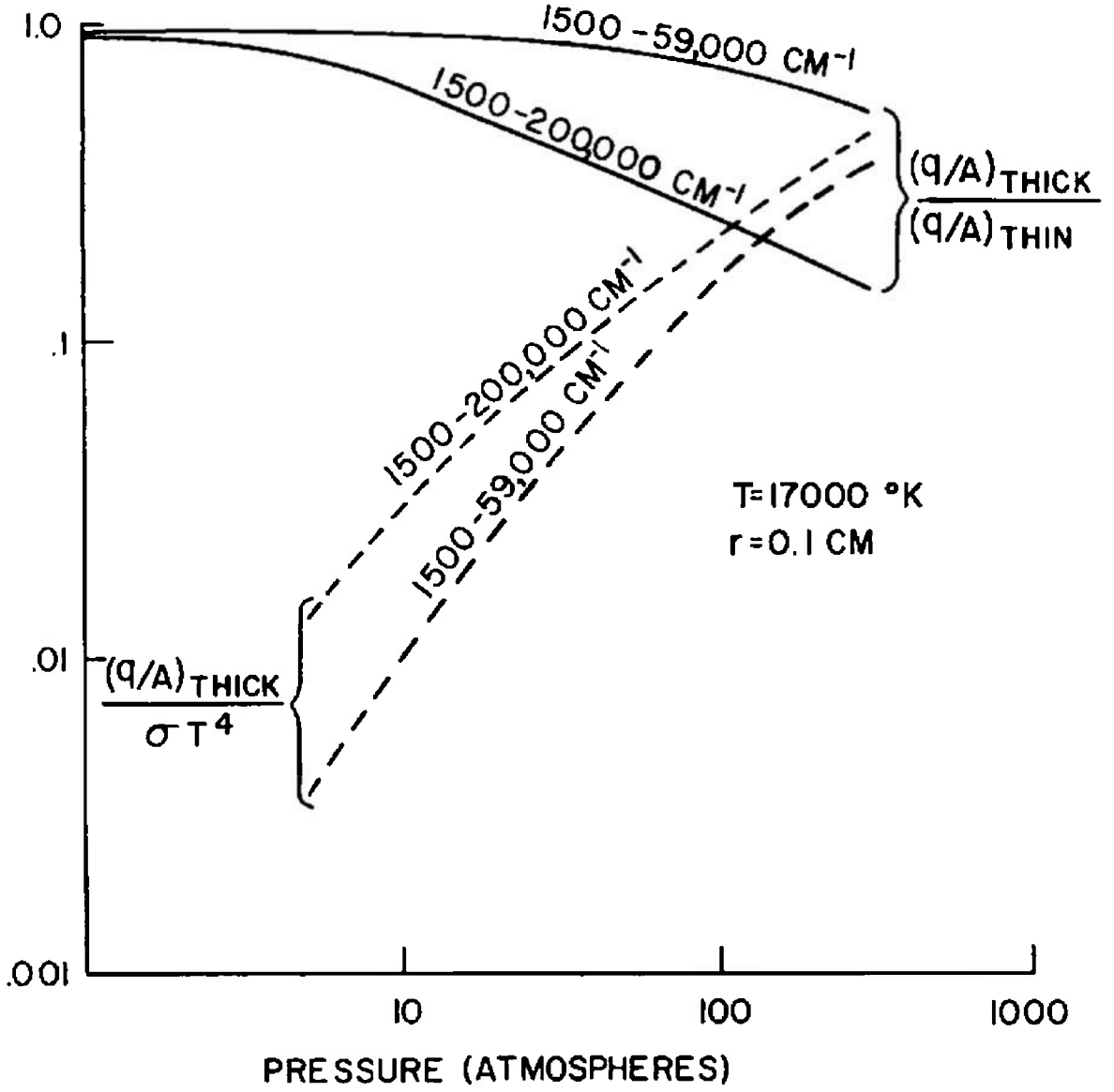

Fig. 11 Self-Absorption in a Uniform Temperature Arc, r_a = .1 cm T = 17,000°K

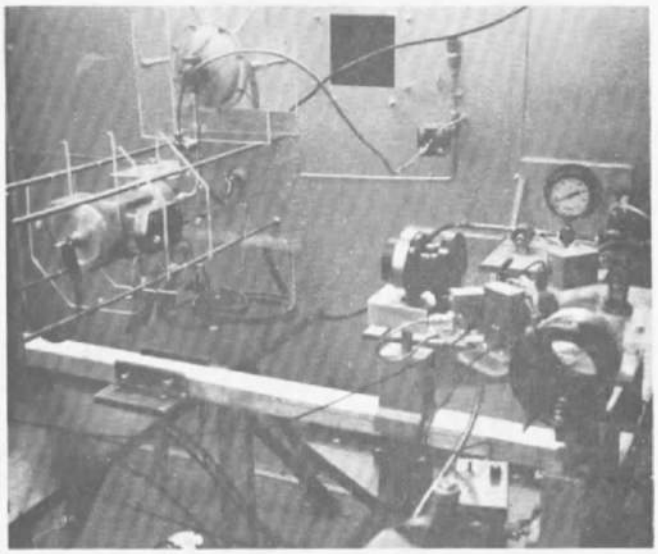

Fig. 12 Experimental Setup. The High Pressure Air Arc is on the Left. On the Right is the Optical System Leading to the Spectragraph, a Small Part of which con be seen, Lower Right of Center

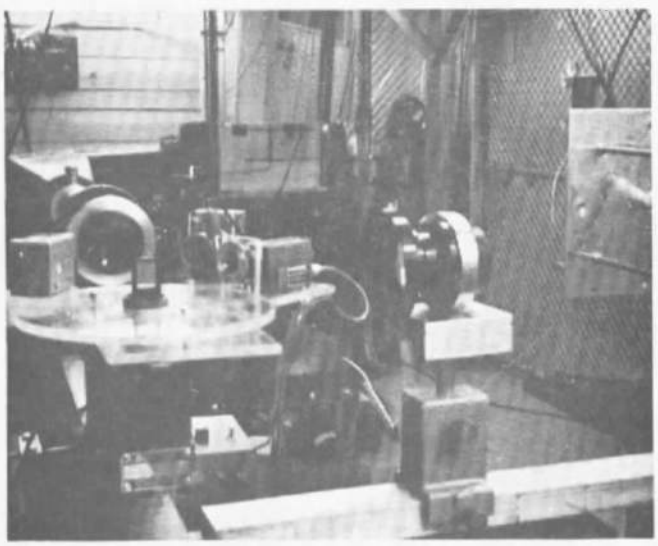

Fig. 13 Optical System with Ratating Mirrar (Rectangle in Center af Large Plexiglas Disc) ond Associated Electronics

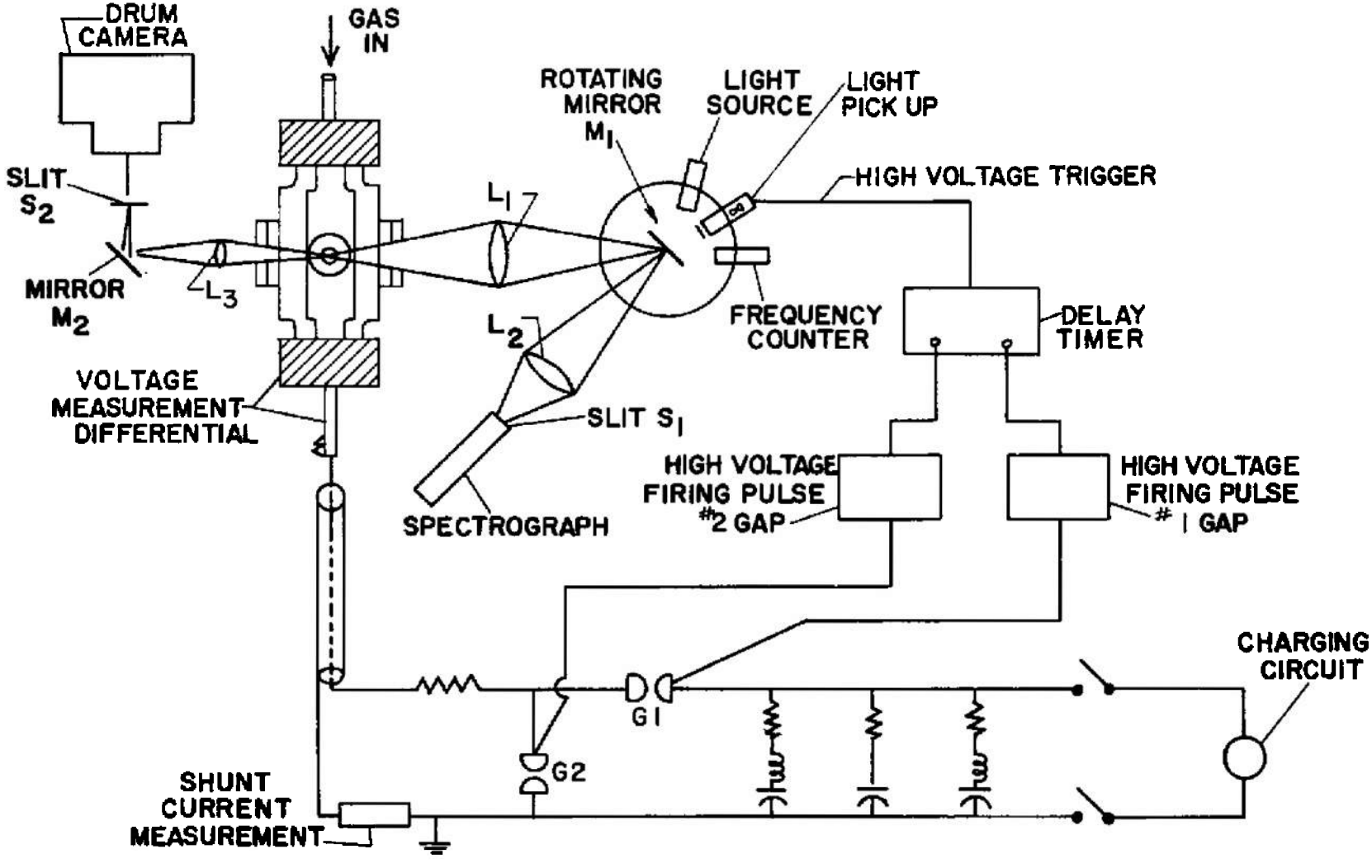

Fig. 14 Schematic Representation of Experimental Apparatus, Showing Arc Chamber, Spectrograph, Drum Camera, Associated Optical Equipment, Power Supply and Synchronization Equipment

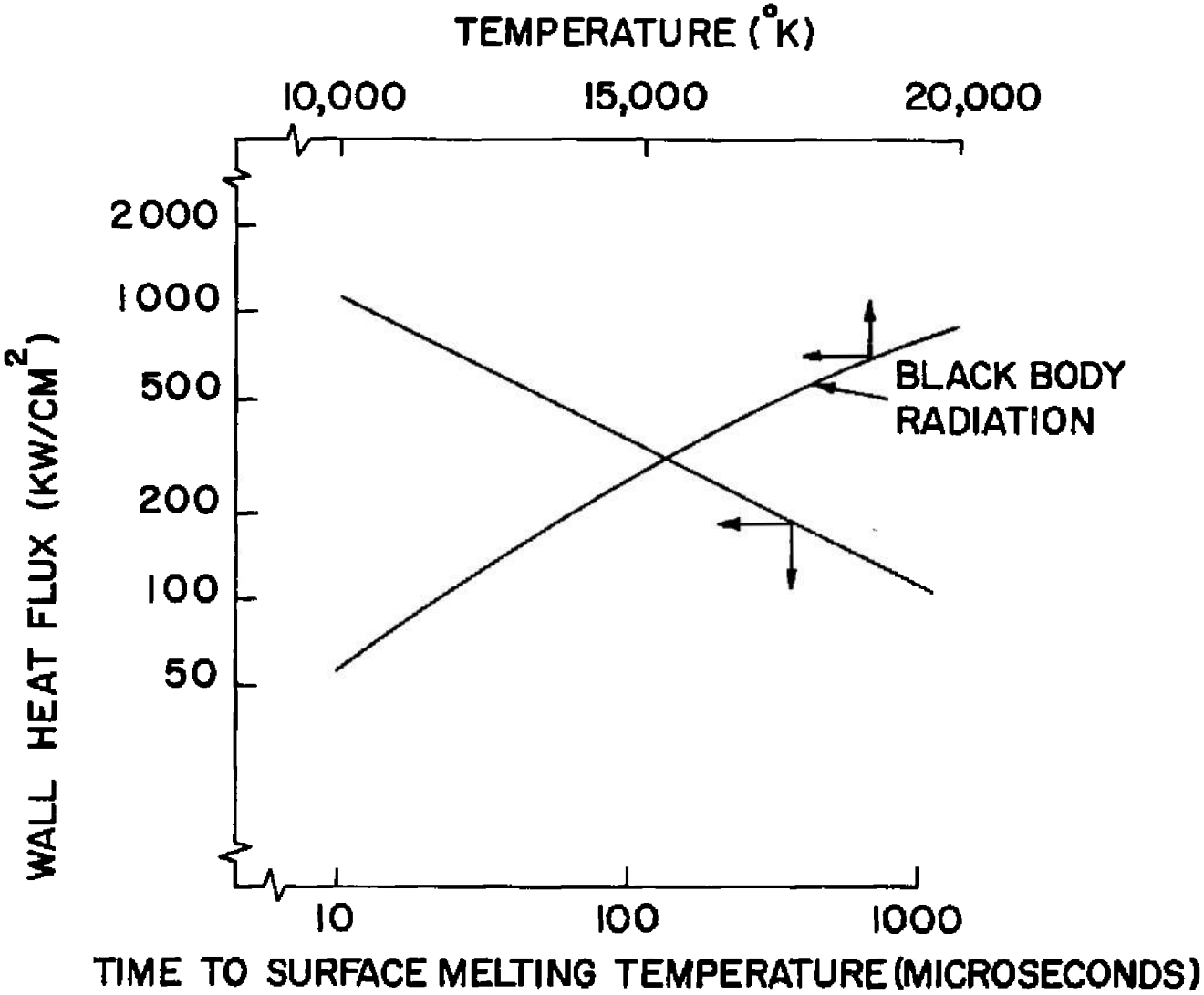

Fig. 15 Design Curve for Copper Constrictor Showing Time to Surface Melting Temperature as a Function of Wall Heat Flux

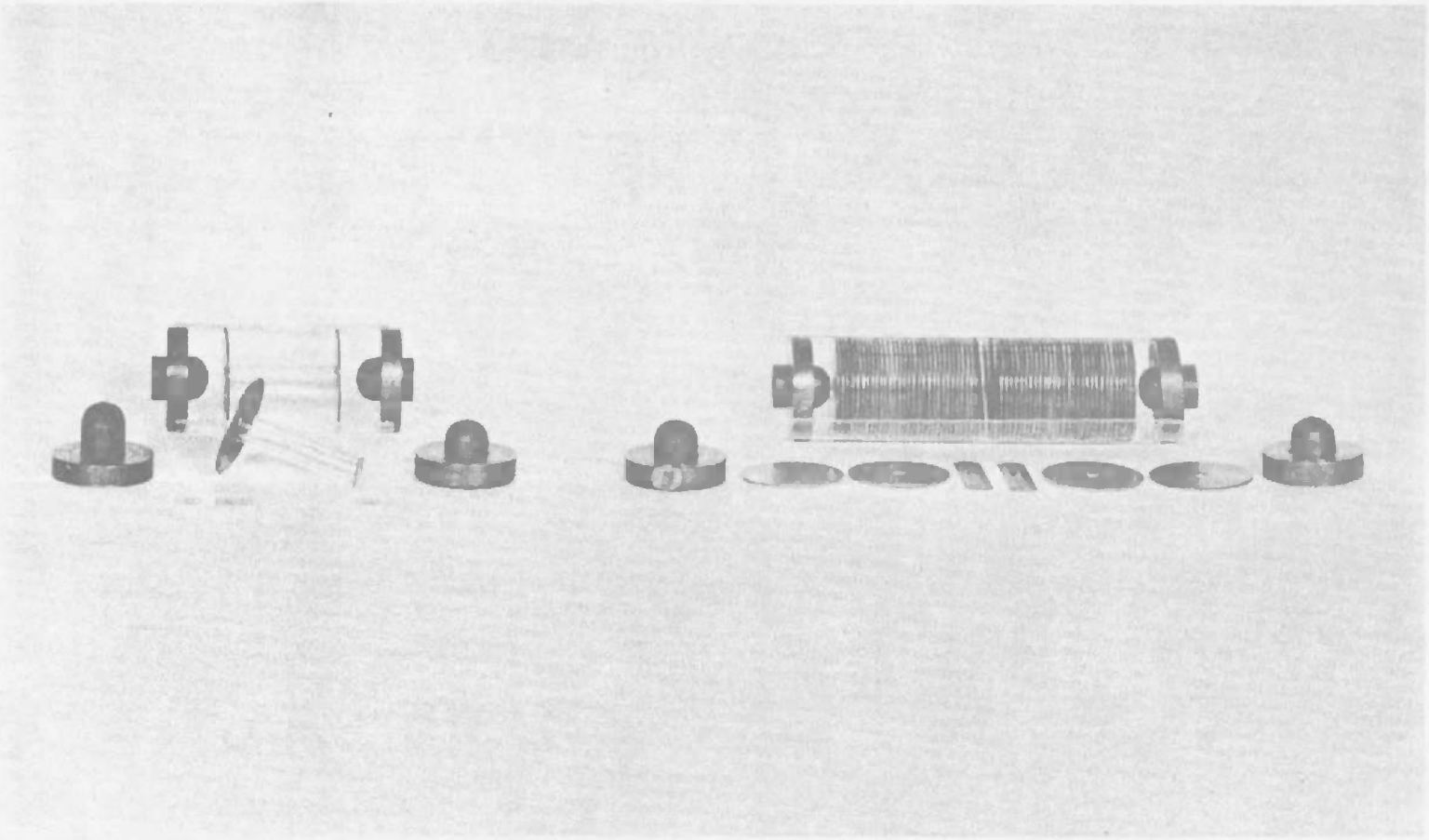

Fig. 16 Exploded Views of a Copper Cascade Constrictor and an Ablation Type Plexiglas Constrictor

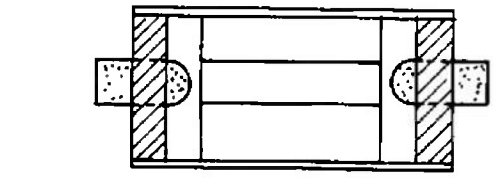

PLEXIGLAS CONSTRICTOR

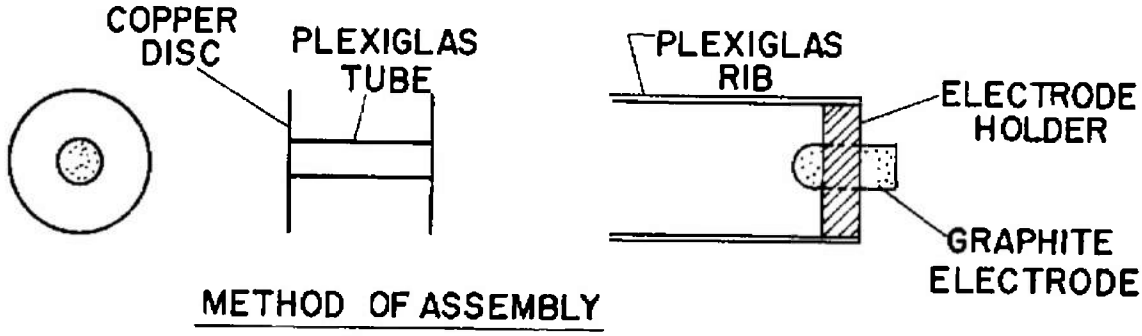

METHOD OF ASSEMBLY

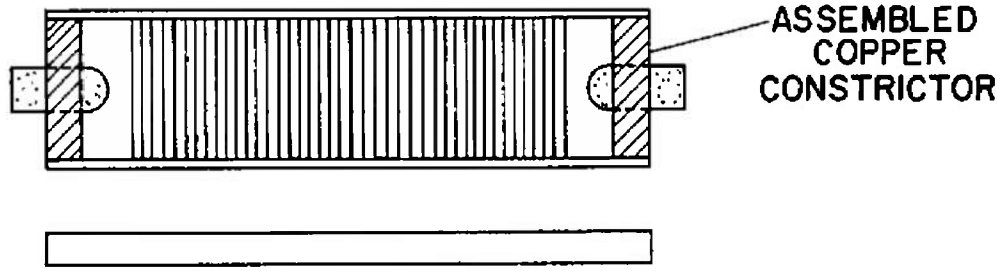

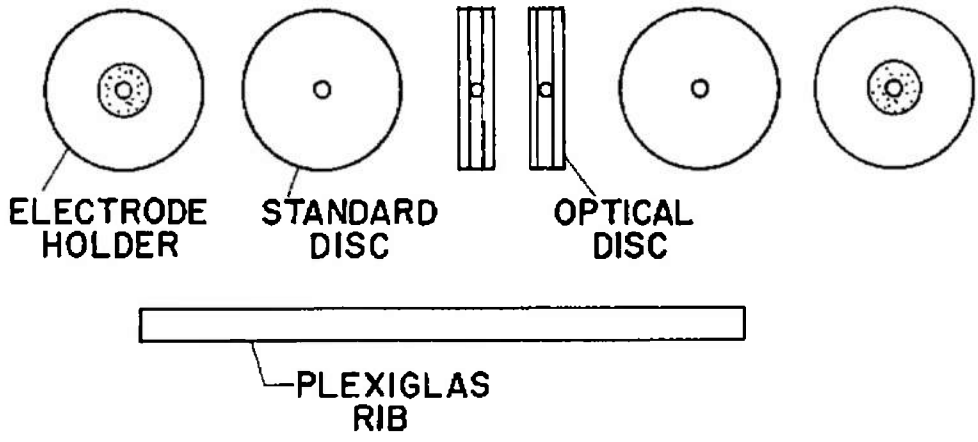

Fig. 17 Schematic View of Copper Constrictor and Components

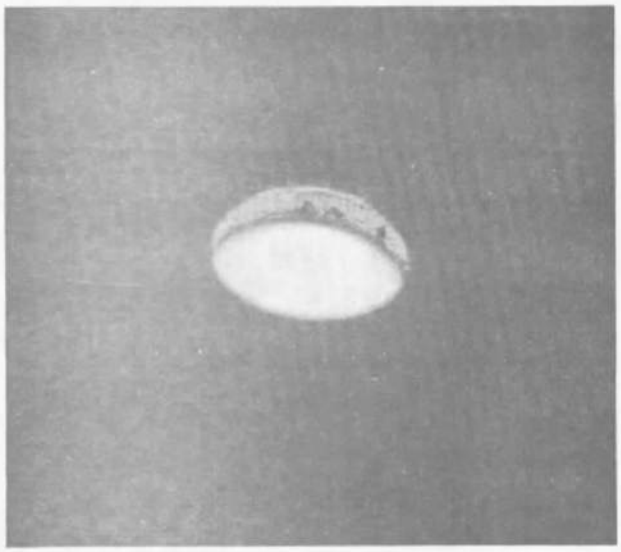

Copper Disc Before Etching

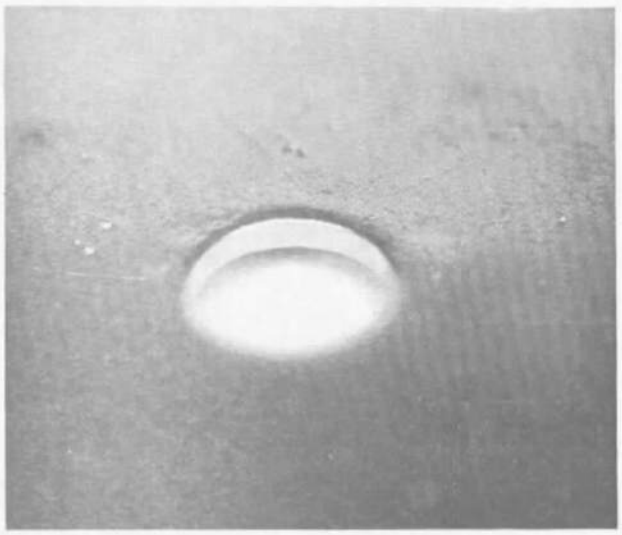

Copper Disc After Etching

Fig. 18 Copper Disc of a Cascade Constrictor Before and After Etching. Observe thot the Loose Copper Particles and Machine Marks are Eliminoted by Etching.

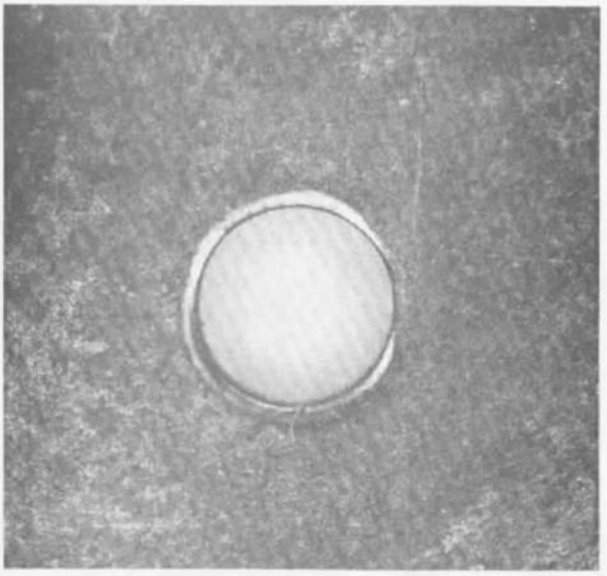

Copper Disc After a Symmetric Operation

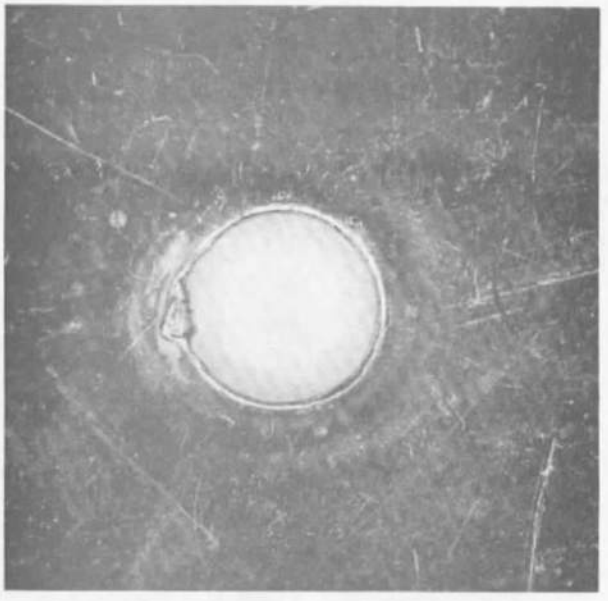

Copper Disc After an Unsymmetric Operation

Fig. 19 Copper Discs of a Cascade Type Constrictor After Symmetric and Unsymmetric Heating by Arc

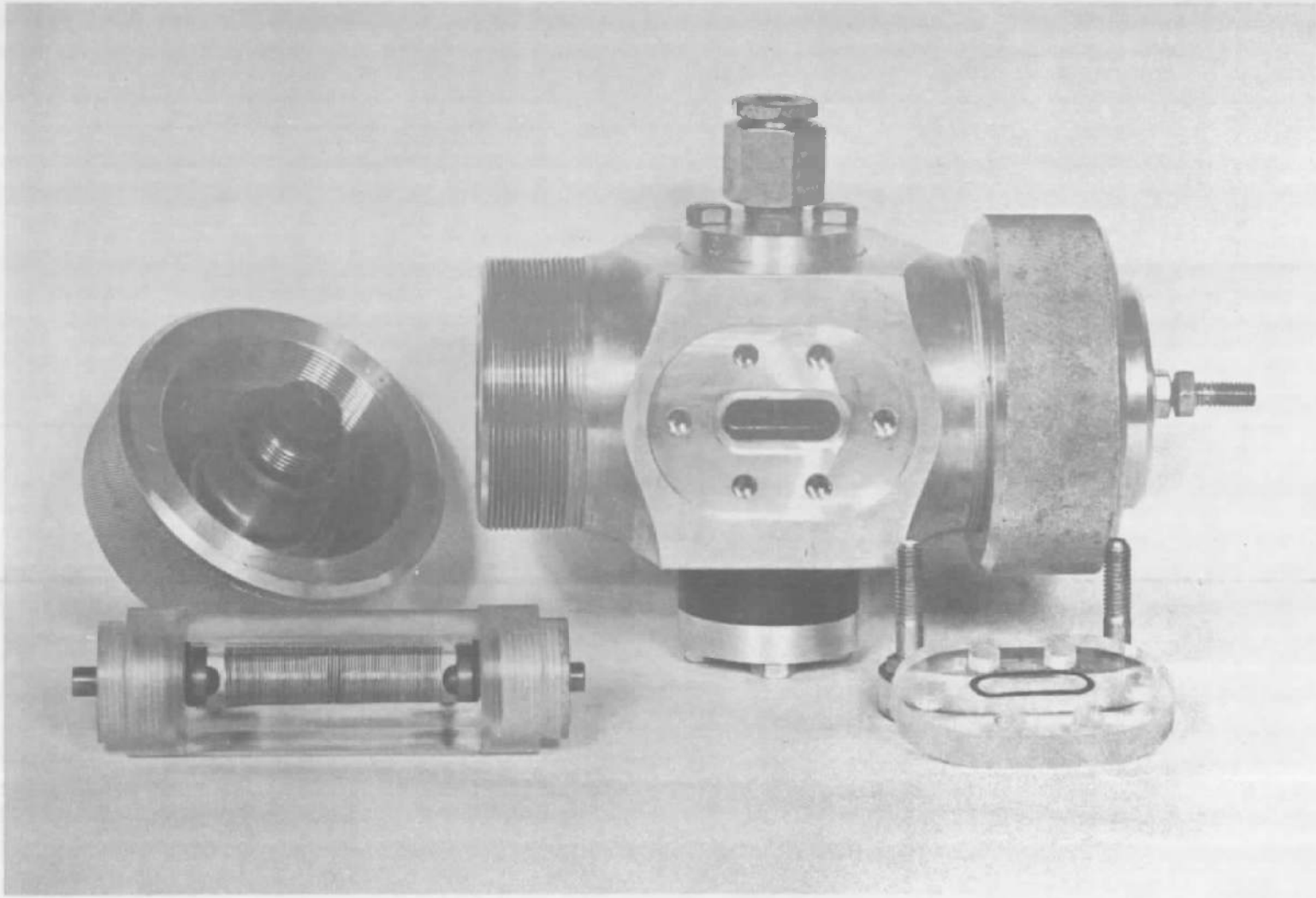

Fig. 20 High Pressure Arc Chamber and Plexiglas Holder with Copper Constrictor

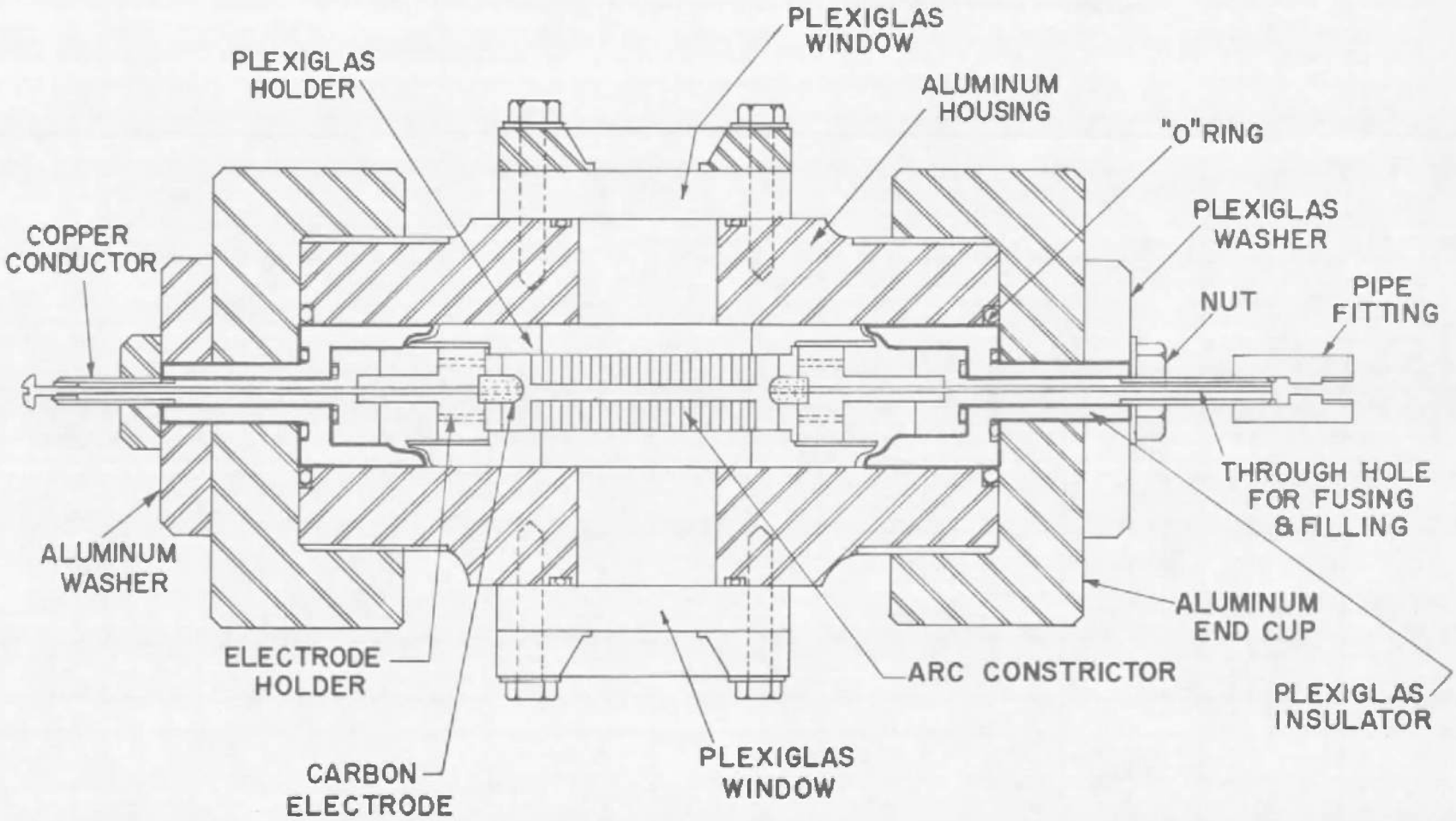

Fig. 21 Schematic View of High Pressure Arc Chamber Assembly

AEDC-TR-66-258

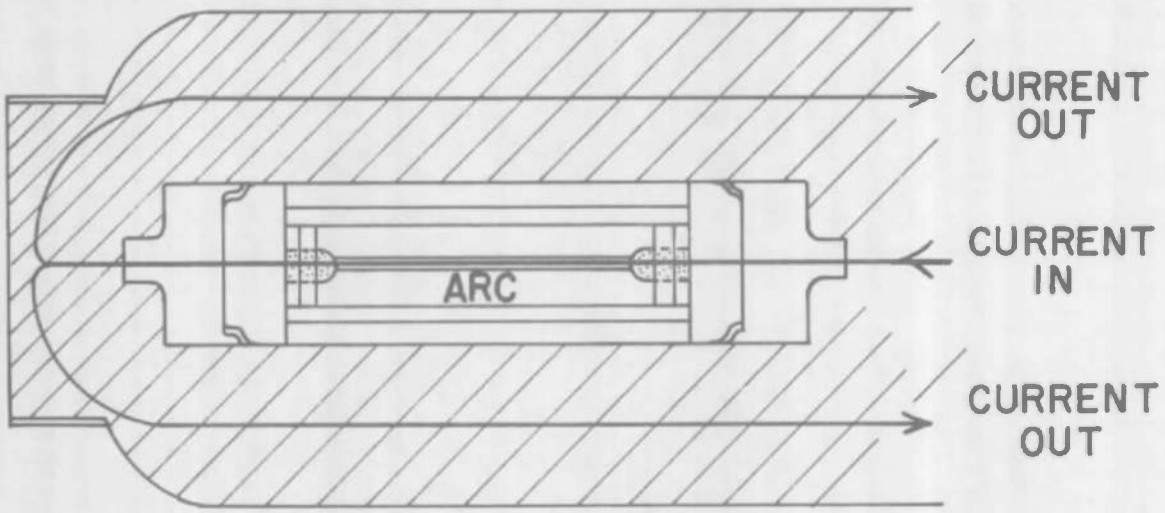

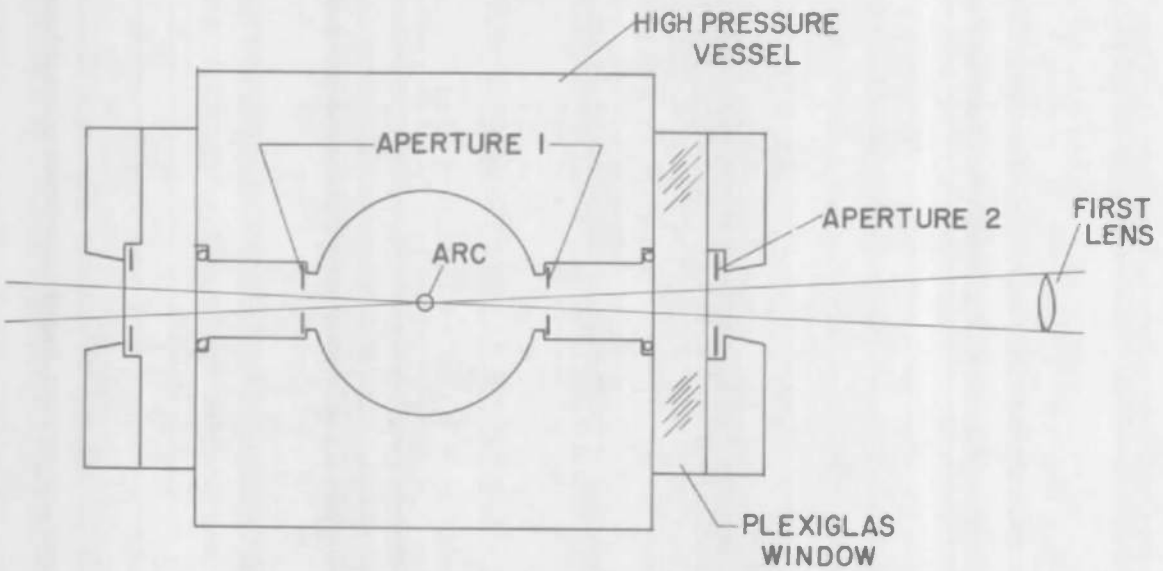

Fig. 22 Details of High Pressure Apparatus:
a) Side View Showing Current Path Through Arc and Return Through High Pressure Vessel; b) Top View Showing Optical Path and Apertures Added to Reduce Stray Light

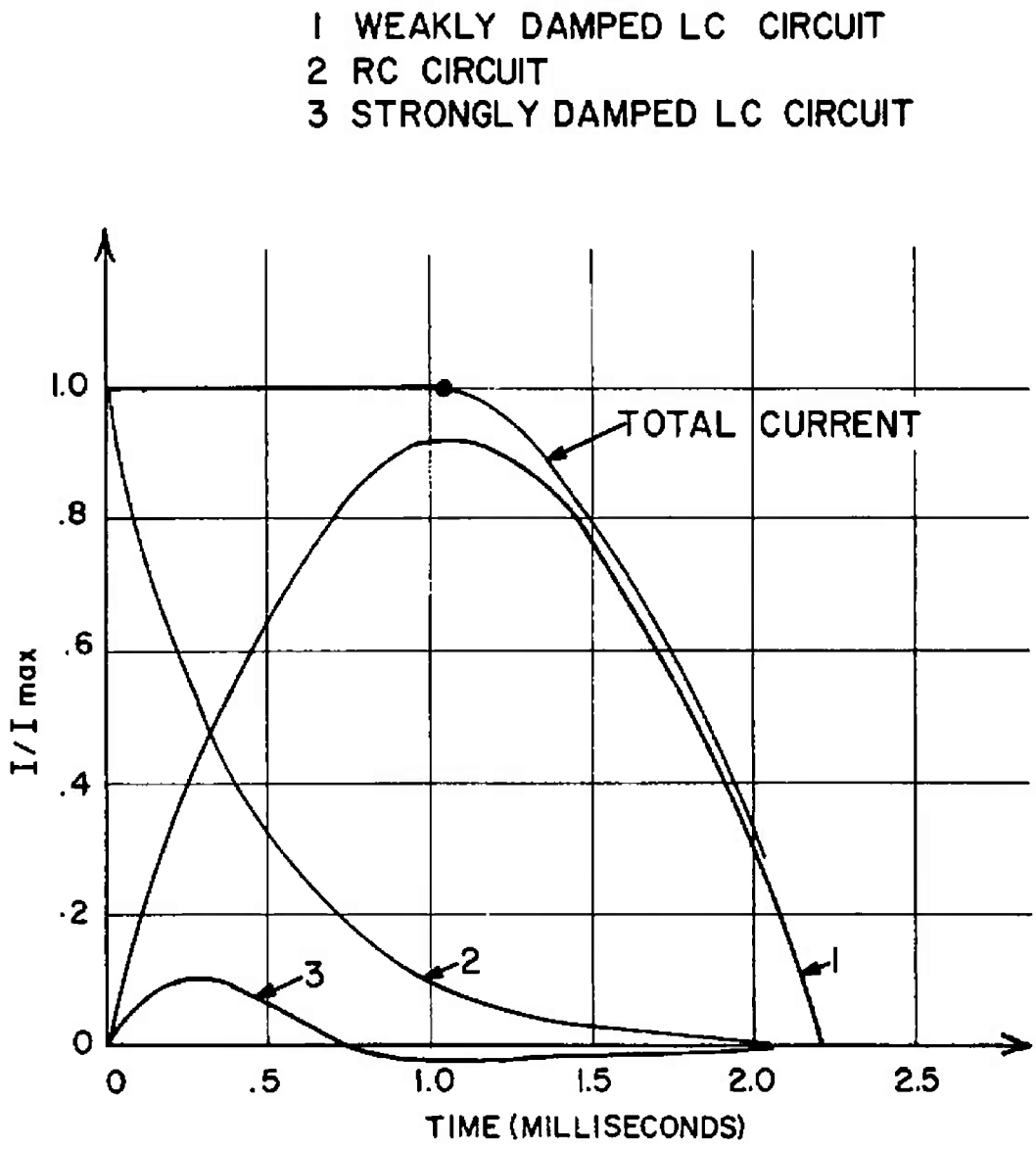

Fig. 23 The Power Pulse and Its Components

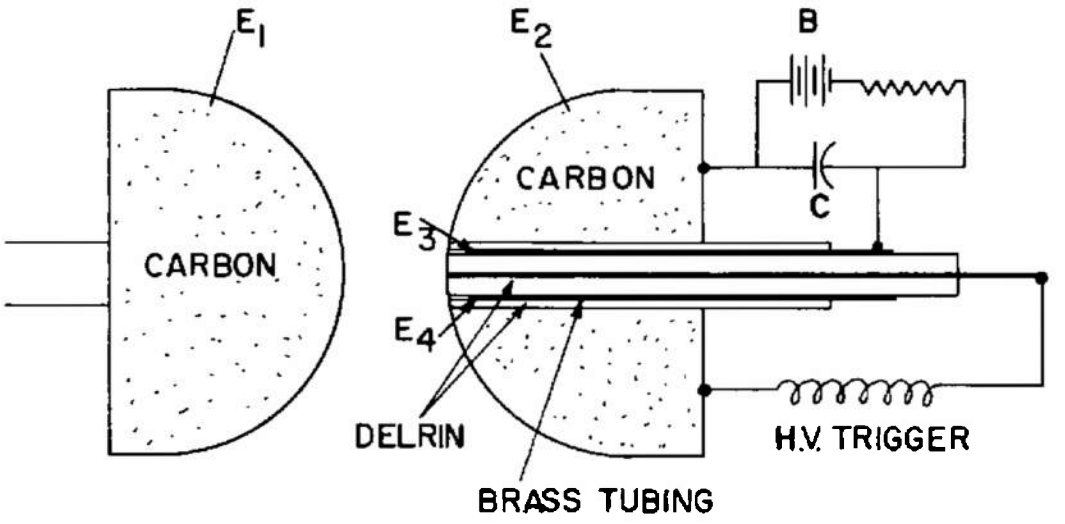

FOUR ELECTRODE GAP

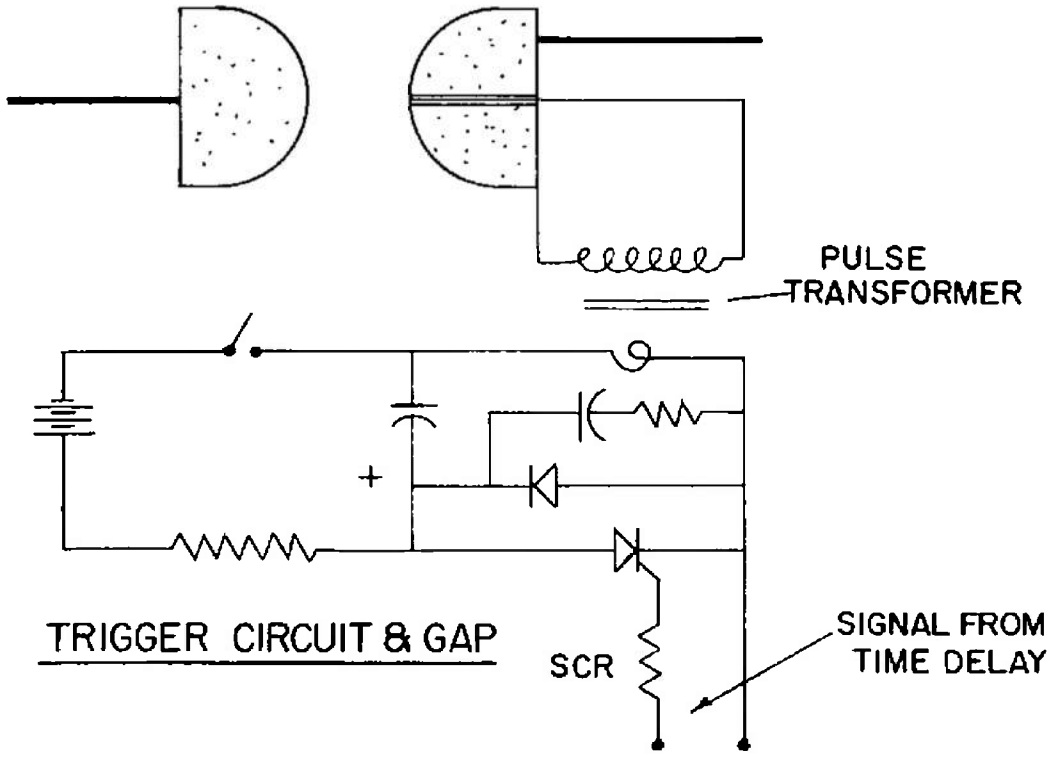

Fig. 24 The Four Electrode Spark Gap

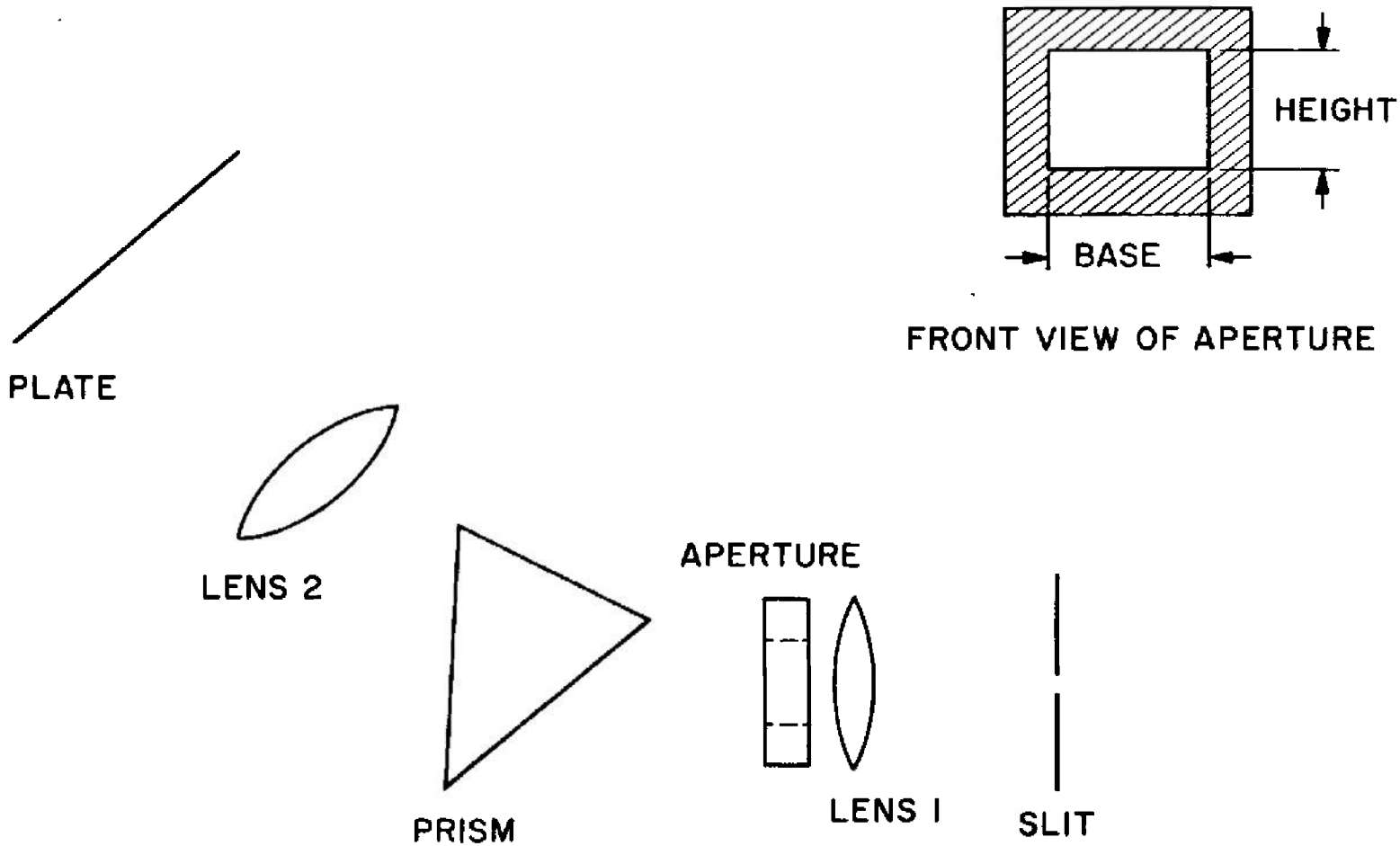

Fig. 25 Arrangement of Apertures in the Spectrograph

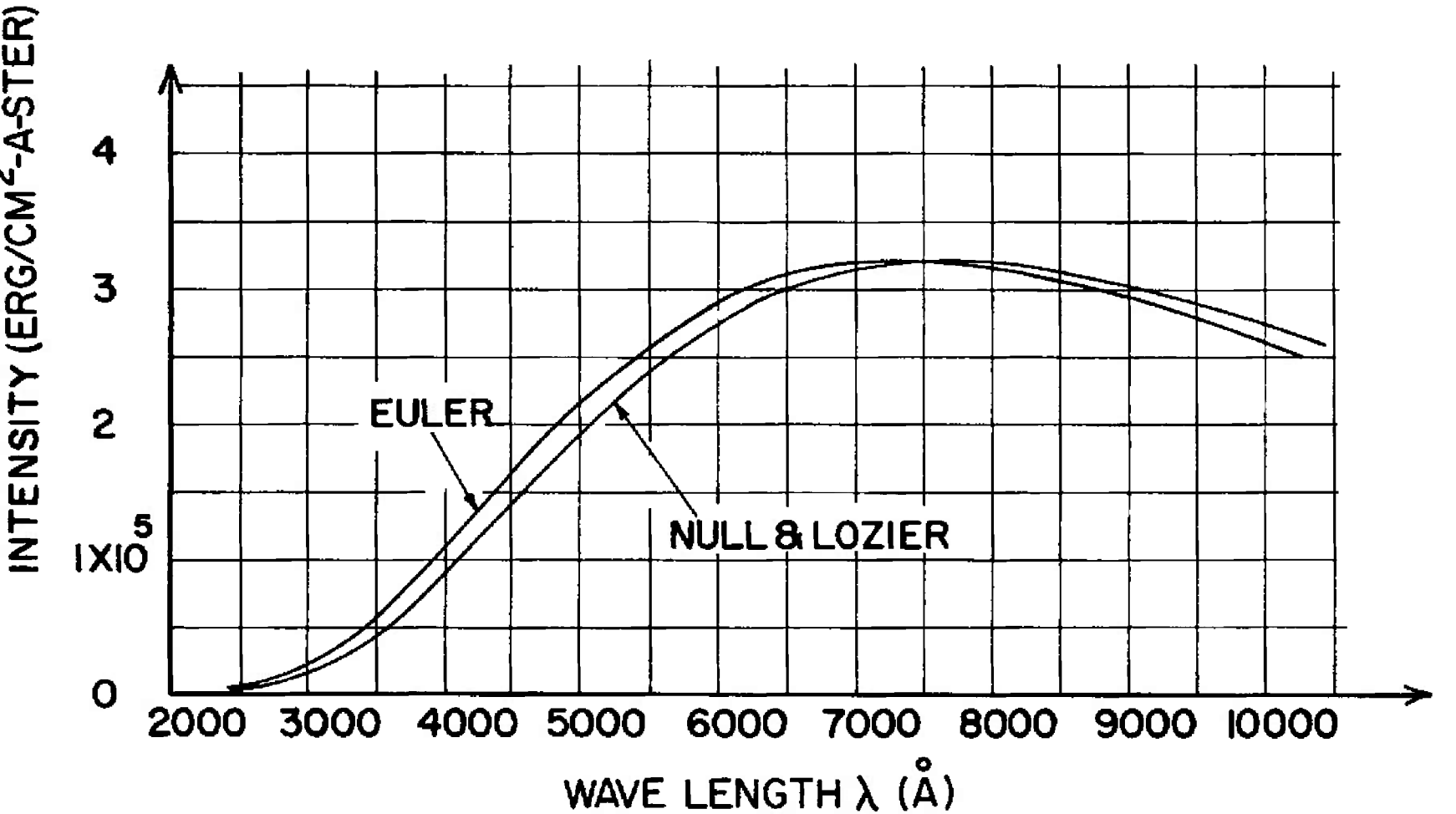

Fig. 26 Intensity of the Carbon Standard

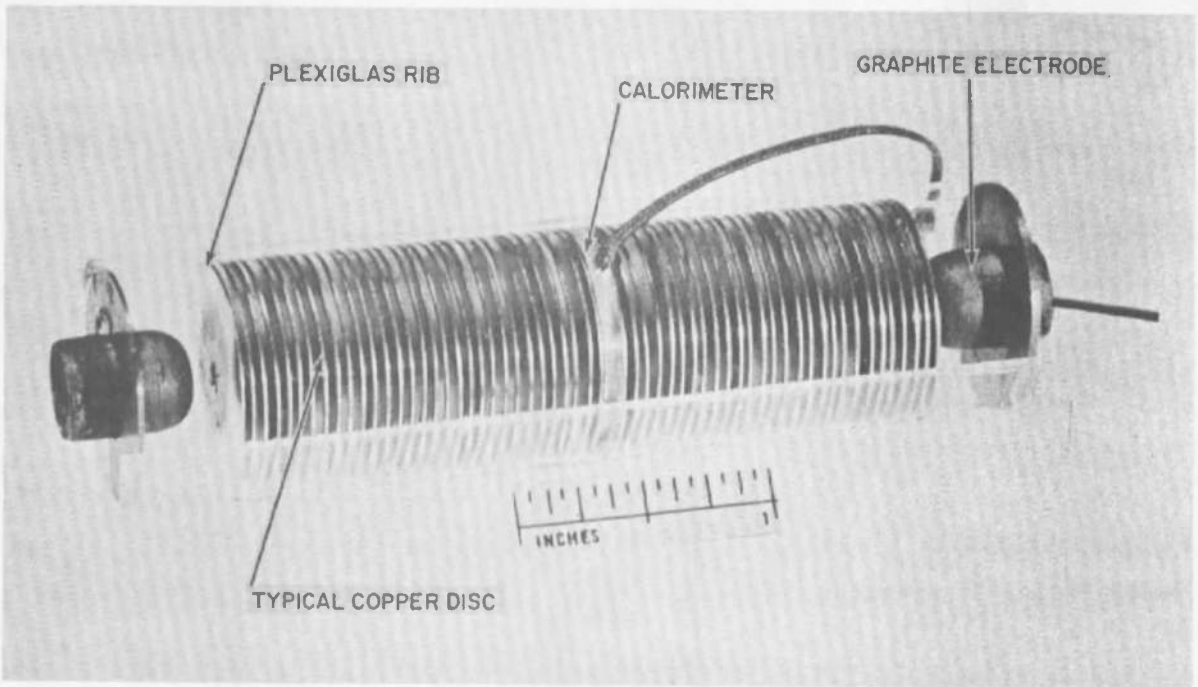

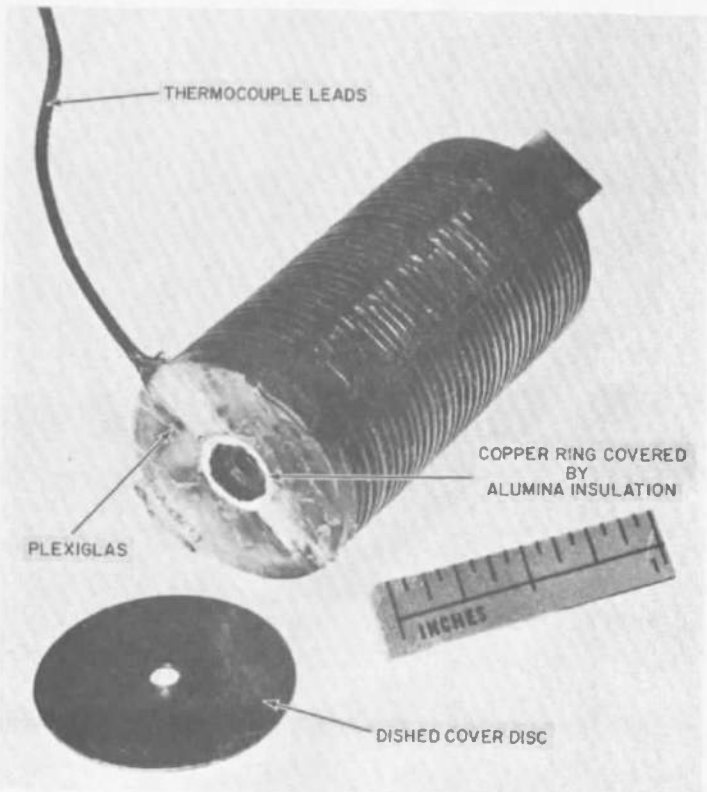

Fig. 27 Arc Cage with Calorimeter Installed and Calorimeter, Partially Disassembled

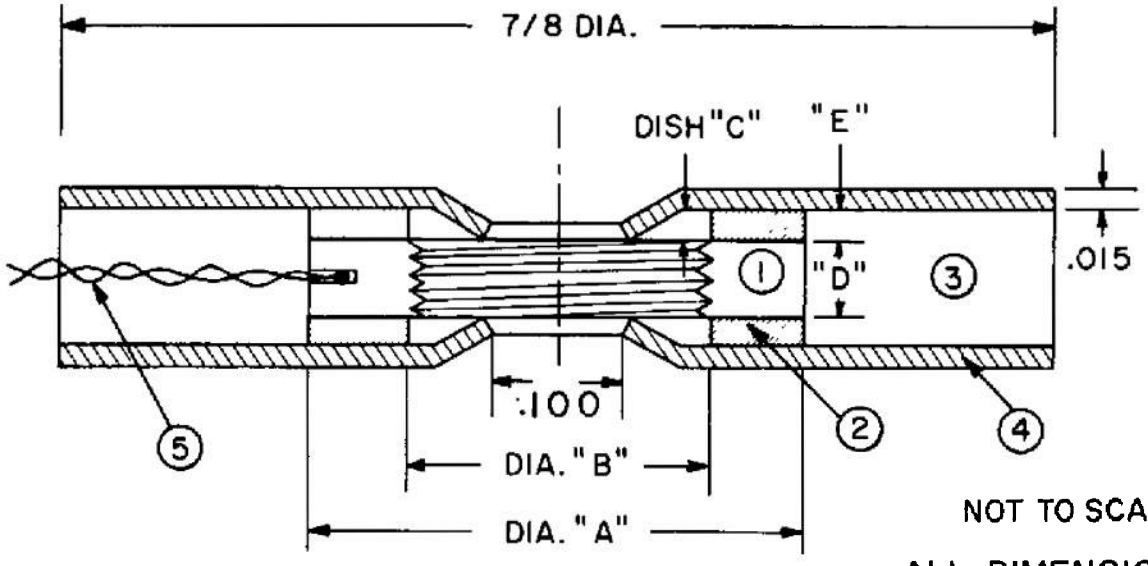

NOT TO SCALE

ALL DIMENSIONS IN INCHES

MODEL	DIMENSIONS				
	A	B	C	D	E
1	.300	.218	.020	.040	.010
2	.300	.218	.000	.040	.010
3	.344	.278	.015	.035	.005

(1) COPPER RING SENSING ELEMENT
(2) ALUMINA CERAMIC
(3) PLEXIGLAS SPACER DISC
(4) COPPER DISC
(5) THERMOCOUPLE

NOTE: INSIDE SURFACE OF SENSING ELEMENT THREADED ON MODEL 3 ONLY

Fig. 28 Section Drawing of Total Radiation Calorimeter

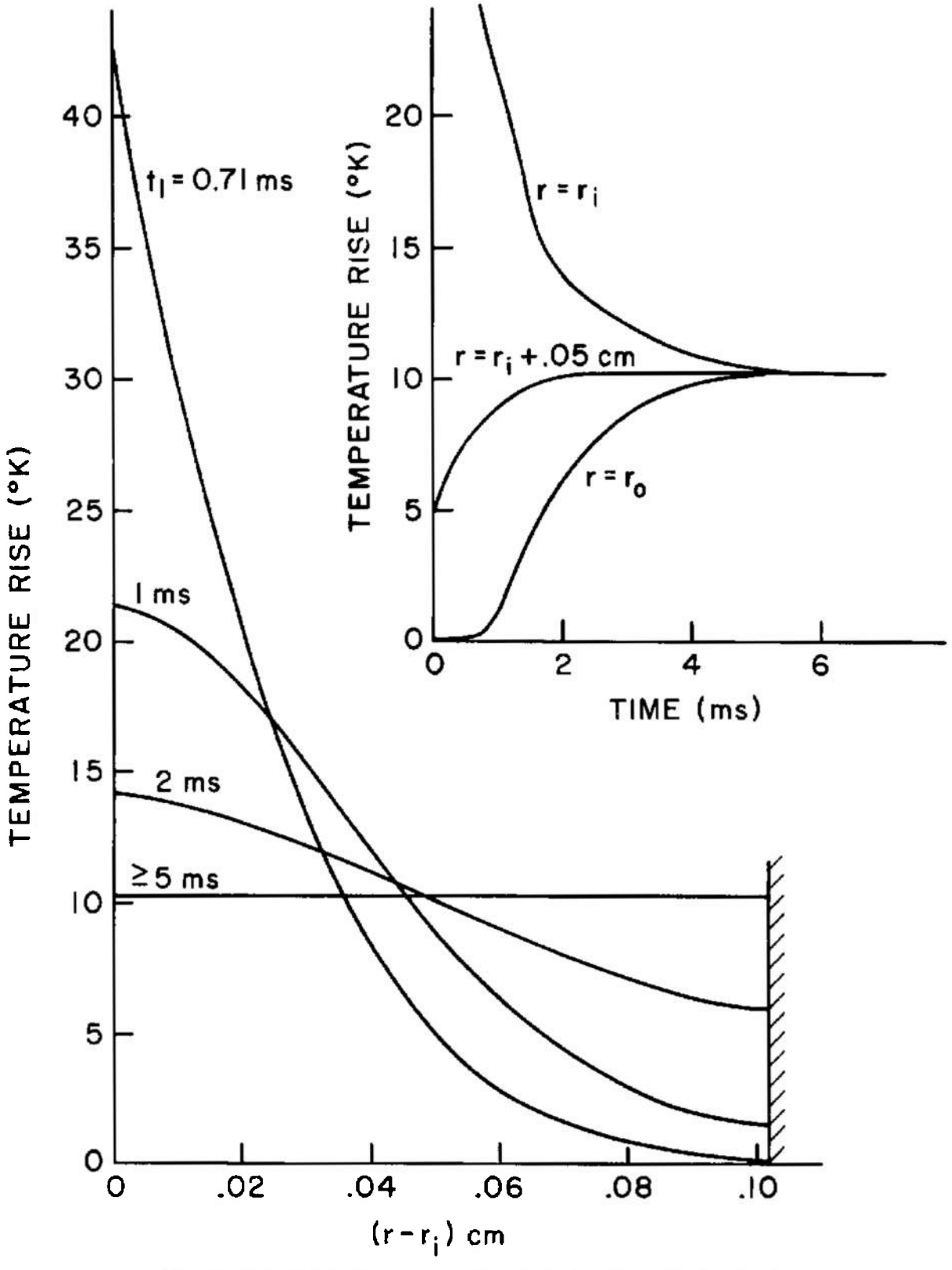

Fig. 29 Calorimeter Response to Constant Heat Flux of 5 KW/cm^2 for 0.71 ms, Followed by Adiabatic Isolation

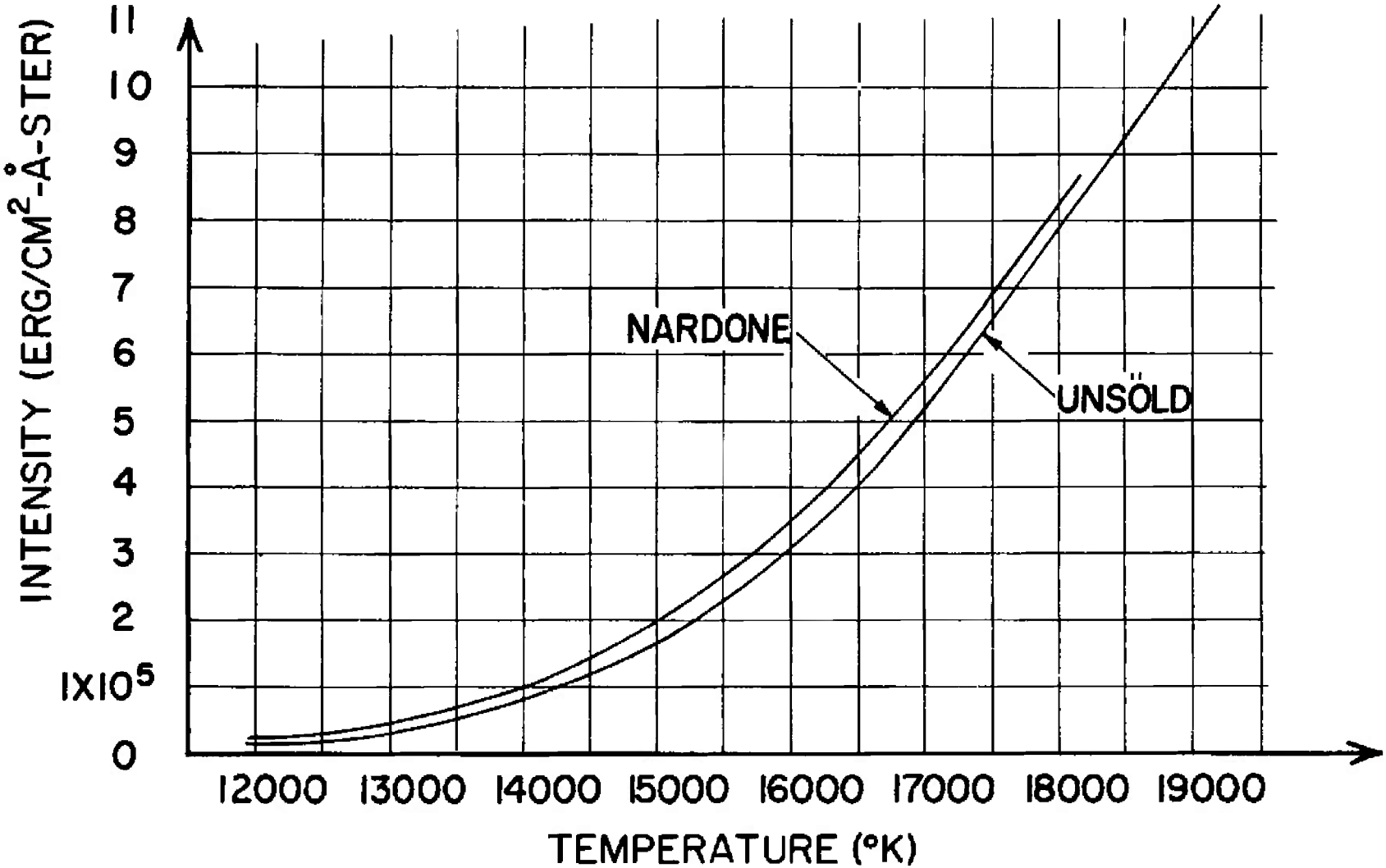

Fig. 30 Intensity of Continuous Radiation of High Pressure Air Plasma in the Temperature Range 12-20,000°K. Pressure 100 Atm; Wave Length 8330Å; Assumed Thickness of Radiating Layer 1/10 mm

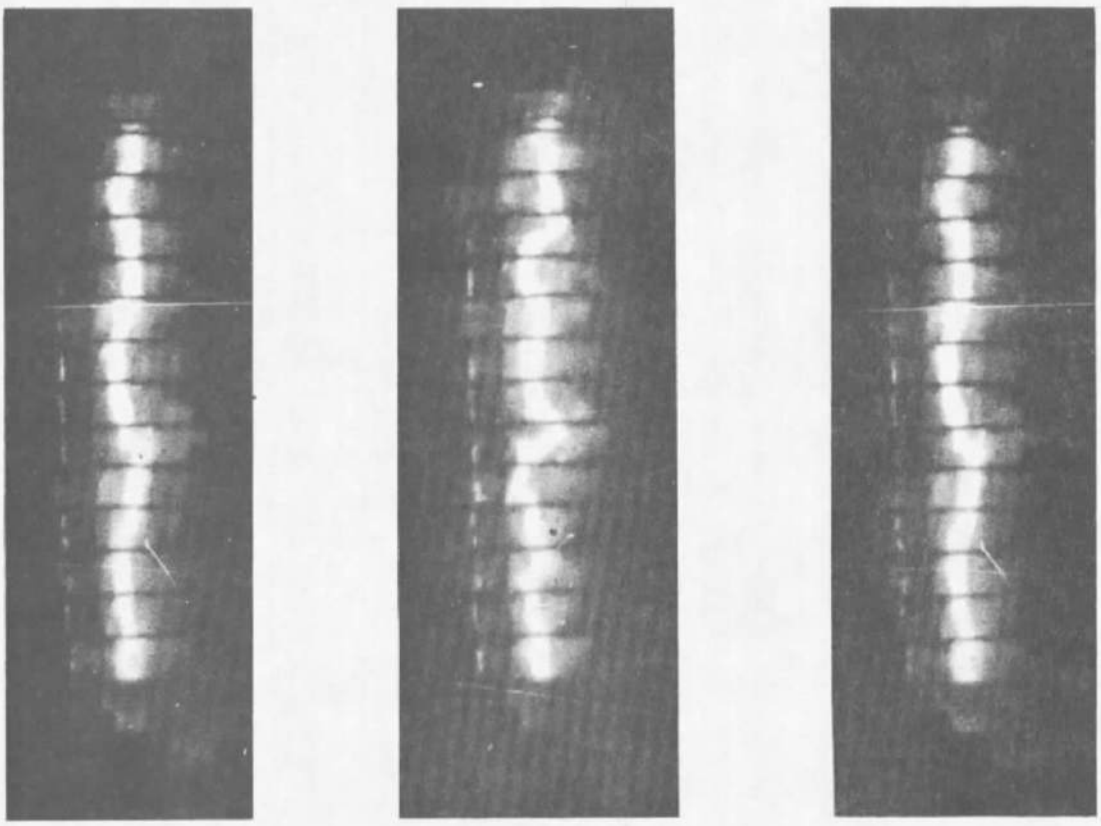

Fig. 31 Typical Instabilities of a High Pressure Arc Column. Constrictor Diameter: 5 mm; Pressure: 31 atm; Gas: Nitrogen; Current: 700 Amp

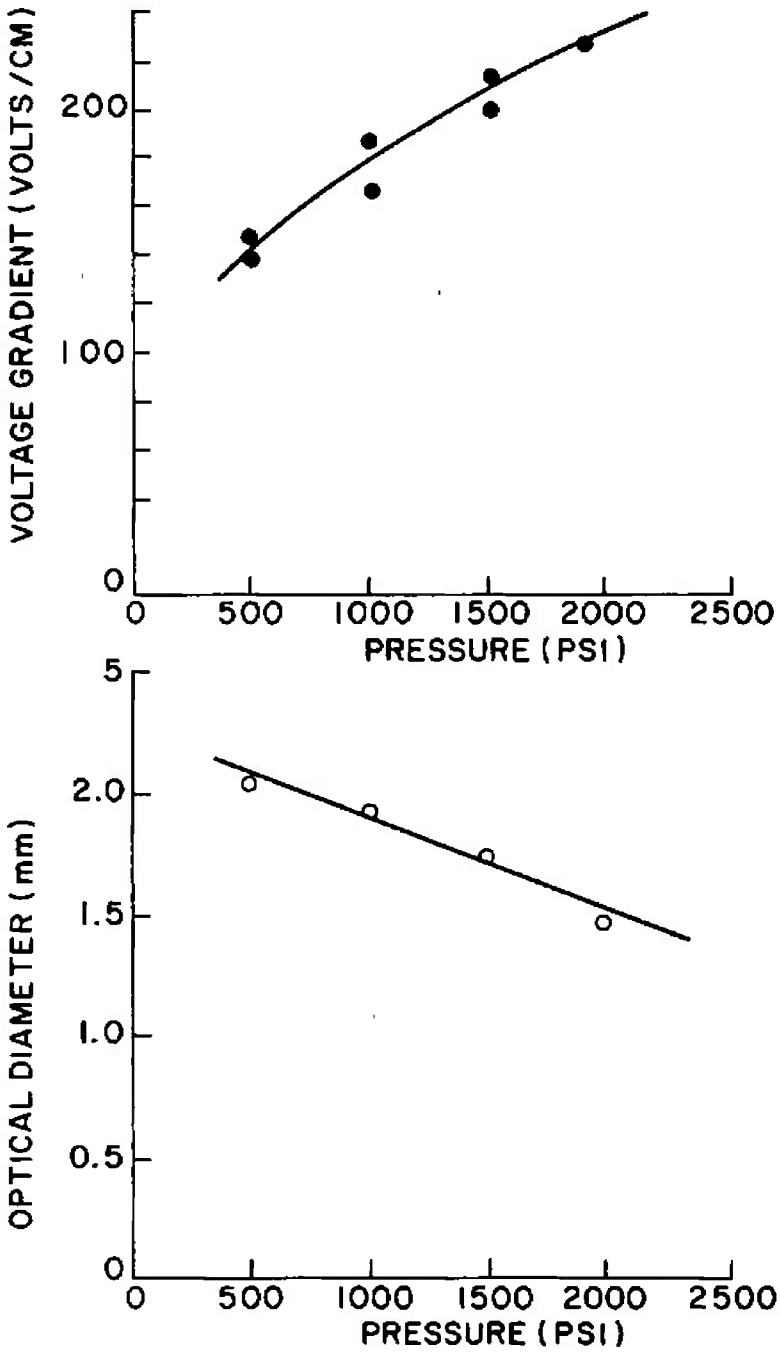

Fig. 32 Pressure Dependence of Voltage Gradient and "Optical" Diameter in a High Pressure Constricted Air Arc I = 500 amp 2.5 mm Diameter Constrictors)

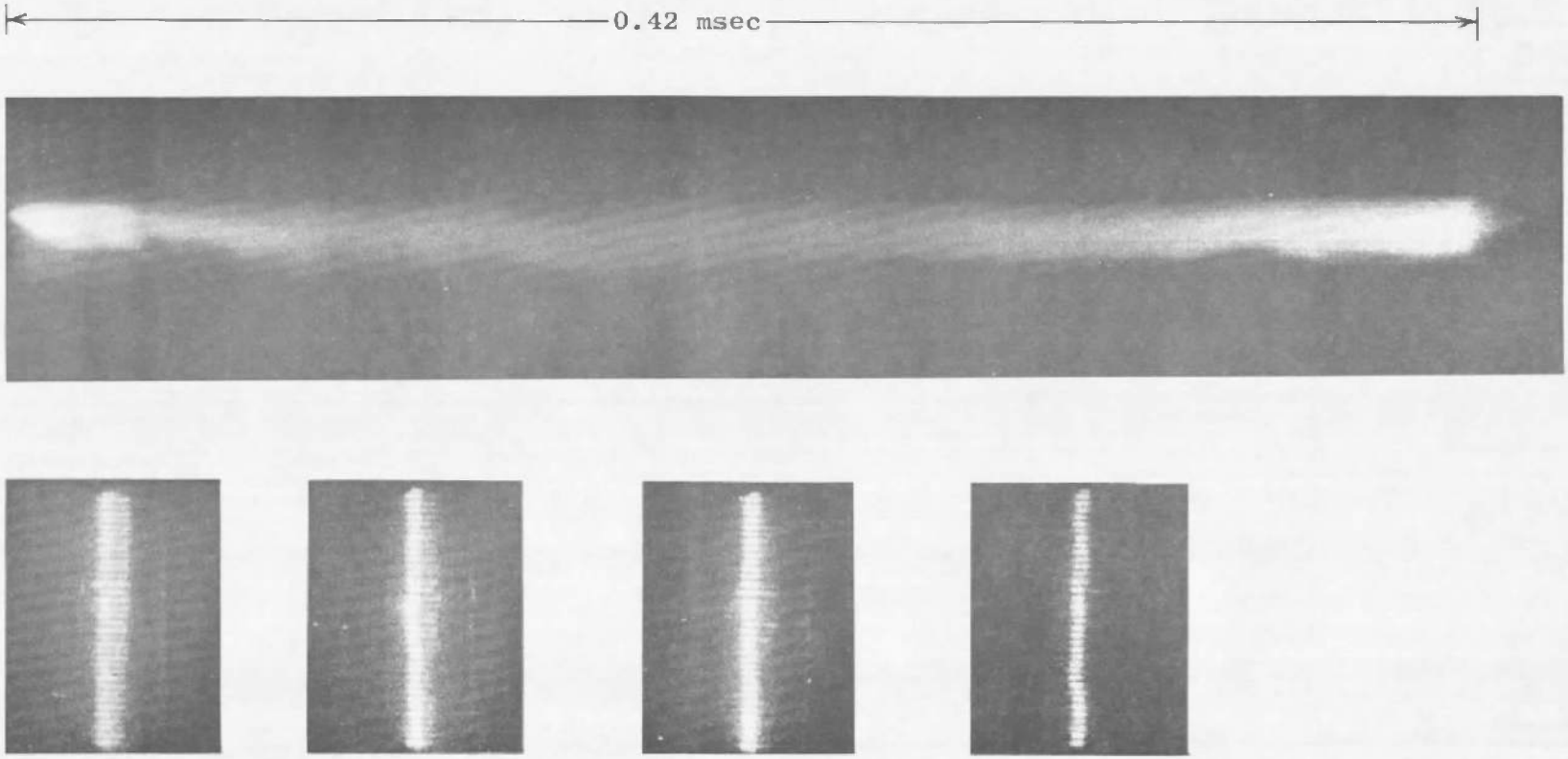

Fig. 33 Discrete and "Smear" Pictures of a 400 Amp, 100 Atm, Air Arc Showing Fluctuations of Arc in Constrictor

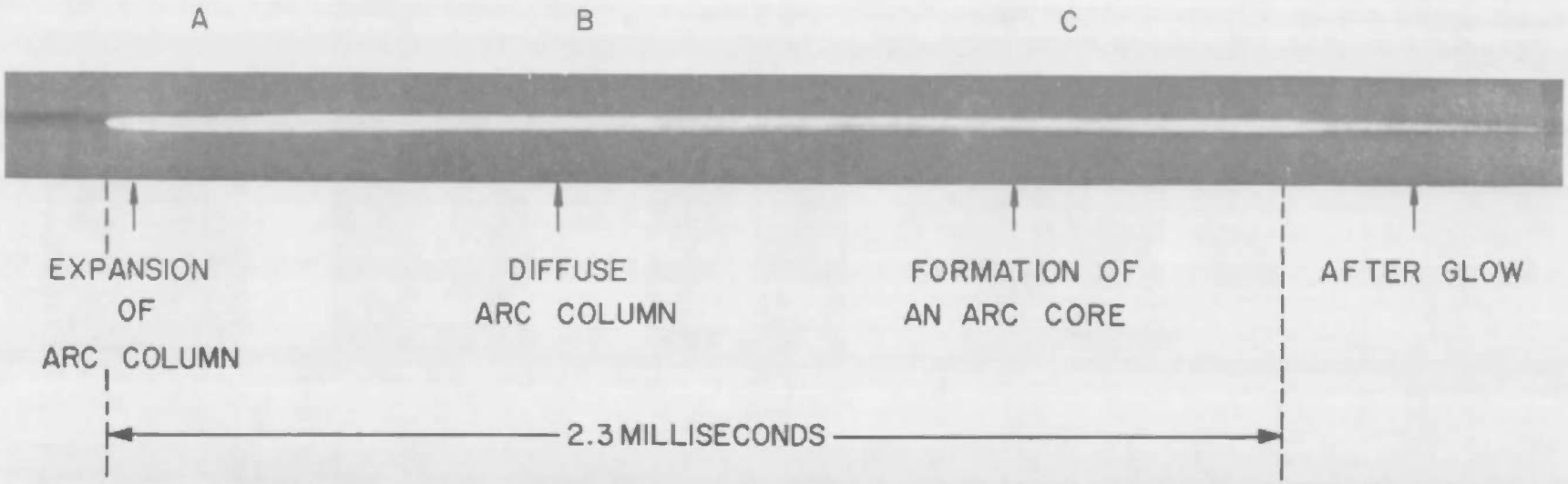

Fig. 34 Drum Camera Film of a 100 Atm Air Arc at a Current of 115 Amp Showing Formation of an Arc Core

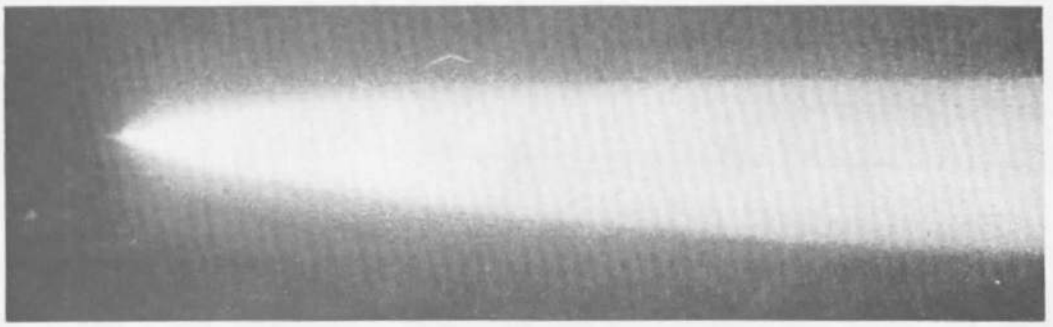

A

Expansion of Arc Column

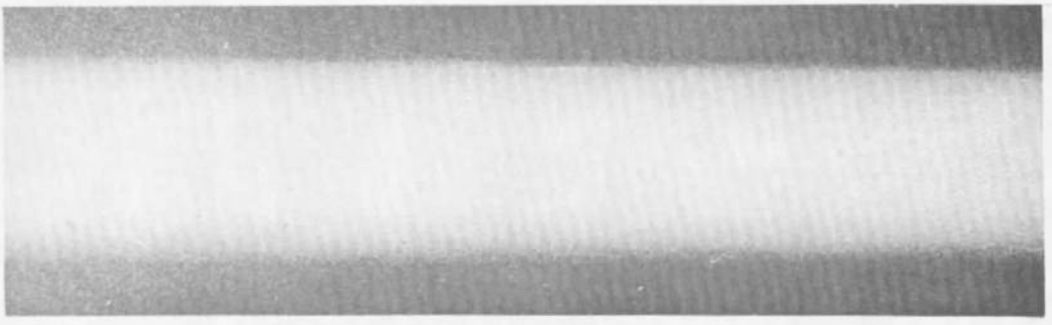

B

Diffuser Arc Column

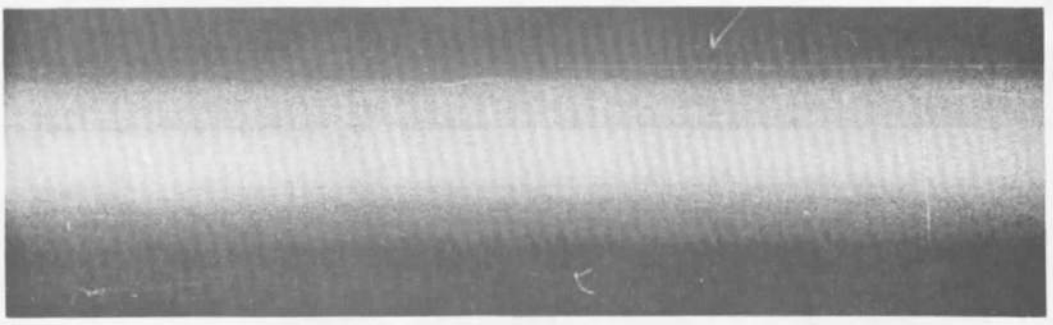

C

Core is Farmed

Fig. 35 Magnified Sections from Drum Camera Film Fig. 34. Characteristic Phases of Arc Develapment are Shown in Detail

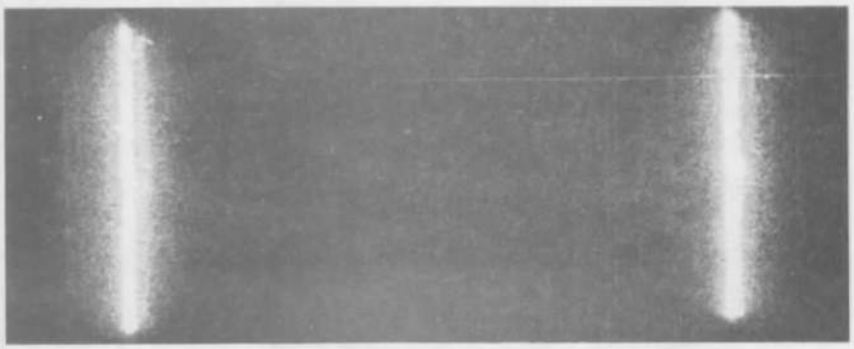

A

Expansion of Arc Column

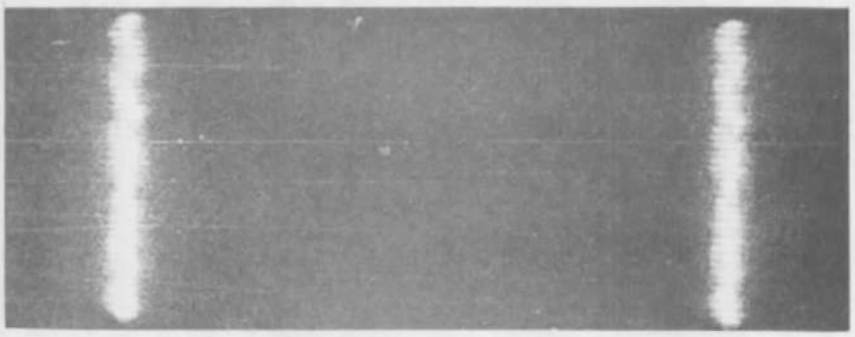

B

Diffuse Arc Column

C

Core is Formed

Fig. 36 Discrete Pictures, Taken Simultaneous with "Smear" Picture of the 115 Amp 100 Atm Air Arc, Fig. 34. Kink Type Instabilities Grow Stranger With Time

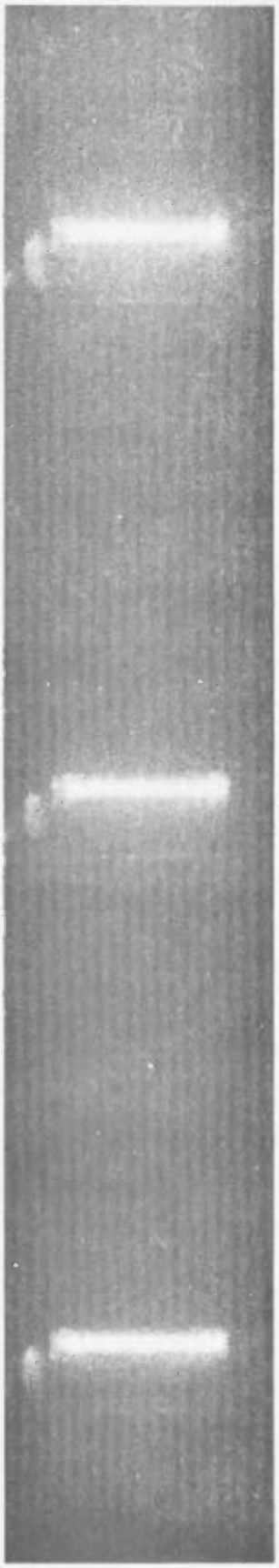

Fig. 37 High Speed Pictures of an Ablation Type Arc, Showing Its Remarkable Stability. Constrictor: Plexiglas; Inner Diameter: 3 mm; Current: 400 Amp; Pressure 150 Atm

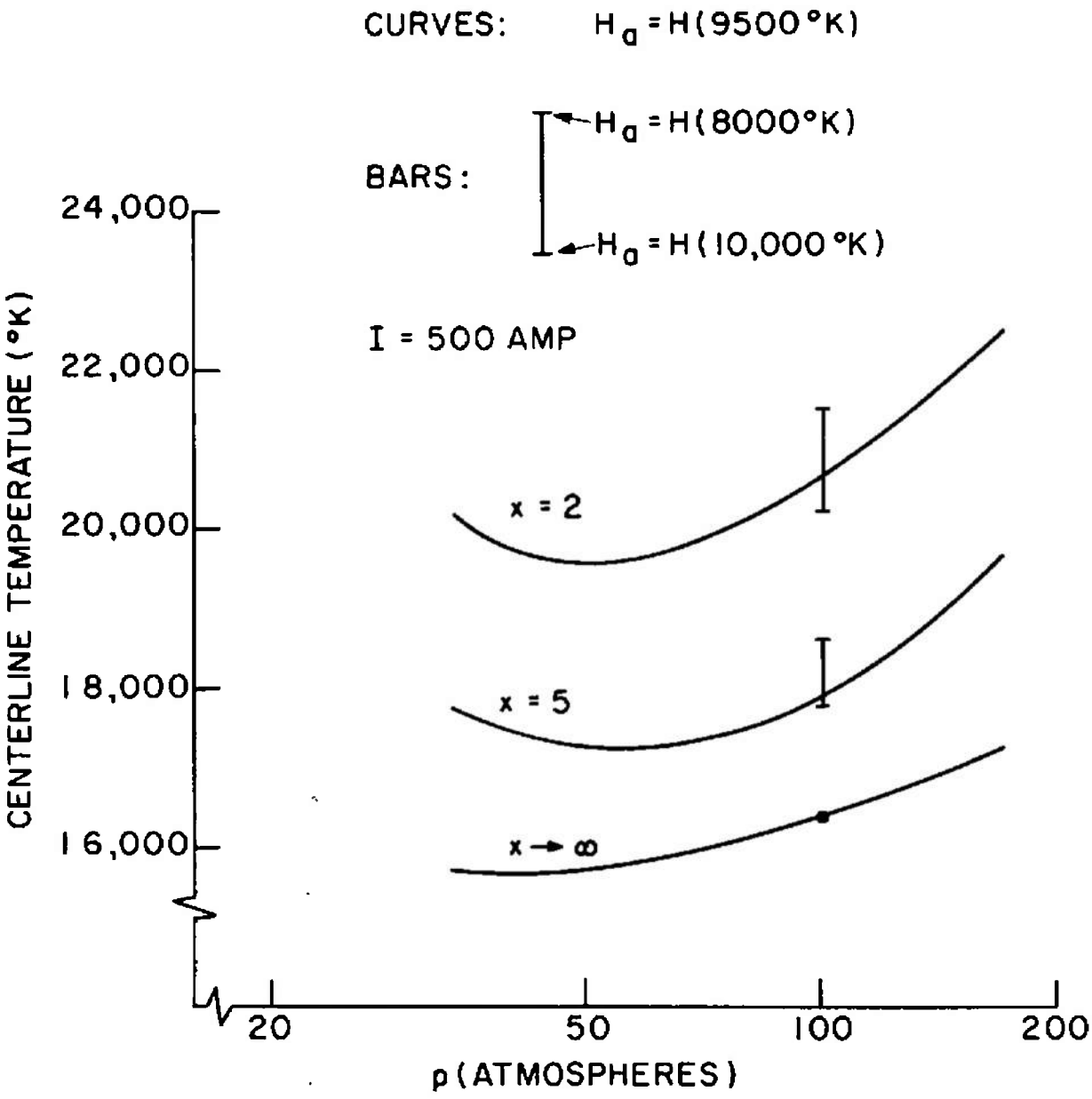

Fig. 38 Air Arc Centerline Temperature Inferred from Electrical Conductivity

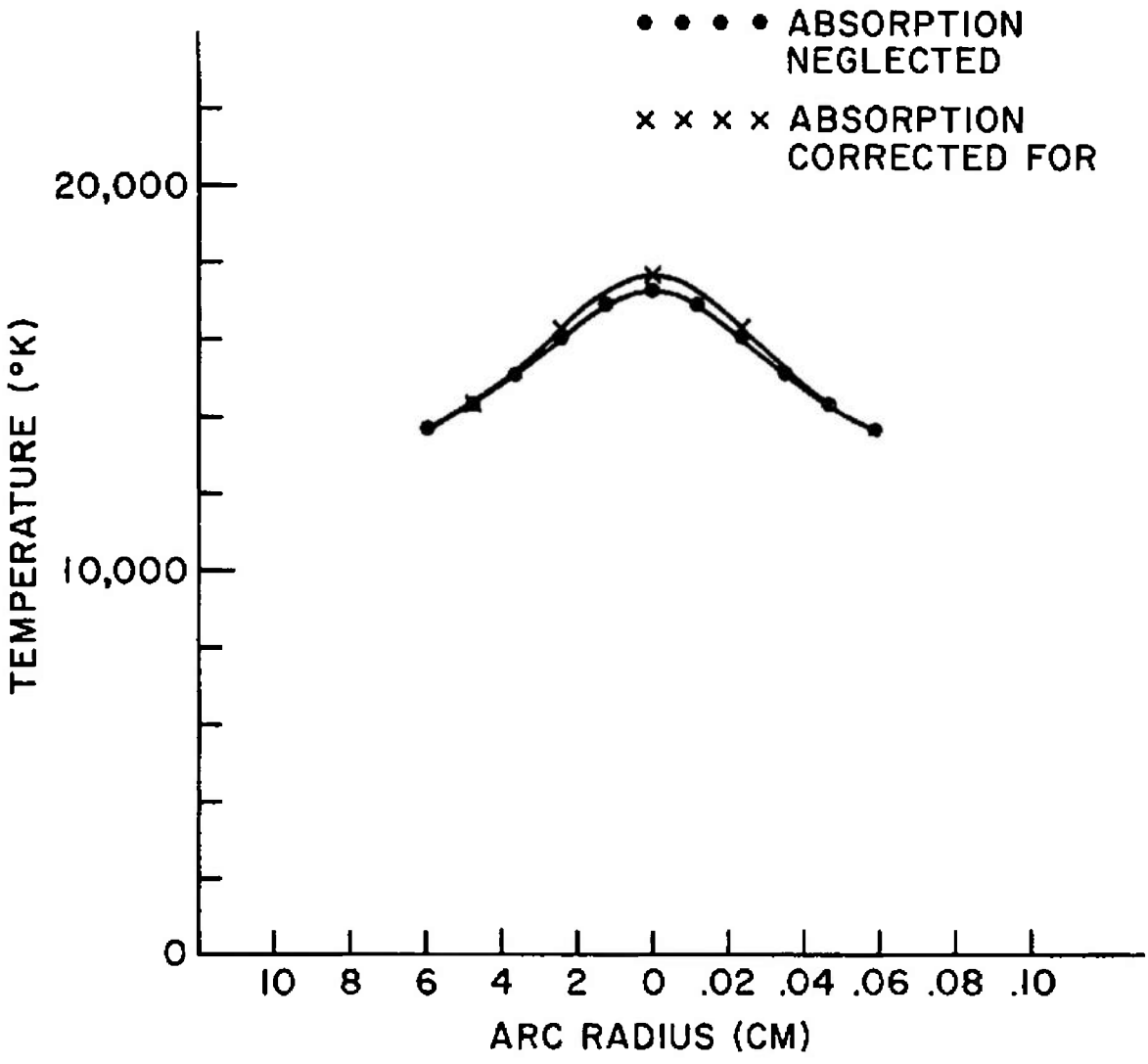

Fig. 39 Measured Temperature Profile: Current; 115 amp, Pressure, 103 Atmospheres; Constrictor Diameter 2.5 mm.

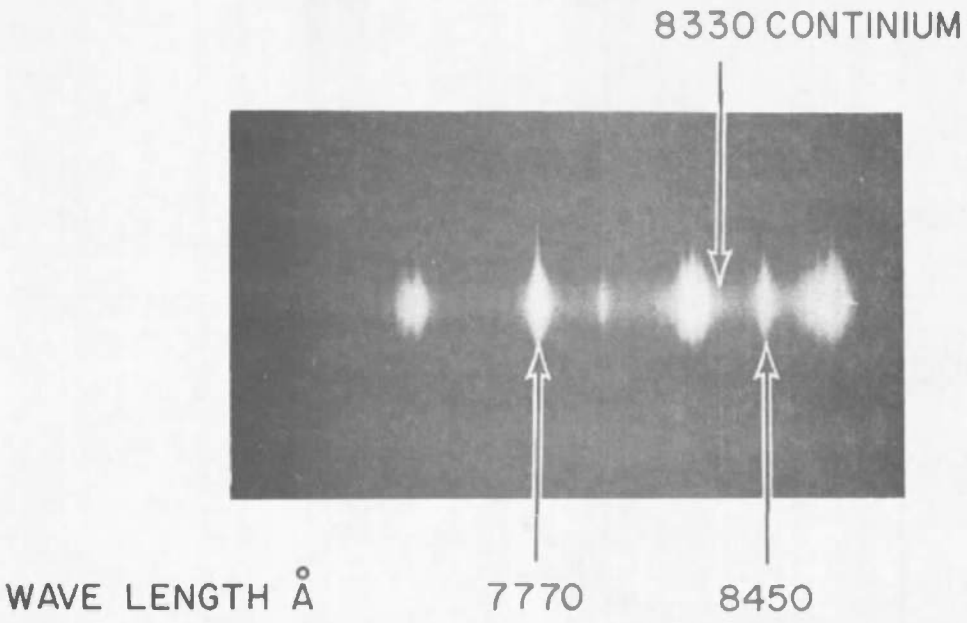

INFRA RED SPECTRUM OF HIGH PRESSURE AIR ARC

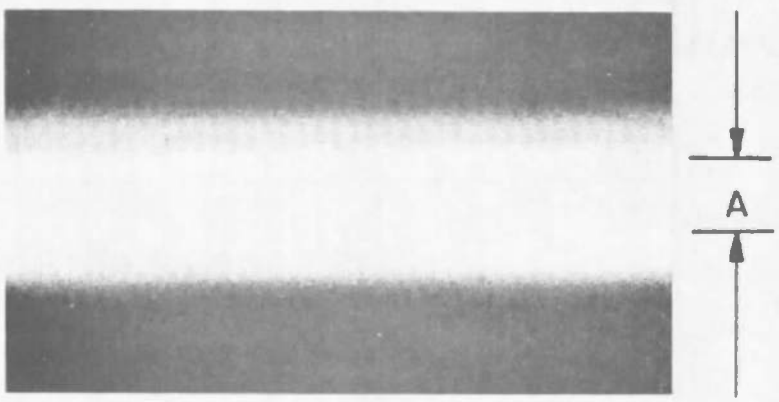

SMEAR PICTURE OF ARC COLUMN DURING SPECTROGRAPHIC EXPOSURE

Fig. 40 Spectrum and Drum Picture of 115 Amp Arc. Temperature Profile was Measured Over Width Marked A in Smear Picture

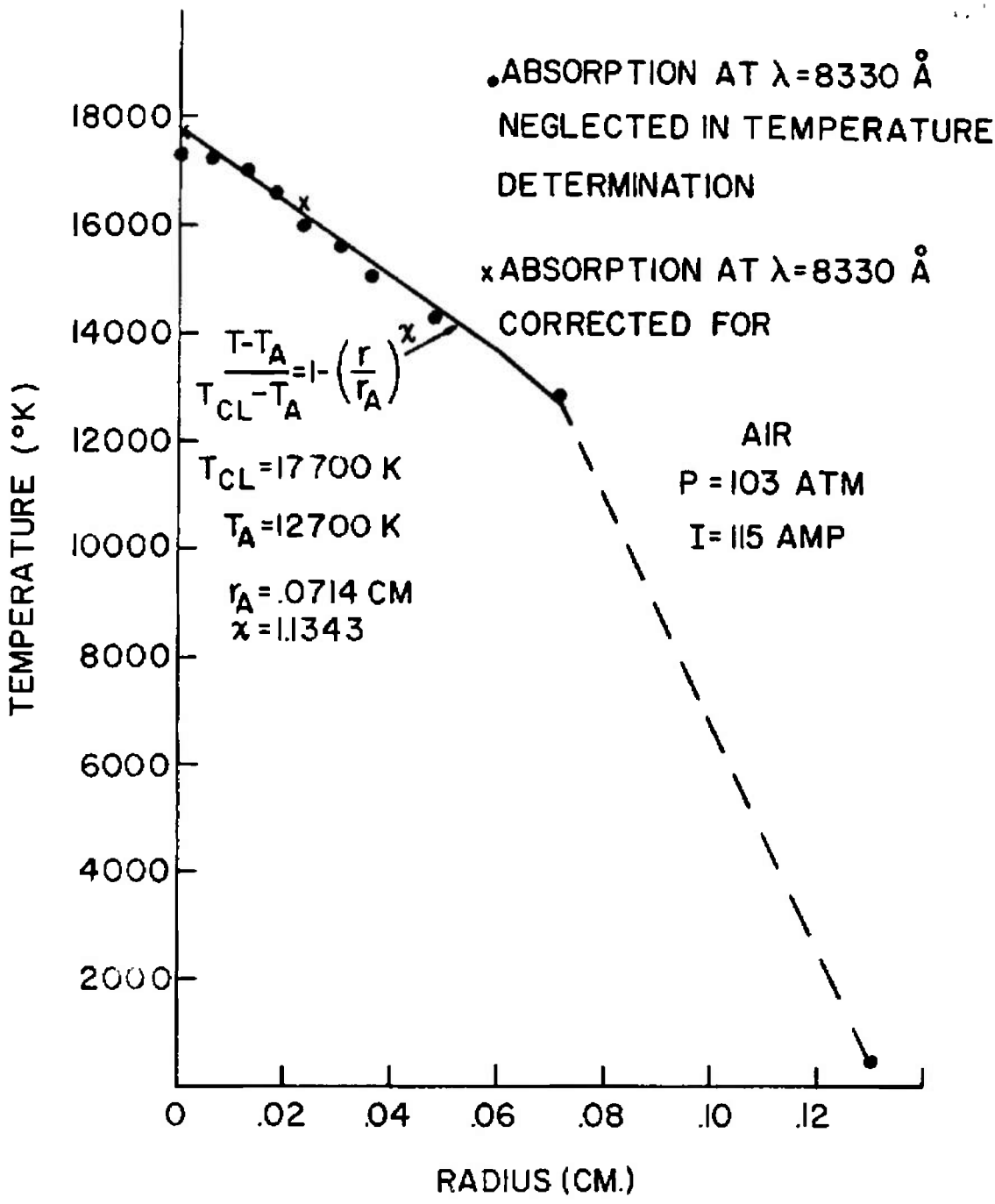

Fig. 41 Curve Fitted to Radial Temperature Distribution of a High Pressure Air Arc, Fig. 39

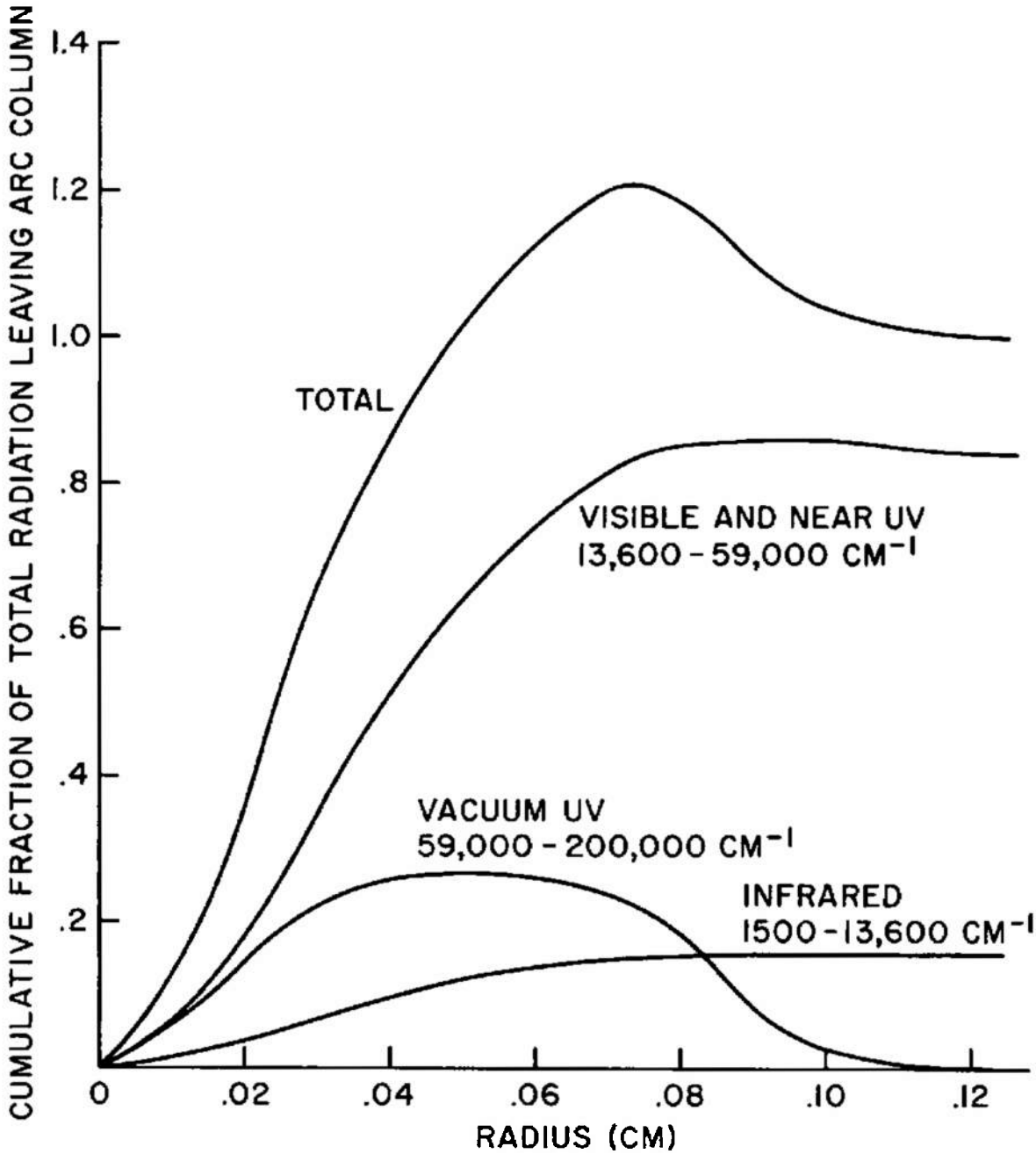

Fig. 42 Cumulative Net Radiation Based on Measured Temperature Profile.
p = 100 atm, I = 100 amp, T_{CL} = 17,700°K

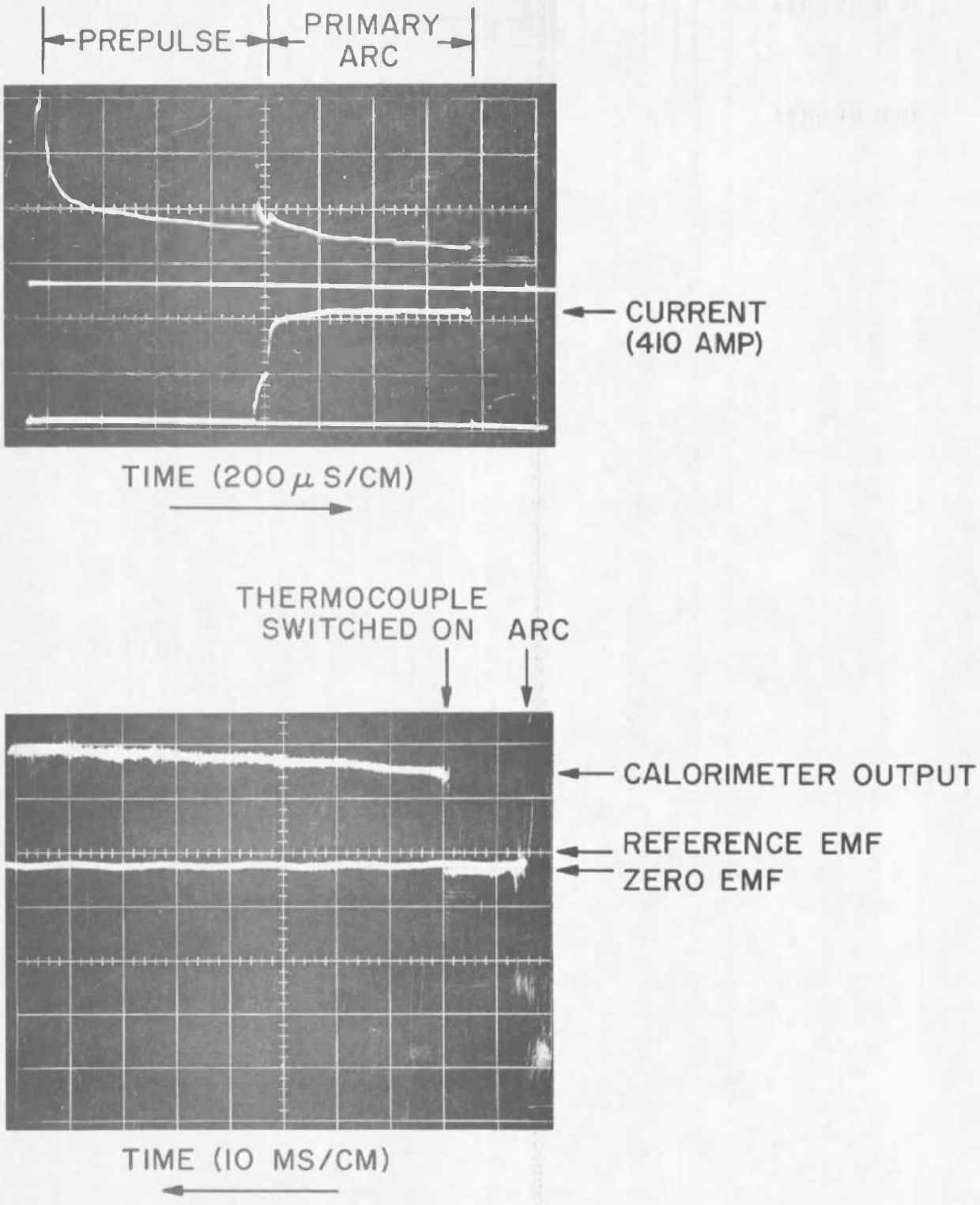

Fig. 43 Calorimeter Traces; P = 100 Atm, I = 410 Amperes

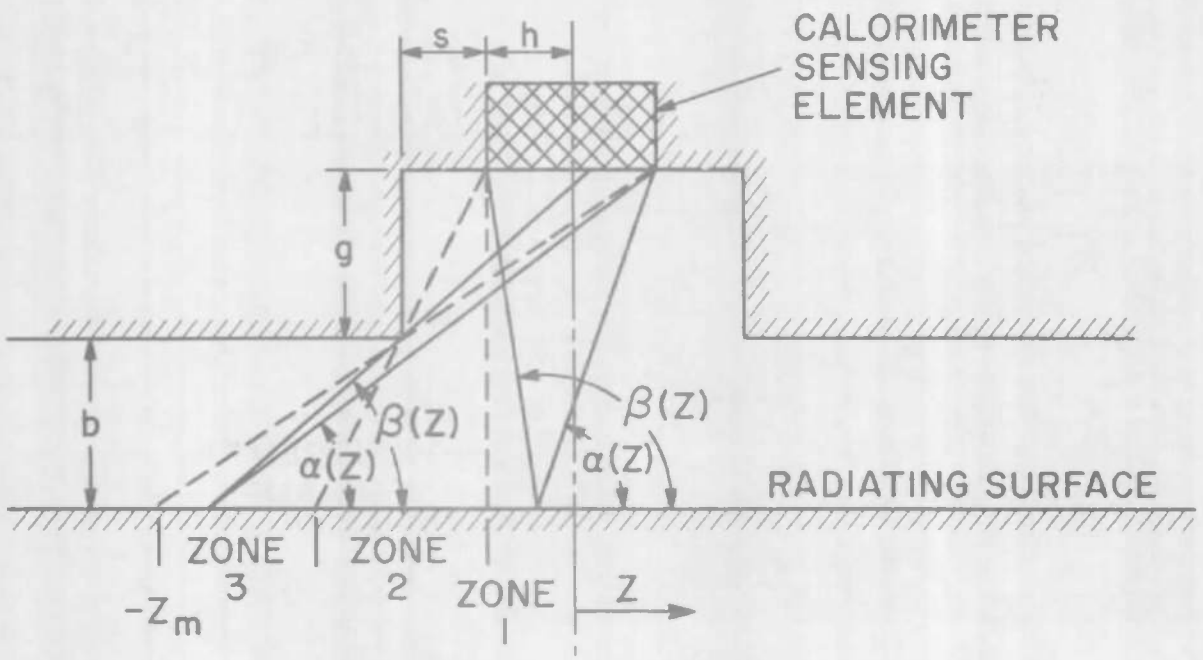

a. Shield Does Not Overlap Sensing Element (S > 0)

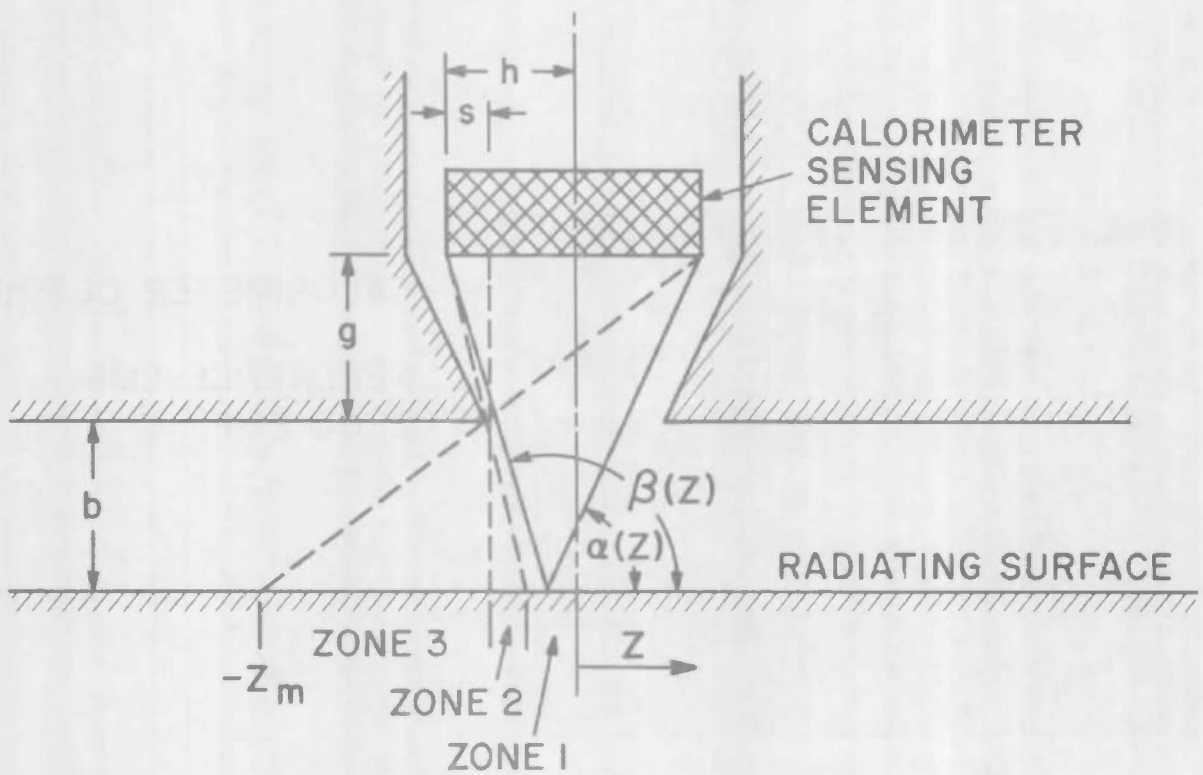

b. Shield Overlaps Sensing Element (S < 0)

Fig. 44 Calorimeter View of Arc Column

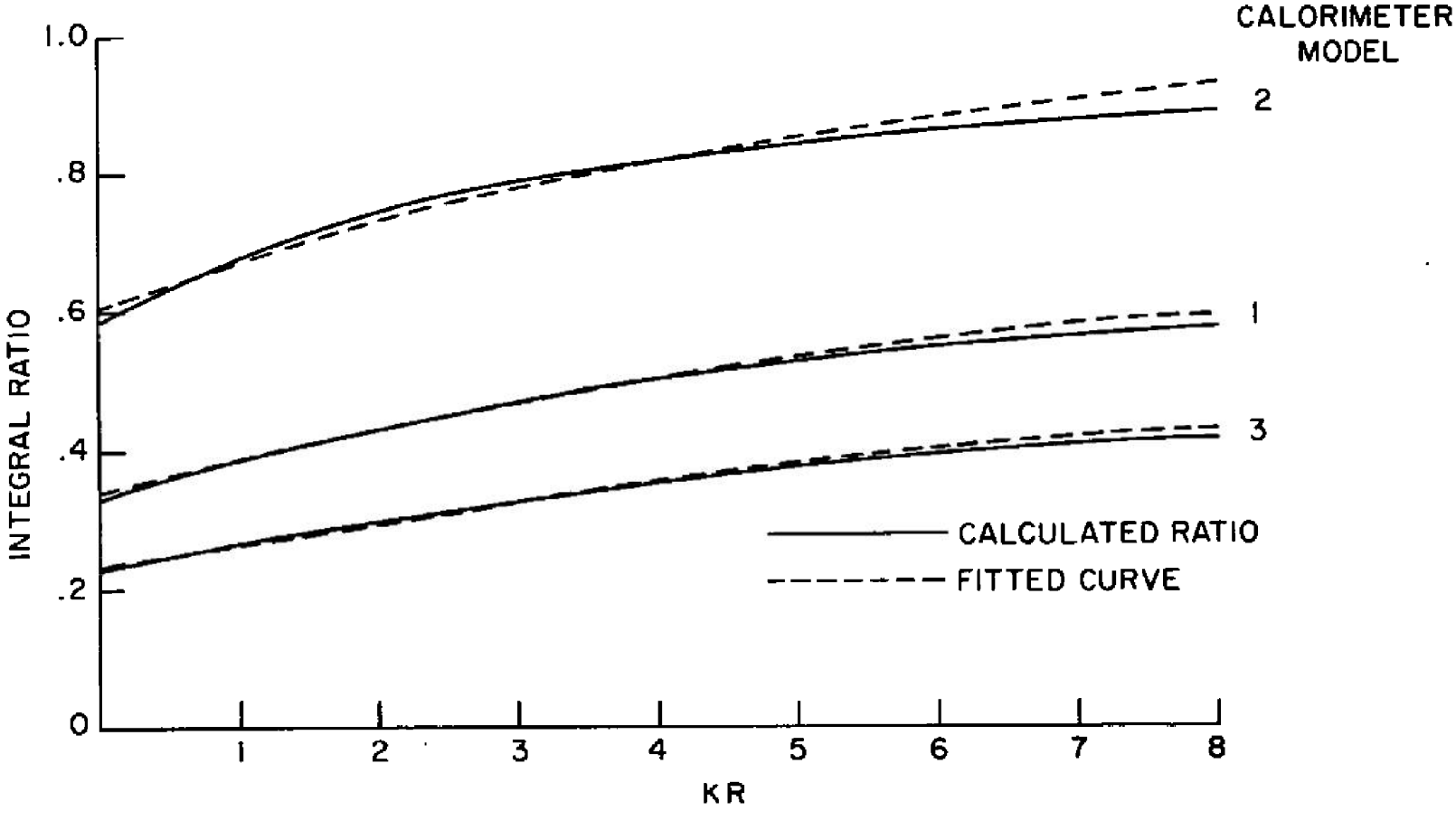

Fig. 45 Ratio of Calorimeter Integral to Complete Transmission Integral

UNCLASSIFIED

Security Classification

DOCUMENT CONTROL DATA - R&D

(Security classification of title, body of abstract and indexing annotation must be entered when the overall report is classified)

1 ORIGINATING ACTIVITY (Corporate author) General Electric Company Space Sciences Lab., King of Prussia, Penn., and High Power Lab., Philadelphia, Penn.	2a. REPORT SECURITY CLASSIFICATION UNCLASSIFIED 2b GROUP N/A

3 REPORT TITLE

RESEARCH STUDY OF RADIATION HEAT FLUX FROM HIGH PRESSURE AIR ARCS

4 DESCRIPTIVE NOTES (Type of report and inclusive dates)

N/A

5 AUTHOR(S) (Last name, first name, initial)

Marston, C. H., Frind, G. and Mishkovsky, V., General Electric Company

6 REPORT DATE	7a TOTAL NO. OF PAGES	7b. NO OF REFS
December 1966	132	None

8a. CONTRACT OR GRANT NO	9a. ORIGINATOR'S REPORT NUMBER(S)
AF40(600)-1126 b PROJECT NO. 8952 c Program Element 62405334 d Task 895202	AEDC-TR-66-258 9b. OTHER REPORT NO(S) (Any other numbers that may be assigned this report) N/A

10 AVAILABILITY/LIMITATION NOTICES

Distribution of this document is unlimited.

11. SUPPLEMENTARY NOTES	12. SPONSORING MILITARY ACTIVITY
Available in DDC.	Arnold Engineering Development Center, Air Force Systems Command, Arnold Air Force Station, Tennessee

13 ABSTRACT

A method has been developed for computation of radiant interchange within an electric arc where self absorption is important. Most or all radiation in the vacuum u.v. range is reabsorbed before it gets out of the arc. Present values of absorption coefficients are within an order of magnitude of predicting radiation losses as determined by direct experimental measurement. An arc has been operated in air at 100 atmospheres sufficiently quiescent to measure a temperature profile at 100 amperes but great care must be taken to start symmetrically and avoid disturbances. At 400 amperes even extreme precautions are not sufficient to forestall instabilities. The air arc constrictor is uncooled and is designed for quasi-steady operation for 1 to 5 milliseconds depending on current level.

DD FORM 1 JAN 64 1473

UNCLASSIFIED

Security Classification

14 KEY WORDS	LINK A		LINK B		LINK C	
	ROLE	WT	ROLE	WT	ROLE	WT
radiation heat flux air arcs self absorption heat transmission temperature testing						

INSTRUCTIONS

1. ORIGINATING ACTIVITY: Enter the name and address of the contractor, subcontractor, grantee, Department of Defense activity or other organization *(corporate author)* issuing the report.

2a. REPORT SECURITY CLASSIFICATION: Enter the overall security classification of the report. Indicate whether "Restricted Data" is included. Marking is to be in accordance with appropriate security regulations.

2b. GROUP: Automatic downgrading is specified in DoD Directive 5200.10 and Armed Forces Industrial Manual. Enter the group number. Also, when applicable, show that optional markings have been used for Group 3 and Group 4 as authorized.

3. REPORT TITLE: Enter the complete report title in all capital letters. Titles in all cases should be unclassified. If a meaningful title cannot be selected without classification, show title classification in all capitals in parenthesis immediately following the title.

4. DESCRIPTIVE NOTES: If appropriate, enter the type of report, e.g., interim, progress, summary, annual, or final. Give the inclusive dates when a specific reporting period is covered.

5. AUTHOR(S): Enter the name(s) of author(s) as shown on or in the report. Enter last name, first name, middle initial. If military, show rank and branch of service. The name of the principal author is an absolute minimum requirement.

6. REPORT DATE: Enter the date of the report as day, month, year, or month, year. If more than one date appears on the report, use date of publication.

7a. TOTAL NUMBER OF PAGES: The total page count should follow normal pagination procedures, i.e., enter the number of pages containing information.

7b. NUMBER OF REFERENCES: Enter the total number of references cited in the report.

8a. CONTRACT OR GRANT NUMBER: If appropriate, enter the applicable number of the contract or grant under which the report was written.

8b, 8c, & 8d. PROJECT NUMBER: Enter the appropriate military department identification, such as project number, subproject number, system numbers, task number, etc.

9a. ORIGINATOR'S REPORT NUMBER(S): Enter the official report number by which the document will be identified and controlled by the originating activity. This number must be unique to this report.

9b. OTHER REPORT NUMBER(S): If the report has been assigned any other report numbers *(either by the originator or by the sponsor)*, also enter this number(s).

10. AVAILABILITY/LIMITATION NOTICES: Enter any limitations on further dissemination of the report, other than those imposed by security classification, using standard statements such as:

(1) "Qualified requesters may obtain copies of this report from DDC."

(2) "Foreign announcement and dissemination of this report by DDC is not authorized."

(3) "U. S. Government agencies may obtain copies of this report directly from DDC. Other qualified DDC users shall request through _____."

(4) "U. S. military agencies may obtain copies of this report directly from DDC. Other qualified users shall request through _____."

(5) "All distribution of this report is controlled. Qualified DDC users shall request through _____."

If the report has been furnished to the Office of Technical Services, Department of Commerce, for sale to the public, indicate this fact and enter the price, if known.

11. SUPPLEMENTARY NOTES: Use for additional explanatory notes.

12. SPONSORING MILITARY ACTIVITY: Enter the name of the departmental project office or laboratory sponsoring *(paying for)* the research and development. Include address.

13. ABSTRACT: Enter an abstract giving a brief and factual summary of the document indicative of the report, even though it may also appear elsewhere in the body of the technical report. If additional space is required, a continuation sheet shall be attached.

It is highly desirable that the abstract of classified reports be unclassified. Each paragraph of the abstract shall end with an indication of the military security classification of the information in the paragraph, represented as *(TS)*, *(S)*, *(C)*, or *(U)*.

There is no limitation on the length of the abstract. However, the suggested length is from 150 to 225 words.

14. KEY WORDS: Key words are technically meaningful terms or short phrases that characterize a report and may be used as index entries for cataloging the report. Key words must be selected so that no security classification is required. Identifiers, such as equipment model designation, trade name, military project code name, geographic location, may be used as key words but will be followed by an indication of technical context. The assignment of links, rules, and weights is optional.

ARNOLD ENGINEERING DEVELOPMENT CENTER
AIR FORCE SYSTEMS COMMAND
UNITED STATES AIR FORCE
ARNOLD AIR FORCE STATION, TENNESSEE

TRANSMITTAL NOTE

1. The attached report is forwarded for your information and retention.

2. Inquiries relative to any feature of this report should be addressed to this Headquarters, ATTN: AETS.

Leonard T. Glaser

LEONARD T. GLASER, Colonel, USAF
Director of Test